University of Alberta

Development of a 3D Finite Element Model for the Biomechanical Study of Maxillary Expansion Treatments Using Bone-Anchors

by

Yi Fang

A thesis submitted to the Faculty of Graduate Studies and Research
in partial fulfillment of the requirements for the degree of

Master of Science

Department of Mechanical Engineering

Edmonton, Alberta
Fall 2006

Library and Archives Canada

Published Heritage Branch

395 Wellington Street
Ottawa ON K1A 0N4
Canada

Bibliothèque et Archives Canada

Direction du Patrimoine de l'édition

395, rue Wellington
Ottawa ON K1A 0N4
Canada

Your file Votre référence
ISBN: 978-0-494-22263-8
Our file Notre référence
ISBN: 978-0-494-22263-8

NOTICE:
The author has granted a non-exclusive license allowing Library and Archives Canada to reproduce, publish, archive, preserve, conserve, communicate to the public by telecommunication or on the Internet, loan, distribute and sell theses worldwide, for commercial or non-commercial purposes, in microform, paper, electronic and/or any other formats.

The author retains copyright ownership and moral rights in this thesis. Neither the thesis nor substantial extracts from it may be printed or otherwise reproduced without the author's permission.

AVIS:
L'auteur a accordé une licence non exclusive permettant à la Bibliothèque et Archives Canada de reproduire, publier, archiver, sauvegarder, conserver, transmettre au public par télécommunication ou par l'Internet, prêter, distribuer et vendre des thèses partout dans le monde, à des fins commerciales ou autres, sur support microforme, papier, électronique et/ou autres formats.

L'auteur conserve la propriété du droit d'auteur et des droits moraux qui protège cette thèse. Ni la thèse ni des extraits substantiels de celle-ci ne doivent être imprimés ou autrement reproduits sans son autorisation.

In compliance with the Canadian Privacy Act some supporting forms may have been removed from this thesis.

While these forms may be included in the document page count, their removal does not represent any loss of content from the thesis.

Conformément à la loi canadienne sur la protection de la vie privée, quelques formulaires secondaires ont été enlevés de cette thèse.

Bien que ces formulaires aient inclus dans la pagination, il n'y aura aucun contenu manquant.

Canada

ABSTRACT

Maxillary expansion (ME) treatments using bone anchors (BA) have been recently developed to correct maxillary transverse deficiencies. The treatments use BA instead of teeth as abutments to apply the expansion load directly to the palatine process of the maxilla, which eliminate the disadvantages of traditional ME treatments. The success of the treatment is mainly dependent on the correct understanding and prediction of the biomechanical responses of craniofacial bones and stress distribution in the bone-anchor osseointegration interface (BAOI) induced by an expansion load applied on bone anchors. The objectives of this thesis were to develop a reliable 3D finite element (FE) model and perform biomechanical studies for BA-ME treatments.

A subject-specific 3D FE skull model was developed based on Cone-Beam Computerized Tomography (CBCT) scan image data of a dry skull. Biomechanical studies of BA-ME treatments showed similar strain and stress patterns compared with experimental results and the literature, respectively.

The evaluation of bone elastic constants indicated that FE models assigned with heterogeneous bone properties provide more reliable FE analysis than those assigned with homogeneous bone properties.

Furthermore, the evaluation of BA anchorage inclination angles showed that BA anchored perpendicular to the palatal bone surface lead to optimal stress distribution in Bone-Anchor Osseointegration Interface (BAOI).

This work was performed as a preliminary step towards the development of a patient-specific FE model for predicting BA-ME treatment; to this end, the objectives of the thesis were met.

ACKNOWLEDGEMENTS

I would like to express my deep gratitude to my supervisor, Dr. Carey Jason, for giving me the opportunity and freedom to work in this interesting field. Without his encouragements and guidance, I could not be able to finish my Master's study. In addition, his understanding and consideration provided me a comfortable environment throughout the years I worked in his group.

I would like to give my thanks to my co-supervisor, Dr. Roger Toogood. He gave me great help on the understanding and application of 3D modeling and finite element analysis. Without his help, I could not overcome those problems quickly.

I would also like to give my thanks to Dr. Paul W. Major, for the support to work in the Orthodontic Graduate Program with the Faculty of Medicine and Dentistry, and Dr. Alidad Amirfazli, his advice helped me better understanding this field.

Especially, I would like to express my appreciation for Manuel O. Lagravère. He provided me a lot of help on the understanding and application of this work related to the orthodontic treatments, which made this work more significant and relevant. Without his cooperation and suggestion, my work could not reach such result as our expectation.

Finally, I would like to extend my thanks to other professors, staff and graduate students in the Department of Mechanical Engineering, such as professor Mark Y. Ackerman, Professor Zihui Xia, Gail Anderson, Bernie Faulkner, Anthony Au, Chengye Fan, Gang Tao, Doug, Cagri and so on, for their help, information and the friendly environment they created during my graduate studies.

This work is dedicated to my family and friends.

TABLE OF CONTENTS

Abstract
Acknowledgements
List of Tablesvii
List of Figures
Abbreviations
Chapter 1 Introduction 1
1.1 Motivation: Maxillary Expansion Treatment Prediction 1
1.2 Thesis Objectives 6
1.3 Background Information 7
1.3.1 Anatomical Coordinate System Nomenclature 7
1.3.2 The Finite Element Method 8
1.3.3 Imaging Techniques for FE Model Development 9
1.4 Thesis Outline 13
Chapter 2 Literature Review 14
2.1 Introduction 14
2.2 Development of FE Models for ME Treatments 14
2.3 Effect of Bone Elastic Properties 16
2.4 Effect of Bone Implant Anchorage Inclination Angles 17
2.5 Conclusions 19
Chapter 3 Development of a Skull Finite Element Model 21
3.1 Introduction 21
3.2 Materials and Methods 23
3.2.1 CBCT Data Acquisition 23
3.2.2 Segmenting and Generating Bone Structures 25
3.2.3 Assigning Elastic Constants 26
3.2.4 Dry Skull Finite Element Model 29
3.2.5 Bone Anchor Model 32
3.3 Discussion and Conclusion 35
Chapter 4 Fresh Skull Experimental Study of Maxillary Expansion Treatment 38
4.1 Introduction 38
4.2 Materials and Methods 39
4.3 Results and Discussion 42
4.4 Conclusions 45
Chapter 5 Study of Craniofacial Response to ME Treatment using Bone Anchors 46
5.1 Introduction 46
5.2 Materials and Methods 46
5.3 Results 47
5.3.1 Displacement Distribution in Craniofacial and Maxillary Structures . 47
5.3.2 Stress Distribution in Craniofacial and Maxillary Structures 57
5.3.2 Strain Distribution in Craniofacial and Maxillary Structures 59
5.4 Discussion 61
5.5 Conclusions 65

Chapter 6 Evaluation of the Effect of Elastic Properties on the Proposed Model ... 67
6.1 Introduction ... 67
6.2 Materials and Methods ... 68
6.2.1 Elastic Property Assignment ... 68
6.2.2 Bone Anchor Osseointegration Interface ... 69
6.2.3 Osseointegration Boundary and Constraint Conditions ... 70
6.3 Results ... 70
6.3.1 Model Sensitivity to Number of Assigned EPs ... 70
6.3.2 BAOI Von Mises Stresses Sensitivity to EP ... 79
6.4 Discussion ... 81
6.5 Conclusion ... 85
Chapter 7 Evaluation of Bone Anchor Implantation Inclination Angle and Position in the Palate ... 86
7.1 Introduction ... 86
7.2 Materials and Methods ... 87
7.3 Results ... 91
7.3.1 BAOI FE Predicted Stress Results ... 91
7.3.2 Predicted Expansion Treatment Results ... 96
7.4 Discussion ... 99
7.5 Conclusion ... 100
Chapter 8 Summary, Conclusions and Future Work ... 102
8.1 Summary ... 102
8.1.1 Development of a 3D FE Model of Skull with Bone Anchors ... 102
8.1.2 Finite Element Analysis of Maxillary Expansion Treatments ... 103
8.1.3 Effect of Elastic Properties ... 103
8.1.4 Effect of Anchorage Inclination Angles of Bone Anchors ... 104
8.2 Conclusion ... 105
8.3 Future Work ... 106
References ... 107
Appendix 1 ... 114
Appendix 2 ... 118
Appendix 3 ... 122

LIST OF TABLES

Table 1-1: Programs developed recently for the medical research 11
Table 3-1: Material properties for bones, titanium bone anchor and BAOI 29
Table 4-1: Micro strains (με) at three sutures in terms of unilateral maxillary expansion (mm), NS: Nasomaxillary Suture; PS: Pterygomaxillary Suture; ZS: Zygomaticomaxillary Suture 44
Table 5-1: Displacement, stress and strain obtained in 25 regions following 4mm transverse expansion (T: transverse direction; V: Vertical direction; S: Sagittal direction; R: Resultant). * Negative value (-) represents a medial displacement in transverse direction, upward displacement in vertical direction and anterior displacement in sagittal direction respectively. 50
Table 5-2: Comparison of stress results with those of Jafari et al 64
Table 6-1: Summary of six material assignment schemes. 69
Table 6-2: Maximum von Mises stress distributed in craniofacial and maxillary structures obtained with 6 material assignment schemes 71
Table 6-3: Equivalent strain distribution in craniofacial and maxillary structures obtained with 6 material assignment schemes 72
Table 6-4: Resultant displacement distribution in craniofacial and maxillary structures obtained with 6 material assignment schemes 73
Table 6-5: Average percentage difference (± standard deviation) between using 2, 20, 39 and 78 versus 156 material properties for displacement, von Mises stresses and strains at 25 bony landmark positions detailed in Figure 5-1 74
Table 6-6: Average percentage difference of von Mises stress distributed in BAOI between control and four trial models. 75
Table 7-1: Displacement distribution under 6 implantation inclination angles. Comparison is done with 0-T, clinically accepted AIA. 97
Table 7-2: Stress (MPa) distribution through the skull under 6 implantation inclination angles. Comparison is done with 0-T, clinically accepted AIA. 98

LIST OF FIGURES

Figure 1-1: Anatomy figure for maxillary transverse deficiency 2
Figure 1-2: Conventional maxillary expansion treatments [Provided by Lagravère, 2006] 3
Figure 1-3: Maxillary expansion treatment using bone anchors; (a) bone anchor placed in palatal bones; (b) maxillary expansion applied with jackscrew [Provided by Lagravère, 2006] 4
Figure 1-4: Conventional imaging methods [Provided by Russett, 2006] 5
Figure 1-5: Anatomical planes as related to skull 7
Figure 3-1: Schematic of the imaging process to build bone solid model based on CT image data 22
Figure 3-2: Schematic of the imaging process to develop a 3D solid model of a skull using CBCT data 24
Figure 3-3: Newtom CBCT machine (Department of Graduate Orthodontics, University of Alberta) 25
Figure 3-4: Elastic modulus (GPa) versus bone apparent density (kg/m^3) 29
Figure 3-5: 3D subject-specific finite element model of skull 31
Figure 3-6: Bone anchor position and full model. a) CT image before placing bone anchor; b) CT image after placing bone anchor 33
Figure 3-7: FE model with inserted bone anchor. a) Transverse view of FE model with bone anchor; b) cross section view A-A (Sagittal view); and c) a zoom in view 34
Figure 4-1: Maxillary expansion experiment on fresh skull; (a) strain gauge positions, (b) strain gauge configuration, and (c) expander in fresh skull (strain gauge shown) 41
Figure 4-2: Micro strains (με) at three sutures in terms of unilateral maxillary expansion (mm), NS: Nasomaxillary Suture; PS: Pterygomaxillary Suture; ZS: Zygomaticomaxillary Suture 43
Figure 5-1: Schematic of constraint conditions 47
Figure 5-2: Investigated regions of craniofacial and maxillary complex 49
Figure 5-3: Contour plot of displacement of nodes in transverse direction after 4mm expansion (+ Lateral; - Medial). Deformed skull shown 52
Figure 5-4: Contour plot of displacement of nodes in vertical direction after 4mm expansion (+ Inferior; - Superior). Deformed skull shown 53
Figure 5-5: Contour plot of displacement of nodes in sagittal direction after 4mm expansion (+ Posterior; - Anterior). Deformed skull shown 54
56Figure 5-6: Contour plot of resultant displacement of nodes after 4mm expansion56
Figure 5-7: Contour plot of von Mises stress of nodes 58
Figure 5-8: Contour plot of equivalent strain of nodes 60
Figure 5-9: Comparison of strain in three craniofacial sutures between experiment and model. Pterygo: Pterygomaxillary suture; Zygo: Zygomaticomaxillary suture; Naso: Nasomaxillary suture 62

Figure 6-1: (a) Bone anchor cross section and evaluation lines; (b) front view of FE model; (c) cut view B of (b) showing the stress at the implant 77
Figure 6-2: Comparison of von Mises stress distribution along (a) line 2 and (b) line 8 78
Figure 6-3: Von Mises stress distribution in (a) line 2 and (b) line 8 with a ± 50% variation of BAOI elastic modulus. 80
Figure 6-4: Von Mises stress and strain at 25 reference position for (a) 2 EP and (b) 156 EP. 82
Figure 7-1: Schematic of implant anchorage position and inclination direction; a) BA long axis projection along transverse axis (T) and along a 15° offset from the transverse axis in the transverse plane (15T); b) implant anchorage position in skull in coronal view 88
Figure 7-2: FE skull model with 6 AIA conditions 90
Figure 7-3: Average stress and standard deviations on BA 92
Figure 7-4: Average maximum stress 93
Figure 7-5: Stress distribution in BAOI from model with 6 implantation inclination angles found along (a) line 5 and (b) line 8. 95

ABBREVIATIONS

AIA: Anchorage inclination angle

BA: Bone anchor

BA-ME: Maxillary expansion treatments using bone anchors

BAOI: Bone-anchor osseointegration interface

CAD: Computer-aided design

CBCT: Cone-Beam Computerized Tomography

CR: Cephalometric radiography

CT: Computed tomography

EP: Elastic property

FE: Finite element

FEA: Finite element analysis

HU: Hounsfield Unit

ME: Maxillary expansion

RME: Rapid maxillary expansion

SME: Slow maxillary expansion

SAME: Surgically assisted maxillary expansion

CHAPTER 1 INTRODUCTION

1.1 Motivation: Maxillary Expansion Treatment Prediction

Maxillary transverse deficiency is a medical condition resulting from a narrow maxilla (Figure 1-1). This condition prevents proper occlusion and causes posterior crossbite. When eating, the mandible may have to move side to side to allow the back teeth to bite together. It has been reported that the abnormal movement of the lower jaw associated with a posterior crossbite can have long term effects on the growth and development of the teeth and jaws (McNamara et al, 2000).

Maxillary expansion (ME) treatments have been used to correct maxillary transverse deficiency problems since the end of 1900's. Since then, different types of ME treatment protocols have been developed and applied. The most widely applied treatments are rapid maxillary expansion (RME), slow maxillary expansion (SME), and surgically assisted maxillary expansion (SAME) (Ficarelli, 1978; Bell, 1982). During these conventional ME treatments, the expansion is typically achieved by using teeth as force abutments to the palatine process of the maxilla (Figure 1-2). This limits the applicable force and causes undesirable teeth movement; it further lacks firm anchorage to retain suture expansion and limits palatal bone movement (Shapiro and Kokich, 1989; Smalley et al, 1988; Erverdi et al, 1994). An additional limitation for the use of teeth as force abutments for expansion is that many patients with craniofacial anomalies have multiple congenitally missing teeth (Parr et al, 1997). A

typical narrow maxilla with apparatus, pre and post intervention is shown in Figure 1-2a,b.

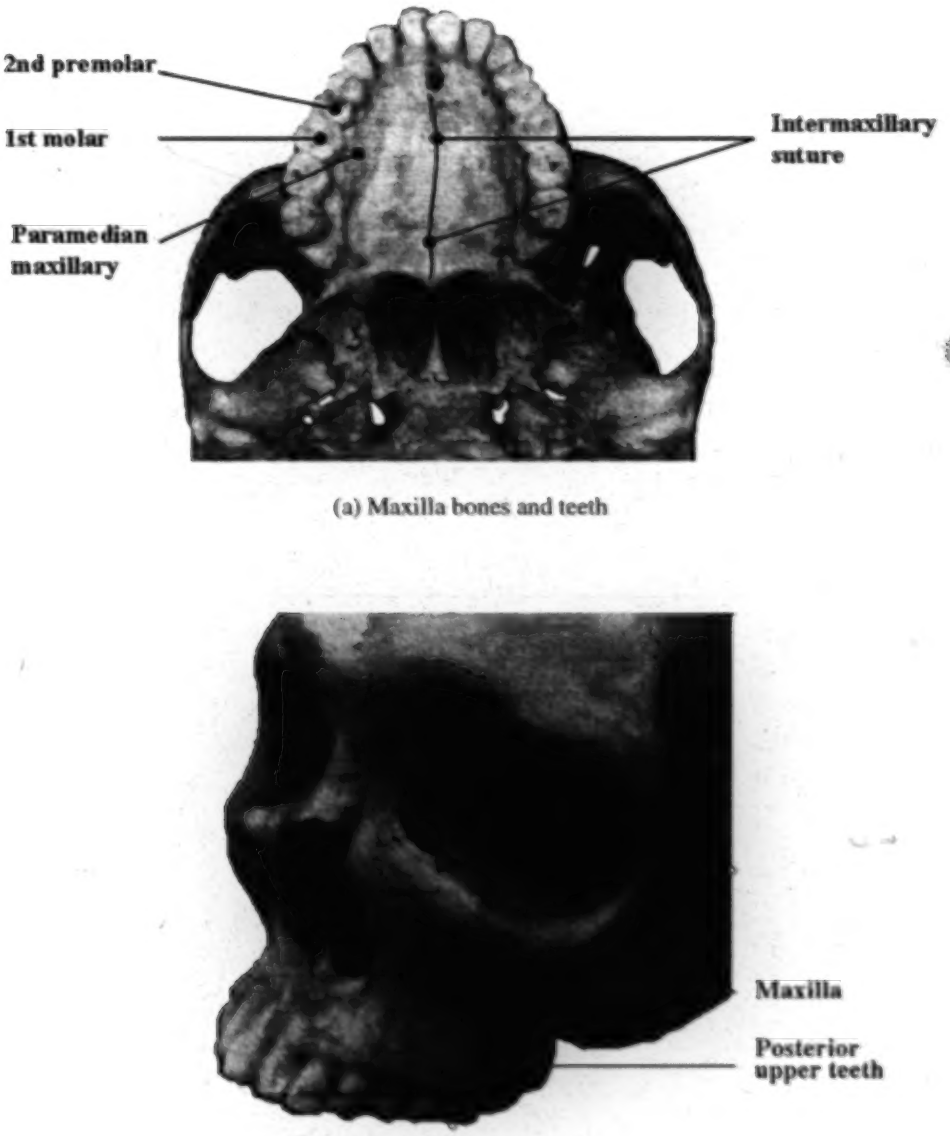

(a) Maxilla bones and teeth

(b) Maxilla and mandible

Figure 1-1: Anatomy figure for maxillary transverse deficiency

(a) Before treatment (b) After treatment

Figure 1-2: Conventional maxillary expansion treatments [Provided by Lagravère, 2006]

To overcome these drawbacks, a new ME treatment was recently developed (Harzer et al, 2004, Shapiro and Kokich, 1989). This treatment uses bone anchor (BA) instead of teeth as abutments to apply expansion load directly to the palatine process of the maxilla. During the early stage of the treatment, two bone anchors are inserted in each of the two halves of the maxilla (Figure 1-3a). One month after insertion, a bone-anchor osseointegration interface (BAOI) generates. The osseointegration interface is defined *"as the contact established without interposition of non-bone tissue between normal remodeled bone and a bone anchor entailing a sustained transfer and distribution of load from the implant to and within bone tissue"* (Roberts et al, 1984). Through the BAOI, BA is bonded with the surrounding bones. After BAOI formation, an expansion appliance, consisting of jackscrew and connectors (Figure 1-3b), is attached to the BA. The extension can be easily controlled by adjusting the activation

of the jackscrew. The expansion process is typically performed at a rate of 1/4mm every 2 days (Harzer et al, 2004). Typically, a total of 4mm unilateral transverse expansion is applied on each BA during clinical treatments (8mm total expansion).

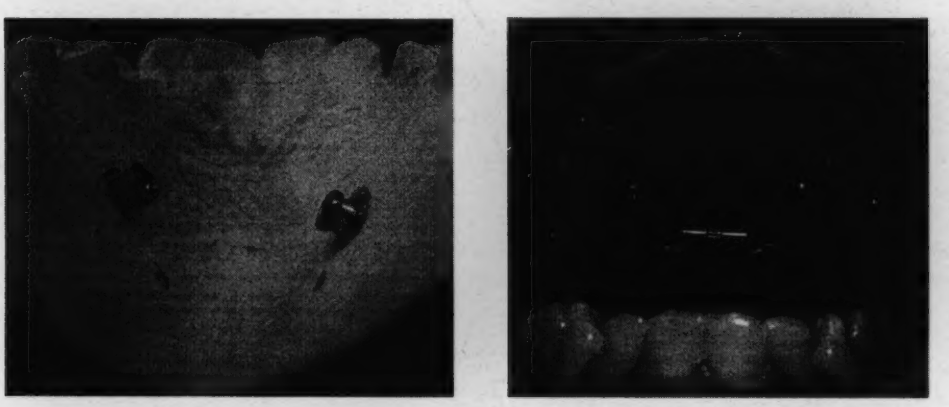

(a) (b)

Figure 1-3: Maxillary expansion treatment using bone anchors; (a) bone anchor placed in palatal bones; (b) maxillary expansion applied with jackscrew [Provided by Lagravère, 2006]

Following expansion force application to the bone anchors, craniofacial structures undergo a remodeling process related to the bone anchors load transmission. The imaging and understanding of the bone remodeling is critically important to orthodontists to deliver a satisfactory treatment. Rigid endosseous bone anchors are ideal orthodontic anchorages since they provide stable abutment for expansion load (Roberts et al, 1984 and 1989; Gray et al, 1983). The loss of stable abutment is related to the failure of osseointegrated bone anchors, which mainly results from an excessive load applied to bone anchors (Hoshaw et al, 1994; Duyck et al, 2001).

Craniofacial imaging has always been an integral part of orthodontic treatment. Cephalometric radiography (CR) and computed tomography (CT), Figure 1-4(a) and (b) respectively, are conventional imaging tools used by orthodontists for diagnostic purposes. CR technique only provides 2D images, and is subject to projection, landmark identification and measurement errors (Athanasiou et al, Major et al, 1994). Due to these limits, it could not be used to analyze force transmission from bone anchors to craniofacial structures, nor predict the remodeling of craniofacial structures, a possible fracture of craniofacial structures and failure of the endosseous BA.

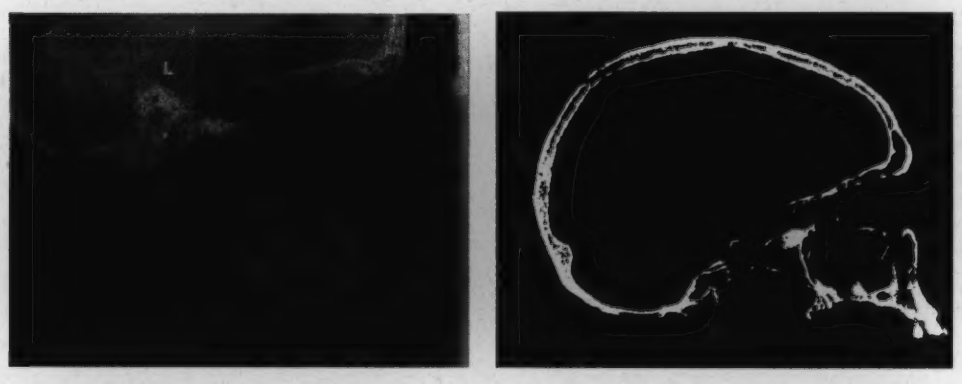

(a) Cephalometric radiography image (b) Computed tomography (CT) image

Figure 1-4: Conventional imaging methods [Provided by Russett, 2006]

1.2 Thesis Objectives

Finite element (FE) analysis is an effective tool to perform biomechanical studies for bony structures without using invasive procedures. It has been widely used to study the displacement, stress and strain responses of bony structures following external force or displacement load in clinic treatments for several decades [Pugh et al, 1973; Lavernia et al, 1981; Chang et al, 1993; Nuno et al, 2002]. The primary objective of the thesis was to develop a proof-of-concept three dimensional (3D) subject-specific FE model for the simulation and biomechanical studies of ME treatments using bone anchors (BA-ME).

A secondary objective of the thesis was to evaluate the validation of the proposed FE model by comparing predicted results with those obtained by performing simple experimental work, specifically a fresh skull ME, and with the available literature. The model will then be used to verify two hypotheses. First, that the number of elastic properties used in the model has an influence on the expansion treatment analysis (anatomical landmark displacement, von Mises stress and strain). Second, that bone anchor anchorage inclination angle must be set perpendicular to the bone surface to minimize local von Mises stresses and BAOI failure from offset loading and stress concentration.

This work was performed as a preliminary step towards the development of a patient-specific FE model for predicting maxillary expansion treatment. Using the approach

developed in this thesis, the FE analysis will hopefully provide more reliable predictions and analysis of maxillary expansion treatments than previous reported work.

1.3 Background Information

1.3.1 Anatomical Coordinate System Nomenclature

The coordinate system used in the current work is that which is defined for anatomical structures. The anatomical planes, as they relate to the skull are shown in Figure 1-5.

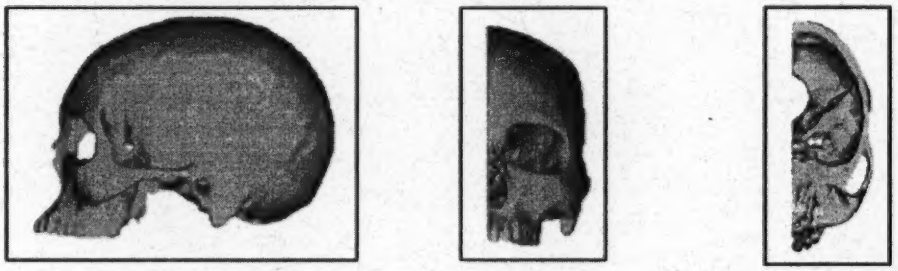

a. Sagittal Plane right view

b. Coronal plane front view

c. Transverse plane left view

Figure 1-5: Anatomical planes as related to skull

The sagittal plane divides the body in left to right sections; the coronal plane divides the body anterior/posterior sections (front/back); the transverse plane divides the body in superior/inferior sections.

Directional terms of interest are:

- Anterior direction: towards the front.
- Posterior direction: towards the back.

- Inferior direction: towards the feet.
- Superior direction: towards the head.
- Medial direction: towards the midline of the body. .
- Lateral direction: away from the midline of the body.

1.3.2 The Finite Element Method

Finite element (FE) analysis has been used extensively and the underlying theory has been discussed in numerous texts. FE analysis has been used in biomechanical studies for more than three decades. The basic principle of FE method is that by using a finite number of well-defined components (element) to represent an adequate model, the approximate solution to the continuum problem can be obtained by assembling the solution to individual components following properly defined approximation method. The general process of performing FE analysis of elastic structures can be briefly described as following:

1. Based on accuracy requirements and geometrical features of structures, choose appropriate element type and size to divide original continuum structures with finite number elements, which connect with common nodes;
2. Construct equations for forces acting at nodes and element stiffness matrix related to material properties;
3. Assemble stiffness matrix and force for the entire structure;
4. Apply boundary constraints and use defined equations to find displacement at every node;
5. Solve the stress and strain for every node and element.

It is clear that the accuracy of the solution of the composed continuum system is dependent on the accuracy of the model composed with finite number elements. The smaller elements result in better approximated solutions for the continuum systems. However, in the development of such models it will be explained in a later section that such issues as model geometry, elastic property definition, boundary conditions and loading are critical to the development of an accurate and representative model.

1.3.3 Imaging Techniques for FE Model Development

1.3.3.1 Computed Tomography Scanning Technique

To perform a reliable FE analysis for BA-ME treatments, it is crucial to develop a 3D FE skull model that is an accurate representation of the geometrical features of the structure and of the bone heterogeneous properties.

Various techniques have been used for constructing 3D FE models of bony structures, such as Magnetic resonance imaging (MRI), computed tomography scanning (CT scan), and ultrasound imaging techniques (UI) (Mehta et al, 1997).

Because CT scanning permits modeling of in vivo human bones, provides accurate information about bone geometry, and outputs digital data that can be used in conjunction with computer-aided design (CAD) and imaging processing programs, this technique has been broadly used in the modeling of bony structures (Ulrich et al,

1998; Cattaneo et al, 2001; Lim et al, 2002; Jaecques et al, 2004).

CT is a powerful evaluation technique for producing 2-D and 3-D cross-sectional images of an object from flat X-ray images. Characteristics of the internal structure of an object such as dimensions and density are readily available from CT images. When taking CT scan, scanned objects are placed on a turntable stage that is between a radiation source and an imaging system. The turntable and the imaging system are connected to a computer so that X-ray images collected can be correlated to the position of the scanned object. The imaging system produces a 2-D grayscale image of a specific slice of the object. Using specific computer software, a 3D model of the object can be produced using many slices. The grayscale of an image is of critical importance since it is a representation of the attenuation of the rays due to the objects in the scanner and thus the density of the objects.

1.3.3.2 Cone-beam Computed Tomography (CBCT) Scanning Technique

CBCT is a CT system that uses a cone-shaped x-ray beam with special image intensifiers and a solid-state sensor for capturing the image (Danforth et al, 2003). Since CBCT captures the entire volume with one scan, there is no redundant overlap of slices and results in major reduction of radiation. Such low intensity radiation is very practical in clinical studies/treatments.

1.3.3.3 Hounsfield Unit (HU)

CT measures and computes the spatial distribution of the tissue attenuation coefficient.

The computed attenuation coefficient is displayed as CT number, also referred to as Hounsfield units (HU), relative to the attenuation of water and air, where water is assigned a HU value of zero and air is assigned a HU value of -1000. Using spiral CT (GE ProSpeed helical scanner, General Electric, Slough UK), Norton and Gamble found that the bone density in the anterior mandible was bigger than +850 HU, posterior mandible/anterior maxilla was from +500 to +850 HU, posterior maxilla was 0 to +500 HU, and tuberosity region was smaller than 0 HU.

1.3.3.4 CT Imaging Processing Programs

Various programs have been developed and applied to build 3D FE models or solid models for bony structures based on CT image data. Table 1-1 shows these programs and an example of the studies for which they were used.

Table 1-1: Programs developed recently for the medical research

Name	Research field
Computer Assisted Tomography to Finite Element Modeling (CATFEM) (Finnigan et al, 1990)	FE model for metallic components, data obtained from CT images
ScanIP&FE (Simpleware Ltd, England) (Weber and Youngs, 2004)	FE Analysis of head response to impact
NIM Image (Coleman et al, 2000)	Construct a solid geometrical model of a long bone from CT image
MIMICS (Materialise, Belgium) & MSC.Patran (Gouda, The Netherland) (Jaecques et al, 2004)	Micro CT based FE models of guinea pigs with titanium implants

Since the CT image information including the soft tissue and bone tissue are represented by voxels with different gray values, the CT imaging processing program can detect, display and record the inner and outer borders of bony structure in each

cross section and therefore, segment the bone tissue from surrounding soft tissue. In addition, volumes of bones and 3D finite element meshes constructed by the CT imaging processing program can be transferred to FE programs.

To perform FE analysis for BA-ME treatments, a FE skull model with BA inserted in palatal bones was required to be developed. Since skulls are geometrically more complicated than most other bony structures and that bone heterogeneous properties were important for an accurate FE analysis, the optimal CT image processing program used in our studies was required to:

1. Automatically generate 3D finite element model which can be read by FEM program, ANSYS, with higher accuracy of model and less time cost.
2. Automatically convert the apparent bone density information to bone elastic constants and assign them to the meshed 3D finite element model.
3. Automatically generate FE models that could be easily edited using a CAD package or text editor.

The ScanIP&FE developed by Simpleware Ltd. (England) was used in this work because of its availability and because it met all the requirements. No other system was tested in our studies.

1.4 Thesis Outline

The thesis will have the following structure. A general introduction of the work was presented in Chapter 1. In Chapter 2 a thorough review of the relevant literature is provided. In Chapter 3 the proposed FE model of the skull and the process by which it was developed is detailed. The methods and results of the maxillary expansion experiments performed to verify the model are presented in Chapter 4. Chapter 5, 6 and 7 could be looked as a further evaluation or practical application of the developed FE model and of the approach developed in Chapter 3. In Chapter 5 the proposed FE model is used to simulate and predict the results of a clinically representative maxillary expansion treatment. The results of the FE analysis are presented and compared with those from literature and those from the experiments described in Chapter 3. The practical advantage and disadvantage of the approach applied are also discussed. The influences of bone elastic constants are examined in Chapter 6. In Chapter 7 a case study of the approach developed in current work is presented; the influence of the bone anchor anchorage inclination angle (AIA) is presented and an optimal AIA which could reduce the failure rate of endosseous BA is suggested. A general discussion and conclusions are given in Chapter 8.

CHAPTER 2 LITERATURE REVIEW

2.1 Introduction

FE method was first applied in biomechanical studies for orthodontic treatments in 1989 by Tanne et al, since then, FE analysis has been extensively applied in similar studies. In this chapter previous studies that focus on the approaches they applied to develop models for FE studies of maxillary expansion are presented. Furthermore, studies discussing the impact of bone Elastic Properties (EP) on FE analysis of maxillary expansion are also reviewed. Finally, since in the latest ME treatments, maxillary expansion loads are applied on bone anchors, the stress distribution in the bone anchor osseointegrated interface are also important to predict the possible interface failure. Therefore, previous studies that focused on the considerations for successful orthodontic implantation are discussed.

2.2 Development of FE Models for ME Treatments

To perform a reliable FE analysis for BA-ME treatments, it is imperative that developed FE models accurately represent skull geometric features and heterogeneous distribution of bone properties. Since traditional CT imaging provides high resolution digital image data which includes pixel spacing information and corresponding individual Hounsfield Units (HU) value for said pixels, recent studies have used CT image data to develop three dimensional FE models for biomechanical studies of conventional rapid expansion treatments.

In studies on the effect of rapid maxillary expansion on the craniofacial structures by Iseri et al (1998), Jafari et al (2003) and Provatidis et al (2003a,b) , 3D FE models were built by segmenting greyscale contour of pixels representing bone structures and generating appropriate points and lines on individual CT slices. By connecting the corresponding points and lines on successive CT slices, 3D surface and eventually 3D solid models that represent bone structures were built and converted to 3D FE models with specific CAD & FE packages.

Another approach was used in the 2005 study by Holberg. They generated a point cloud representing bone structure surfaces based on CT image data of a skull. Using an optimization process, appropriate points were linked, followed by the generation and conversion of polygonal meshes to build a sphenoid[i] FE model.

In these earlier studies, only three bone elastic properties were used for developed FE models, namely for cortical bone, cancellous bone and teeth, respectively. Properties were assigned based on bone location using average values found in the literature. This is not representative of the heterogeneous distribution of bone properties for specific subjects; this will be discussed in the next section.

---

[i] Sinus cavity behind nose

Weber and Young (2004) used another approach to develop a 3D FE model of a dry cadaveric femur. In their approach, the FE model was developed by directly converting CT image pixels/voxels representing bone structures into FE elements. This approach provides an automatic method to eventually develop FE models representing subject-specific geometrical features and includes property heterogeneity of bone structures.

2.3 Effect of Bone Elastic Properties

The assignment, range and number of elastic properties (EP), such as elastic modulus (E), shear modulus (G) and major Poisson's ratio (ν), used in FE modeling has long been seen as a critical issue to obtaining accurate predictions (Strait et al, 2005). Several studies have evaluated the reliability of FE analyses of biological system by evaluating the effect of EP (Cattaneo et all, 2001; Strait et al, 2005). Bone is an anisotropic material and has different mechanical behaviors in radial, circumferential and superior-inferior directions (Rho et al. 1995). It has been shown that bone EP and directionality, especially for craniofacial structures, are bone shape and density dependent (Peterson and Dechow, 2003). Craniofacial structure EP are usually orthotropic but are typically modeled as isotropic (Strait et al. 2005). Models that have ventured in more complex material assignment were not geometrically complex (Strait et al, 2005; Chen and Chen, 1998; Coleman et al, 2002) but showed that the assignment of EP has an effect on the response of displacement, Von Mises stress and strain distribution of studied bone structures.

Recently, work by Cattaneo et al (2001) was devoted to the development of subject-specific FE models as tools to predict treatment outcome as well as local stress and strains. They found that accurate results can only be achieved using accurate input information. The large variability of biological structure EP has also limited their applicability (Cattaneo et al, 2001). Anthropometric EP data presents large standard deviations that could be linked to age, disease, sex and ethnicity of studied subjects as well as bone type under consideration (Rho and Hobatho, 1995).

As mentioned earlier, FE models used in previous studies of ME treatments were developed based on Computed Tomography (CT) image data and often limited to defining and assigning no more than three average EP (cortical bone, cancellous bone and teeth), obtained from the literature (Iseri et al, 1998; Jafari et al, 2003; Provatidis et al, 2003a,b; Holberg et al, 2005). These models lack the heterogeneous aspect of bone density distribution and could not be deemed to be accurate representations of the bone structure and EP distribution.

2.4 Effect of Implant Anchorage Inclination Angles

The use of implants or bone anchors in orthodontics was first published around 1945. Early reports usually presented unfavorable outcomes (Shapiro and Kokich, 1989). Branemark reported firm anchorage of titanium implants to bone with no adverse effects in rabbits (Branemark et al, 1964) and that titanium implants remained stable for periods of more than 5 years without signs of tissue injury or rejection, even when

excessively loaded (Branemark et al, 1969). This condition, described as osseointegration, implies the direct contact and firm bond of living bone to implant, which remains stable, even under significant loads, and will not shift as teeth do under constant orthodontic forces (Movassaghi et al, 1995).

Since these earlier studies, the use of BA as force abutments instead of teeth in order to apply the expansion load directly on to the palatal bones has become more prevalent (Harzer et al, 2004, Shapiro and Kokich, 1989). Various studies (Roberts et al, 1984 and 1989; Gray et al, 1983; Branemark et al, 1970, 1975 and 1977; Breine et al, 1980, Hansson et al, 1983) analyzed the use of implants in the reconstruction of human mandibles and as abutments to support fixed and removable dental prostheses and showed them to be highly successful. Factors that contributed to this success were the nature of the implant material (titanium), the technique of insertion, and the loading technique applied.

BAOI failure is always a concern. Following expansion force application to the BA, large stresses are induced in the Bone Anchor Osseointegrated Interface (BAOI). Loss of stable abutment can occur due to the failure of osseointegrated bone anchors, which mainly results from an excessive load applied to bone anchors (Bernhart et al, 2001; Schiel et al, 2003). Buser et al (1999) found, depending on surface morphology, that implant removal torque ranged 0.13 to 1.56 Nm. Reddi et al (1987) estimated a failure strain threshold of about 100-150 μm. Watanabe et al (2003) using a Finite

Element (FE) model found that minimum stress distributions in the bone-implant osseointegration interface were found when load and implant were aligned perpendicular to bone surface. However, the FE models used in previous studies only included rigidly fixed bone structures surrounding the implant. It was an unrealistic representation of maxillary expansion and was limited in scope and applicability. Their models and results of FE analysis for implantation conditions could not have been used in this work.

2.5 Conclusions

This chapter reviewed the approaches used in previous studies for developing FE models for biomechanical studies of maxillary expansion treatments as well as other orthodontic treatments. Following the development of FE models, an important issue related to the reliability of the FE models was presented by introducing previous studies on the effect of EP on the FE analysis. Clearly questions remain regarding FE model EP.

Another important clinical consideration, the conditions for successful orthodontic implantation was reviewed and an optimal Anchorage Inclination Angles (AIA) of implant and load condition from previous study was presented. Their application and validation were restricted due to the limitations of the FE models used. From the literature review, some fundamental questions relating to the FE analysis of ME using BA have been introduced and will be addressed further in this thesis.

Based on the above literature survey, the FE skull model that will be developed for predicting maxillary expansion treatment outcomes will be based on information obtained by converting CT image date and represent bone heterogeneity. The development of the model is presented in the next Chapter.

CHAPTER 3 DEVELOPMENT OF A SKULL FINITE ELEMENT MODEL

3.1 Introduction

In this chapter, a finite element model of a dry skull is developed to predict the outcome of maxillary expansion treatments. In the following sections, the approach used to develop the geometric model and assigning elastic properties will be discussed. It was previously mentioned that CT image data provides digital pixel spacing information and corresponding HU value for every individual pixel. CT image processing programs use this information to construct 3D solid models of bony structures. As early as 1998, Ulrich et al presented an approach to generate such solid models based on CT image data. Compared with the pixels of soft tissues or air, those of bone on 2D CT slices have higher greyscale/HU values. By scanning and identifying pixels with HU values greater than a specified threshold, for example, 600 HU shown in Figure 3-1a, this approach segments the pixels representing bone tissues and eliminates the others (4 corners of Figure 3-1a). Using the remaining pixels, the 3D voxels with thickness equal to the slice distance can be built based on every 2D CT slice (Figure 3-1b). Once the voxels representing bone tissues are built for every CT slice, a 3D solid model of the entire scanned bony structures is constructed.

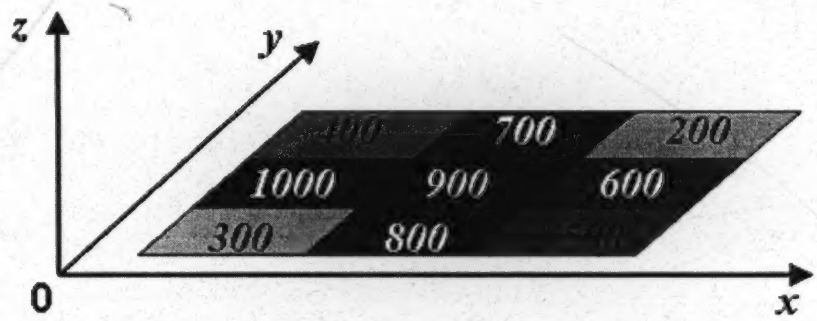

(a) 2D pixels with different HU value

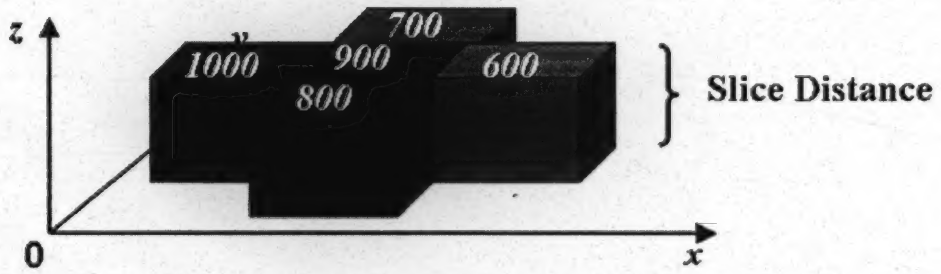

(b) Segmented 3D voxels of bone tissues

Figure 3-1: Schematic of the imaging process to build bone solid model based on CT image data

It has been reported that HU value can be correlated with apparent density of bone tissues using linear regression equations (Rho and Hobatho, 1995). Moreover, experimental equations have been established to define the relationship between apparent density and mechanical properties of bone tissues (Rice et al, 1995; Rho and Hobatho, 1995; Currey et al, 1988; Snyder et al, 1991; Schaffler et al, 1988). Equations depend on the type of bone, bone location and loading, subject age, gender

and race. These empirical relationships can be used to define the elastic properties based on the HU value of pixels. The FE model is then developed by directly converting the voxels into elements with associated elastic properties obtained from the HU value of the original pixels. This approach has been used successfully with ScanIP&FE™ (Simpleware Ltd., England) to build subject-specific 3D FE models of a dry cadaveric femur and a trachea implant by Weber and Young in 2004.

Due to its practical advantage, the same approach will be applied in this work. CBCT scan image data of a dry skull will be used to develop a 3D FE model for the purpose of performing biomechanical studies of ME-BA treatments. An additional advantage of CBCT images is that they are already in voxel form. The objectives of this model are to accurately represent geometric features and bone heterogeneity properties of the skull.

3.2 Materials and Methods

3.2.1 CBCT Data Acquisition

A dry skull shown in Figure 3-2a, excluding the mandible was scanned using a low radiation dosage scanner, CBCT (NewTom 3G, Aperio, Italy, Figure 3-3) scanner as the physical subject of the finite element model. This apparatus was also used since its low radiation dosage makes it possible to eventually perform an in vivo study. Images were collected at every 1mm interval in the transverse plan and converted into DICOM format with pixel spacing size of 1.06mm×1.06mm with 1mm slice thickness.

A CBCT image slice is presented in Figure 3-2b. The dark areas outline the bone structure.

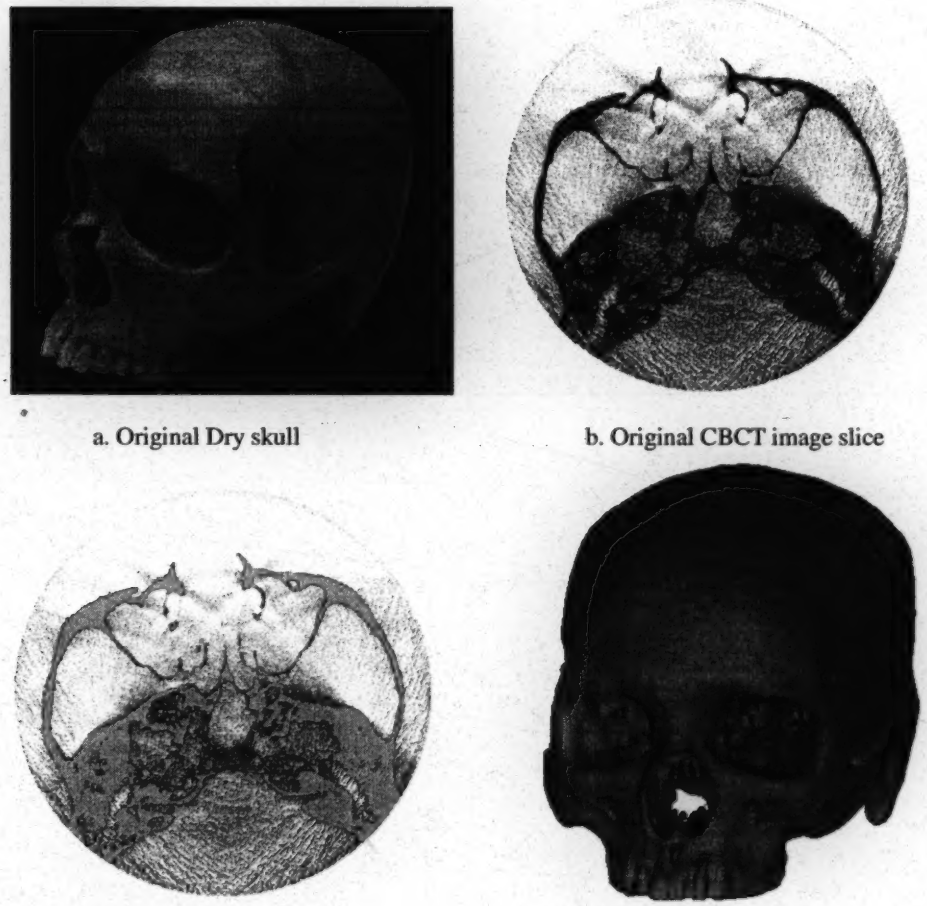

a. Original Dry skull

b. Original CBCT image slice

c. Segmented CBCT image slice

d. Solid model

Figure 3-2: Schematic of the imaging process to develop a 3D solid model of a skull using CBCT data

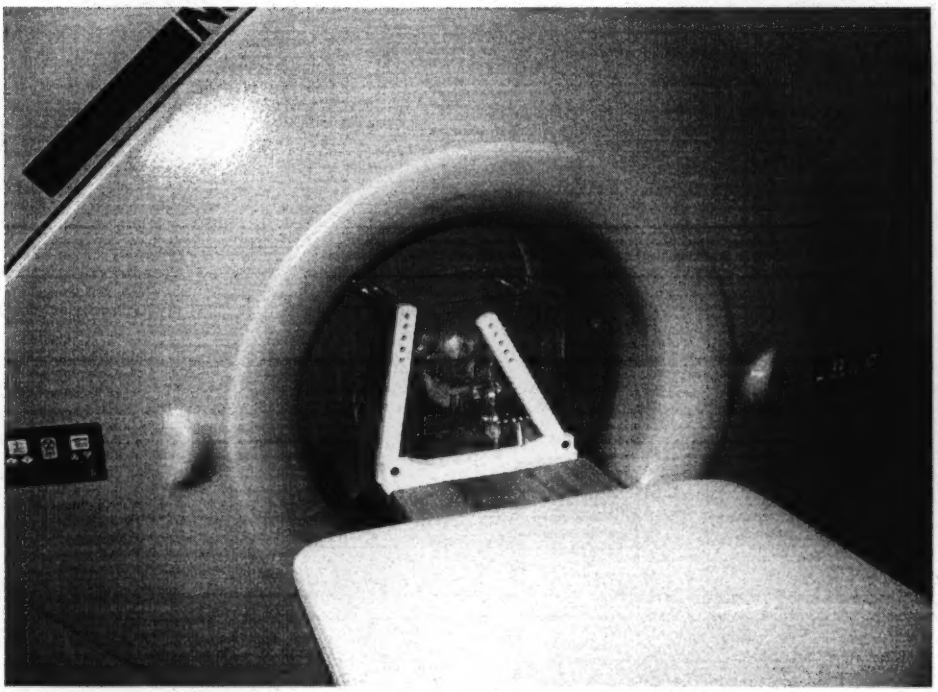

Figure 3-3: Newtom CBCT machine (Department of Graduate Orthodontics, University of Alberta)

3.2.2 Segmenting and Generating Bone Structures

CBCT image data is imported into ScanIP&FE™ (Simpleware Ltd., England) to perform a mostly automated segmentation of the skull with the later use of ScanFE™ to build skull FE models. Figure 3-2 illustrates the process involved in building a 3D solid model of a skull using CBCT data from a dry skull to the solid model. By setting a HU threshold, with which the density is defined bigger than that of surrounding air (i.e. density > 0), the pixels which represent bone structures in Figure 3-2b were segmented in every slice. The segmentation process defines the blue area seen in Figure 3-2c. Based on the 2D coordinates of segmented pixels, voxels representing

bone structures are built. Finally, a smoothed 3D solid skull model is built (Figure 3-2d.

To reduce model complexity, it was assumed reasonable to consider the skull as a perfectly symmetric structure along the sagittal plane, thus only half a skull was built into an FE model. Although human skulls are not perfectly symmetric structures, anatomical differences on both hemispheres are insignificant from an engineering view point and of no consequence for proof-of-concept work.

3.2.3 Assigning Elastic Constants

To assign properties to different regions of bone structure, relationships between HU values and apparent density, and between apparent density and elastic constants are required for cancellous and cortical bone. Contrary to models that use teeth as abutment, teeth EP were not considered in this model since they play no part in the expansion process. A CBCT scanner specific relationship between HU and apparent density was required. An experiment using 5 material specimens known to have densities spanning the required range to envelop the array of bone densities present in the skull was performed using the NewTom QR-DVT 9000 Volume Scanner to obtain the coefficients of a representative linear regression equation between HU and apparent material density (Lagravère et al, 2005). An equation was obtained and used to compute the bone apparent density (ρ in kg/m^3) by converting HU of pixels such that:

$$\rho = 2HU - 362 \qquad R = 0.986 \qquad \textbf{(3-1).}$$

The standard error on the Hounsfield units and the density are 27.104HU and 64 kg/m^3. Rho and Hobatho (1995) reported regression-based equations relating elastic modulus (E in MPa) and bone apparent density (ρ in kg/m^3) for cancellous (Eq. 3.2) and cortical (Eq. 3.3) bones, respectively; as such, this experimental undertaking was not performed in this work. Furthermore, variability in the data found in the literature clearly shows that the error to be expected from new experimental data and that found in the work of others, even for different bones, would not improve the model significantly to currently justify the undertaking.

$$E = 0.82\rho^{1.27} \ (R^2 = 0.54) \qquad \rho < 1958 kg/m^3 \qquad \textbf{(3-2)}$$

$$E = 13\rho - 13050 \ (R^2 = 0.95) \qquad \rho \geq 1958 kg/m^3 \qquad \textbf{(3-3)}$$

Equation 3.2 was obtained from mandible cancellous bone specimens, whose properties are assumed similar to maxillary cancellous bone. Equation 3.3 was obtained from distal femur specimens and selected because of high R^2 value. Clearly, using femur bone can lead to error due to the expected strength difference from the typical bone loading. Figure 3-4 shows the elastic modulus as a function of cancellous and cortical bone densities.

Variability of human bone properties due to age, gender and specific bone make it unfeasible to determine an exact density values which can be used to identify cancellous and cortical bones or a threshold between both. Work is underway to define proper cancellous-cortical HU thresholds (Au et al, 2006). To simplify this issue, the intersection point of both curves was used as cancellous-cortical threshold. Densities less than 1958 kg/m^3 were defined as cancellous bone, while densities greater or equal to 1958 kg/m^3 as cortical bone. Again, this simplification is acceptable for this proof of concept model and provides a reasonable range of EP for defining bone heterogeneity. Elastic moduli were automatically assigned to model elements with the ScanIP/FE™ package. To allow for a maximum of bone heterogeneity, 156 total linear elastic bone material properties were defined using various thresholds in the FE model; these are summarized in Table 3-1. The sensitivity of the model to material properties and convergence of the results are presented in Chapter 6.

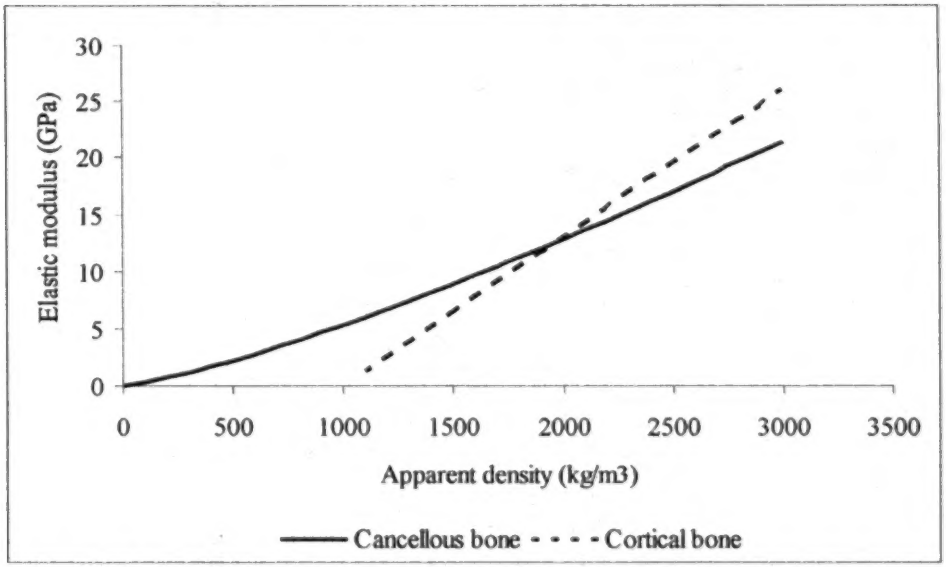

Figure 3-4: Elastic modulus (GPa) versus bone apparent density (kg/m^3)

Table 3-1: Material properties for bones, titanium bone anchor and BAOI

	Number of assigned materials properties	Average Elastic Modulus (MPa)	Minimum Elastic Modulus (MPa)	Maximum Elastic Modulus (MPa)	Poisson's Ratio
Cancellous bone	125	1800	41.56	12509	0.3
Cortical bone	31	15400	12742	18644	0.3
Titanium	1	116000	NA	NA	0.34
BAOI	1	2400	NA	NA	0.3

3.2.4 Dry Skull Finite Element Model

From importing CBCT data to final FE model, the entire imaging process is automated by using the ScanIP/FE™ package with the exception that some noise must be identified and manually deleted. The full process is detailed in section 3.2.2. Through this imaging process, a geometrically accurate 3D FE model of a dry skull with heterogeneous EP distribution was developed and is presented in three

engineering views in Figure 3-5. Since the grid of pixels in every CBCT slice were used to construct the elements as shown in Figure 3-1, the 1.06mm×1.06mm×1mm hexahedral elements were generated, where the 1mm thickness is equal to the slice distance of CBCT image data. Moreover, since smooth surfaces were applied, the tetrahedral elements were generated with the Simpleware smoothing algorithm along the skull inner and outer surfaces. This FE model includes 297,800 nodes and 877,400 hexahedra and tetrahedral elements.

(a) Right view

(b) Front view (c) Left view

Figure 3-5: 3D subject-specific finite element model of skull

3.2.5 Bone Anchor Model

Bone anchors should be placed in the palatine process of the maxilla between 2nd premolar and 1st permanent molar teeth, where support bone is typically strong and plentiful (Bernhart et al, 2000). As shown in Figure 3-6 a,b, representing coronal plane cuts of the skull, using this configuration, long axis of bone anchors would be optimally set perpendicular to palatal bone surface such that bone anchors would avoid teeth roots. Based on the above considerations, a 3mm diameter cylindrical bone anchor was modeled and included in FE skull model (Figure 3-7). It is necessary to mention that bone anchors could not be perfectly bonded in clinical situations; however, for simplicity and due to a lack of available literature based experimental results for specific values on BAOI properties, bone anchor osseointegration interface (BAOI) was defined as perfectly bonded along the 4mm length and at the tip of the bone anchor. Solid tetrahedral elements were selected for bone anchor and BAOI. Functional osseointegrated bone anchors demonstrate interfacial bone density similar to that of the bone in which the bone anchor was placed (Albrektsson et al, 2001), which is mainly cancellous bone. An average of the heterogeneous elastic modulus of surrounding elements was used to define BAOI property as:

$$E_{BAOI} = \frac{\sum_{i=1}^{n} E_i}{n} \qquad (3\text{-}4)$$

where E_{BAOI} is the elastic modulus of BAOI, E_i is the elastic modulus of surrounding

element i, where i = 1, ...n and, n is the total number of surrounding elements. The elastic modulus and major Poisson's ratio of the implant and BAOI are given in Table 3-1. To model the perfectly bonded BAOI and BA, solid models converted from the elements representing BAOI and BA were automatically meshed by ANSYS, where the nodes on the cylinder surface were defined as common nodes shared with BAOI.

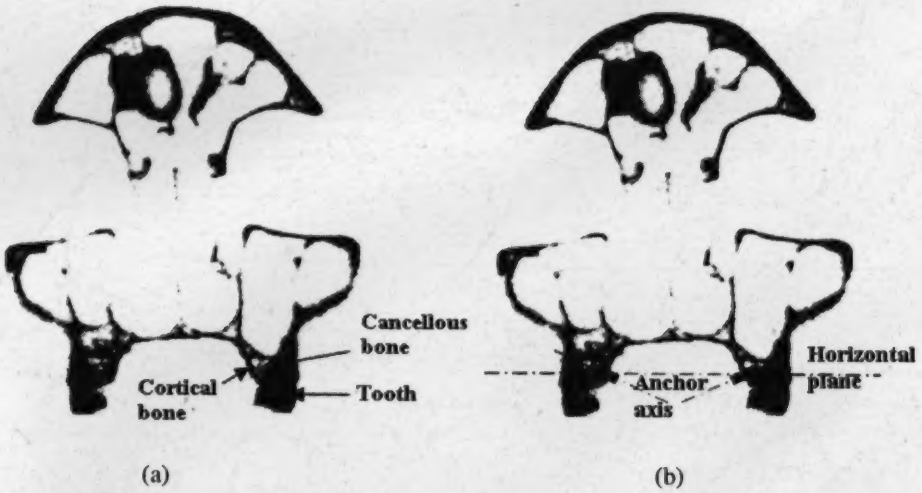

Figure 3-6: Bone anchor position and full model. a) CT image before placing bone anchor; b) CT image after placing bone anchor

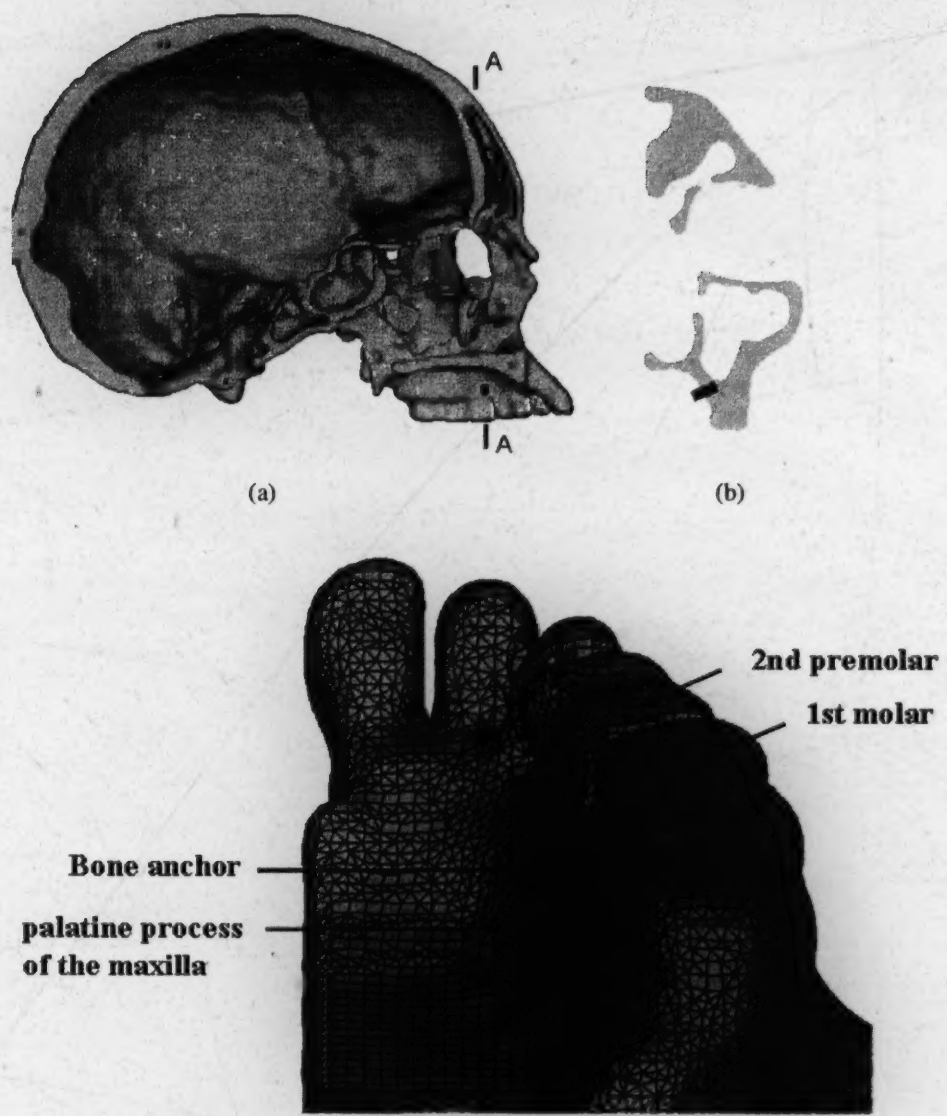

Figure 3-7: FE model with inserted bone anchor. a) Transverse view of FE model with bone anchor; b) cross section view A-A (Sagittal view); and c) a zoom in view

3.3 Discussion and Conclusion

In this Chapter, a finite element model of a dry skull was developed as a first step to the development of a subject-specific treatment prediction tool for orthodontic clinicians. Using individual CBCT image generated voxels to build a skull FE model leads to the automatic assignment of elastic properties based on the HU of individual pixels. However, since skulls are very complicated structures, whose bone thickness varies and shape changes abruptly, the voxels do not always accurately represent skull geometry, especially at the skull inner and outer surface. ScanIP automatically smoothes the edge of models and avoids additional distortion of the models. However, the mesh smoothing process could add or remove some quantity of bone. This imaging resolution problem can be minimized using a high quality CT/CBCT image scanner. This makes the 3D finite element models more geometrically accurate than previous models and its production is less time consuming than previous methods.

One of the differences as compared with previous models is that the current FE model only includes half a skull while others included the whole or most skull structures; the skull was never previously separated along a sagittal plane. However, by setting appropriate boundary conditions, the half skull FE model should be as accurate as other models.

Another difference is that a cylinder-type bone anchor was modeled and implanted at a real clinical situation with a perfect 4mm bonded BAOI effective length. This model

provides more complete simulation conditions and can be used to perform the FE analysis for biomechanical responses of both craniofacial structures and BAOI. Previous FE models can only be used to study the overall biomechanical response of the craniofacial structures.

The FE models used by Tanne et al (1990) included 2918 nodes and 1776 solid elements; that used by Iseri et al (1998) included 2147 nodes and 2349 quadrilateral and triangular thick shell elements; that used by Provatidis et al (2003a,b) included 5288 nodes and 5697 elements; Jafari et al (2003) included 7357 nodes and 6951 elements. Compared with the FE models used in these previous studies, the current FE model has much smaller but many more elements (300,000 nodes, 878,000 hexahedral and tetrahedral elements) and considers only half skull. Since human skulls are complicated geometrical structures, the current FE model could lead to more reliable/accurate FE analysis for ME treatments than most previous studies based on its element specificity (Zienkiewicz et al, 2000). Although small element size is essential to build a reliable FE model of skull, small element size could lead to a massive number of nodes and elements. However, with the introduction of newer and faster computers, element size is no longer a limiting factor.

Besides representing more accurate geometrical features, the presented model provides heterogeneous bone properties by assigning 156 elastic properties into the model based on the HU distribution of CBCT image data. Based on previous studies,

the EP has significant effect on the FE analysis. This kind of effect will be investigated and illustrated further in Chapter 5 and 6. The objectives of this preliminary work were to have geometric representation of the anatomical features which exceed current models in the literature; to select an approach for assigning materials properties to the FE model elements which was representative of the heterogeneity of bone; and to include a titanium bone anchor model to which maxillary expansion treatment loads will be applied. The development of the model appears successful. In Chapter 5 to Chapter 7, the model will be used to predict preliminary ME treatments, to evaluate the effect of elastic property assignment and to determine optimal bone anchor inclination angle and position.

The open literature does not contain results from maxillary expansion treatment experimental studies. To further verify the proposed model, fresh skull maxillary expansion experiments were devised, the results of which are presented in the following chapter.

CHAPTER 4 FRESH SKULL EXPERIMENTAL STUDY OF MAXILLARY EXPANSION TREATMENT

4.1 Introduction

Strain measurements have been widely used for *in vivo* analysis in dental and orthodontic studies (Thomason et al, 2001; Yacoub et al, 1999; Hekimoglu et al, 2004; Brosh et al, 1998). In these studies, the strains measured were used to examine the influence of external load applied to dental implants or to investigate the change of load applied by expansion appliance for maxillary expansion (Brosh et al, 1998).

Furthermore, strain measurements have also been used to verify anatomical FE models (Gupta et al, 2004 Barker et al, 2005). In the current studies, a FE model of a skull was built, but due to the absence of experimental literature, strain measurement experiments are the most reasonable approach for verifying the proposed FE model predictions. Results may only present approximate trends because of the obvious differences between the experimental and modeled situations – these will be discussed in a following section. However, strain measurements cannot be performed on live subjects during maxillary expansion, therefore this was deemed the most appropriate approach.

The dry skull scanned to provide CBCT image data in Chapter 3 can not be used for strain measurement experiment, since bones of dry skulls are brittle, which could be broken even under small expansion condition. Strain measurements also cannot be

performed on live subjects during maxillary expansion. In this work a ME treatment will be performed on fresh skulls in an attempt to verify the FE model. Since the bone structures and properties of the fresh skulls are different from those of the dry skull, the experiments were performed as a concept proof for the developed subject-specific FE model. Due to the above reasons, only the strain distribution pattern or trend from the experiments will be used to compare with that from FE analysis for ME-BA treatments. Another objective of the experiment is to provide pilot experiments for clinical maxillary expansion treatments using bone anchor being conducted at the University of Alberta Orthodontic clinic. Strains will be measured at 3 craniofacial suture positions and will be compared in Chapter 5 to model treatment predictions.

4.2 Materials and Methods

Fresh skull experiments were designed to verify model trends during maxillary expansion treatment. Ethics approval was obtained from the Health Research and Ethics Board for this experimental work [[ii]]. Strains gauges used were type CEA-13-062WT-350 (Vishay Micro-measurements). Position and configuration of strain gauges are shown in Figure 4-1(a) and (b). Six (6) strain gages were used in three 0°-90° configuration on fresh skulls. Gauges were placed on orthodontist interested craniofacial sutures, named nasomaxillary (position 1), zygomaticomaxillary (position

---

[ii] Major, P.W., Maxillary expansion with an implant bone borne appliance; and in vitro skull pilot study, HREB file number B-240704, approved July 2005

2) and pterygomaxillary (position 3) suture respectively with one axis along and one axis perpendicular to suture path. Experiments were done on four skulls of 50 to 60 year old male donors; only two experiments are presented in this Chapter.

The skulls were first dissected to leave only bone. The temperature of lab was kept within 24-25°C. The water content of fresh skulls was assumed to be stable under the experiment environment. After trial experiments to assess its tissue bonding capabilities, M-Bond 200 adhesive (Vishay, micro-measurements) was used to bond the strain gauges to the skull surface. Adhesives appeared to rigidly bond gauges to bone, limiting possible relative motion at the interface. A uniaxial strain gauge was also placed on each arm of the expander appliance. Expansions were done in 0.5mm increments up to 8mm (4mm per side). Analogue signals from the strain gauges were filtered and multiplied using HP/Agilent multimeter and multiplexer modules. A Labview™ (National Instrument, USA) virtual instrument that controlled and recorded strain measurements via a GPIB interface (National Instrument, USA) was developed. Expansion was performed by the instrument shown in Figure 4-1(c).

The first experiment incrementally expanded the skull to 8mm full expansion, using 0.5mm increments. Increments were performed every 10 minutes to verify if any creep occurred in such a short time period. Strain readings were continuously recorded.

The second experiment, performed on a different skull, proceeded to a full 8mm expansion in a single process. Readings were collected over 46 hours to determine the effect of time on the readings. For both experiments, osteotomy of the palate was performed as is clinically done on adult patients prior to ME treatment.

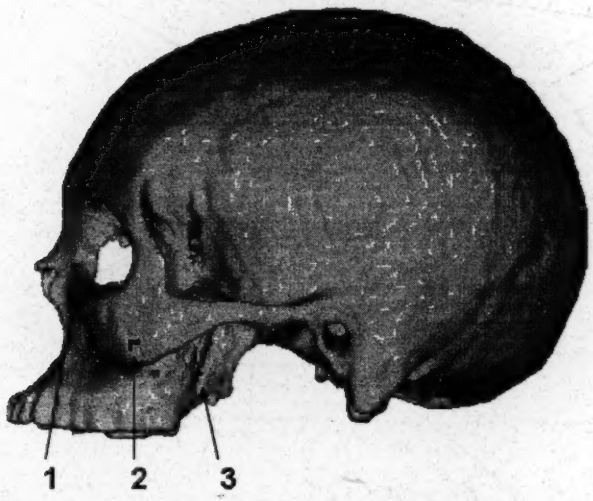

(a)

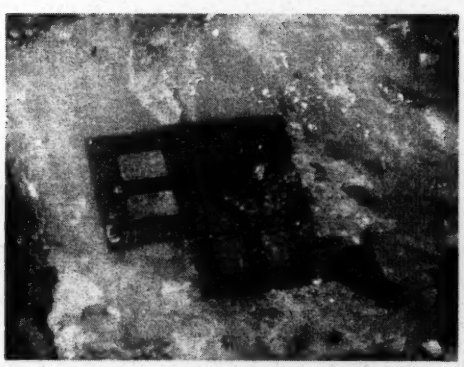

(b)

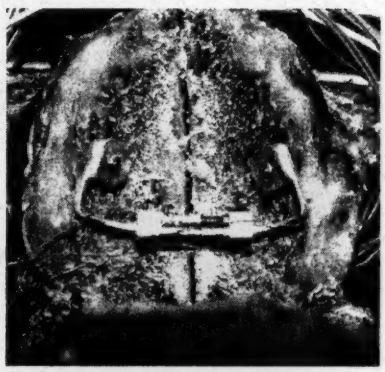

(c)

Figure 4-1: Maxillary expansion experiment on fresh skull; (a) strain gauge positions, (b) strain gauge configuration, and (c) expander in fresh skull (strain gauge shown)

4.3 Results and Discussion

These experimental procedures have sources of errors that cannot be discounted when comparing with FE predictions. It is recognized that subject facial features, age, bone elastic properties, possible illness could largely affect results. Bones of dry skulls, from which the FE model is developed, are brittle and the density may vary significantly from that of fresh or live bone. Furthermore, the glue may affect the bone; it could permeate or harden it as well as degrade it. Also, for the sake of comparison, a two strain gauge rosette cannot provide a complete stress state. Bonding of three gauges was made difficult by the wet skull uneven surface and gauge warping could have effects on the results. However, the results should still provide some general information and basis of comparison.

Some of the strain results from the first experimental procedure are given in Figure 4-2 for the nasomaxillary, zygomaticomaxillary and pterygomaxillary sutures. Positive and negative values indicate tensile and compressive strains, respectively. The results show tensile strains along the nasomaxillary suture (25με) after 2.25mm of expansion and a continuously increasing compressive strain (-135με) perpendicular to the suture. The zygomaticomaxillary suture shows compressive strains peaking at approximately -100με.

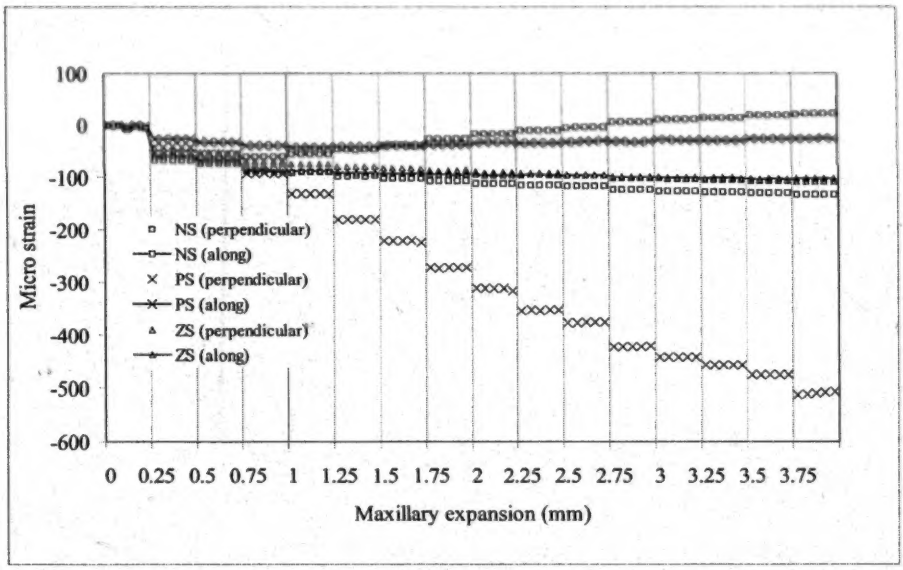

Figure 4-2: Micro strains (με) at three sutures in terms of unilateral maxillary expansion (mm), NS: Nasomaxillary Suture; PS: Pterygomaxillary Suture; ZS: Zygomaticomaxillary Suture

The results of the second experiment (Table 4-1) show the strain at time zero and the strains after 46 hours. The measured strain indicated that the strain on sutures of fresh skull induced by expansion treatment changed after 48 hours. This change could be due to liquids flow inside the bones due to the local compaction at the bone anchor. Strain levels did settle and an actual bone expansion was visible. Strains in the expander arms decreased with time by approximately 2%. Because of space limitations, only one strain gauge was placed on each arm of the expander. It is recognized that there is no compensation for any bending or temperature strain. On the other hand, the strains at the sutures increased significantly over the 46 hour period, with a near leveling off after 40 hours. A final plateau was not reached, but it can be assumed that because of the viscoelastic nature of the sutures, it is likely that

strains would ever stop increasing until they failed.

Table 4-1: Micro strains (με) at three sutures in terms of unilateral maxillary expansion (mm), NS: Nasomaxillary Suture; PS: Pterygomaxillary Suture; ZS: Zygomaticomaxillary Suture

	Strain			
	8mm expansion (0 hour)	8mm expansion (After 46 hours)	Equivalent Strain	Strain change (%)
Expander (Left)	+8319	+8132	NA	-2.25%
Expander (Right)	+5174	+5063	NA	-2.1%
Pterygomaxillary suture (Perpendicular)	-455	-5035		+1006.6%
Pterygomaxillary suture (Along)	-609	-4147	6523	+581%
Zygomaticomaxillary suture (Perpendicular)	-108	-917		+749%
Zygomaticomaxillary suture (Along)	-284	-1298	1589	+357%
Nasomaxillary suture (Perpendicular)	-284	-2828		+895.8%
Nasomaxillary suture (Along)	-664	-6211	6825	+835.4%

Large strain discrepancies were observed at the three craniofacial suture positions from both experiments. Compared the strain induced in the three positions, both strain in nasomaxillary and pterygomaxillary sutures were much larger than that in zygomaticomaxillary suture. Osteotomy of the palate performed before expansion directly resulted in large deformations in nasomaxillary regions. The discrepancies between strain data indicate that maxillary expansion has a greater effect in the pterygomaxillary and nasomaxillary bones than in the zygomaticomaxillary bones. The results concur with the reported pain experienced by patients of the procedure. The pain experience is symptomatic of high strain regions.

The strain data obtained in the second experiment also indicated that the strain

induced in the three sutures have different behaviours. In the nasomaxillary and zygomaticomaxillary sutures, the induced strain perpendicular to the suture path is larger (120% and 40% respectively) than that along to the suture path, while in the pterygomaxillary suture, the strain perpendicular to the suture path is smaller than that along to suture path.

4.4 Conclusions

Experimental work with fresh skulls does not always provide accurate results; this should be expected since fresh but dead tissue will not react as a live tissue. However, the measured strain data could help clinicians to understand the influence of expansion treatments on craniofacial sutures and predict possible failure/damage on these sutures following the maxillary expansion treatments.

The strain data obtained in the second experiment (Table 4-1) will be used to compare with those from FA analysis in Chapter 5, where the FE model developed in Chapter 3 will be used simulate a maxillary expansion using bone anchor. This will be done to obtain preliminary information as to the adequacy of the results obtained by the model.

CHAPTER 5 STUDY OF CRANIOFACIAL RESPONSE TO ME TREATMENTS USING BONE ANCHORS

5.1 Introduction

In Chapter 3, an FE skull model that represents accurate geometrical features and heterogeneous bone properties of a dry skull was presented. In the model, hexahedral and tetrahedral finite elements were used and their linear elastic properties were defined based on Hounsfield Unit distribution of CBCT image data. In Chapter 2 it was stated that the reliability of FE analysis is highly dependent on the accuracy of the model and the boundary conditions applied to simulate the real problems. Therefore, to obtain a more reliable FE analysis for BA-ME treatments, it is crucial to define boundary conditions which are representative of clinical BA-ME treatment conditions; this process will be performed in the following sections.

5.2 Materials and Methods

As introduced in Chapter 1, during the maxillary expansion treatment, once the osseointegrated layer is generated between bone anchors and surrounding bones, the maxillary expansion will be applied by adjusting the expansion appliance level of activation (consisting of jackscrew and connectors), which is attached to the BA (Figure 1-3). During the treatments, the maxillary expansion process is applied at a rate of ¼ mm every 2 days and typically, a total of 4mm unilateral transverse expansion is applied on each BA (Harzer et al, 2004) for a total bilateral expansion of 8 mm.

To simulate the expansion, a 4mm transverse displacement was applied to the bone anchor neck in the model. A zero transverse displacement is defined on the model plane of symmetry. Since for adult patients, an osteotomy of maxillary suture surgery is carried out before expansion (Harzer et al, 2004), no constraint was applied on the regions of maxillary suture. To eliminate rigid body motion, zero displacement constraint is defined at the peripheral region of the foramen magnum and posterior region of the symmetry plane (Figure 5-1). ANSY (ANSYS Inc., Canonsburg, PA, USA) explicit commercial finite element solver was used.

Figure 5-1: Schematic of constraint conditions

5.3 Results

5.3.1 Displacement Distribution in Craniofacial and Maxillary Structures

Twenty five (25) locations on the maxilla and other craniofacial structures were used as test positions in this work; they are shown in Figure 5-2 and listed in Table 5-1. The

locations were selected because they are easily identifiable and have clinical relevance. The model assumes separated maxilla suture. Following 4mm expansion displacement at the bone anchors, displacement, strain and stress values of these locations were obtained and recorded in Table 5-1.

Maximum displacement occurred at the mesial surface of the upper incisor (landmark 1) while minimum displacement occurred at the region nearing the Calvarium (landmark 19). It should be noted that this displacement is in the vertical plane and is an artifact of the boundary conditions.

Maximum von Mises stresses are located along nasal and lower border of the orbital complexes (landmarks 13, 14, 15, 16) indicating that these are lines along which bone strains occur to expand the maxilla and that these are regions of high modulus bone; analogous to having a pivot at landmark 16.

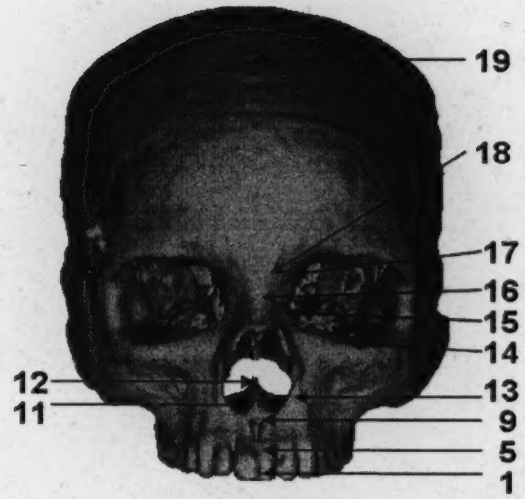

(a) Front view

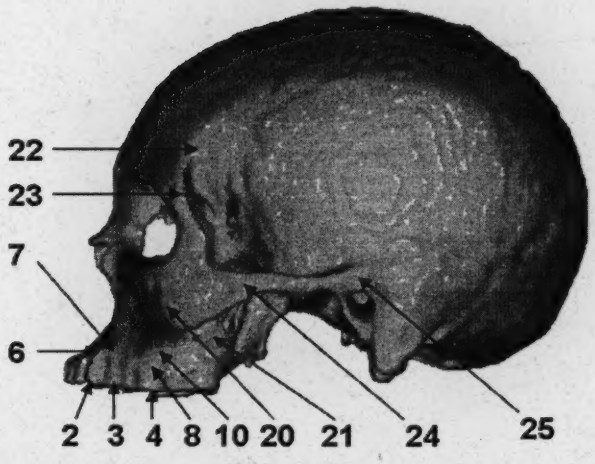

(b) Left view

Figure 5-2: Investigated regions of craniofacial and maxillary complex

Table 5-1: Displacement, stress and strain obtained in 25 regions following 4mm transverse expansion (T: Transverse direction; V: Vertical direction; S: Sagittal direction; R: Resultant). * Negative value (-) represents a medial displacement in transverse direction, superior displacement in vertical direction and anterior displacement in sagittal direction respectively.

Regions analyzed	Displacement (mm) *				Von Mises Stress (MPa)		Equivalent Strain (με)	
	T	V	S	R	Max	Mean	Max	Mean
1. Mesial surface of upper central incisor	4.90	1.02	-1.03	5.11	0	0	0	0
2. Upper canine	4.74	0.56	-0.72	4.82	0.02	0.01	3	2
3. Upper first premolar	4.60	0.44	-0.63	4.67	0.29	0.17	69	36
4. Upper first molar	4.30	0.32	-0.49	4.34	0.94	0.57	217	145
5. Prosthion	4.42	1.04	-0.94	4.64	0.06	0.03	14	10
6. Upper Canine root apex	4.28	0.57	-0.64	4.37	0.39	0.17	134	127
7. Upper first premolar buccal root apex	4.14	0.48	-0.56	4.21	4.09	1.89	917	761
8. Upper first molar mesial buccal root apex	4.10	0.28	-0.42	4.13	3.31	1.88	1110	936
9. Subspinale	3.96	1.17	-0.92	4.23	0.71	0.39	1733	699
10. Ectomolar	3.84	0.25	-0.36	3.87	6.59	4.36	10604	6160
11. Anterior Nasal Spine	3.71	1.38	-1.00	4.09	1.43	0.92	321	276
12. Posterior nasal Spine	3.23	1.64	-1.03	3.77	1.79	1.05	482	353
13. Piriform	3.38	0.68	-0.51	3.49	34.90	16.27	50171	41183
14. Lower border of Orbit	1.36	-0.11	0.14	1.37	16.96	6.86	3717	2558
15. Nasomaxillary suture	0.29	0.68	0.78	1.08	30.31	22.37	11105	6783
16. Nasal suture	0.03	0.88	0.97	1.31	48.50	31.99	15006	10087
17. Frontomaxillary	0.10	0.51	0.63	0.82	6.22	3.16	2134	1265
18. NasoFrontal suture	-0.04	0.76	0.80	1.10	49.35	14.37	21720	12103
19. Calvarium	0.00	0.11	0.00	0.11	2.53	1.54	294	197
20. Zygomaticomaxillary buttress	2.31	-0.33	-0.36	2.36	2.81	2.35	1709	1174
21. Pterygomaxillary suture	3.33	0.99	-0.72	3.55	16.36	7.57	8248	2527
22. External Angular Process	0.22	0.08	0.07	0.24	10.63	4.11	8648	5511
23. Zygomaticofrontal	0.59	-0.16	0.05	0.61	30.57	10.42	3091	2338
24. Zygomatic temporal	1.24	-0.37	0.11	1.30	7.39	5.05	2456	1874
25. Posterior Zygomatic Arch	0.26	0.00	0.07	0.27	1.87	1.87	456	348

The transverse displacement contour plots after 4mm expansion are shown in Figure 5-3. The maximum medial displacements, 4.90 mm and 4.74, in the transverse direction were observed at the upper central incisor (landmark 1) and upper canine (landmark 2). The displacements of teeth and their corresponding root apex were larger than the expansion displacement applied on bone anchor (4mm). This is expected considering a pivot point at Region 16 and since landmarks 1 and 2 are

further than the bone anchor. The displacements of other superior parts of the maxillary, such as the lateral wall of the inferior nasal cavity and the pterygoid plates were smaller than 4mm; again in agreement with the previous line of reasoning. The displacements gradually decreased from inferior-anterior parts to superior-posterior parts of maxillary structures. Besides the maxillary complex, a large medial displacement (2.31 mm) was observed at the zygomaticomaxillary landmark (20), while minor displacements were observed in nasal regions.

Large inferior displacements, 1.64 mm and 1.38 mm, (Figure 5-4) were observed in the posterior nasal spine (landmark 12) and in anterior nasal spine (landmark 11), respectively. The teeth and inferior parts of maxillary structures had inferior displacement ranging from 0.25mm to 1.02mm. Most craniofacial and maxillary structures have inferior displacement except the zygomaticomaxillary region which has small superior or zero displacement.

Smaller magnitude displacements were noticed in the sagittal plane (Figure 5-5). Anterior and posterior displacements of the order of 1.2 mm were noticed. Similar to the transverse displacement, most large anterior displacements were observed in the maxillary structures including the pterygomaxillary suture. Small posterior displacements (~ 0.5mm) were observed in the nasal regions. No sagittal displacement was observed in zygomaticomaxillary regions.

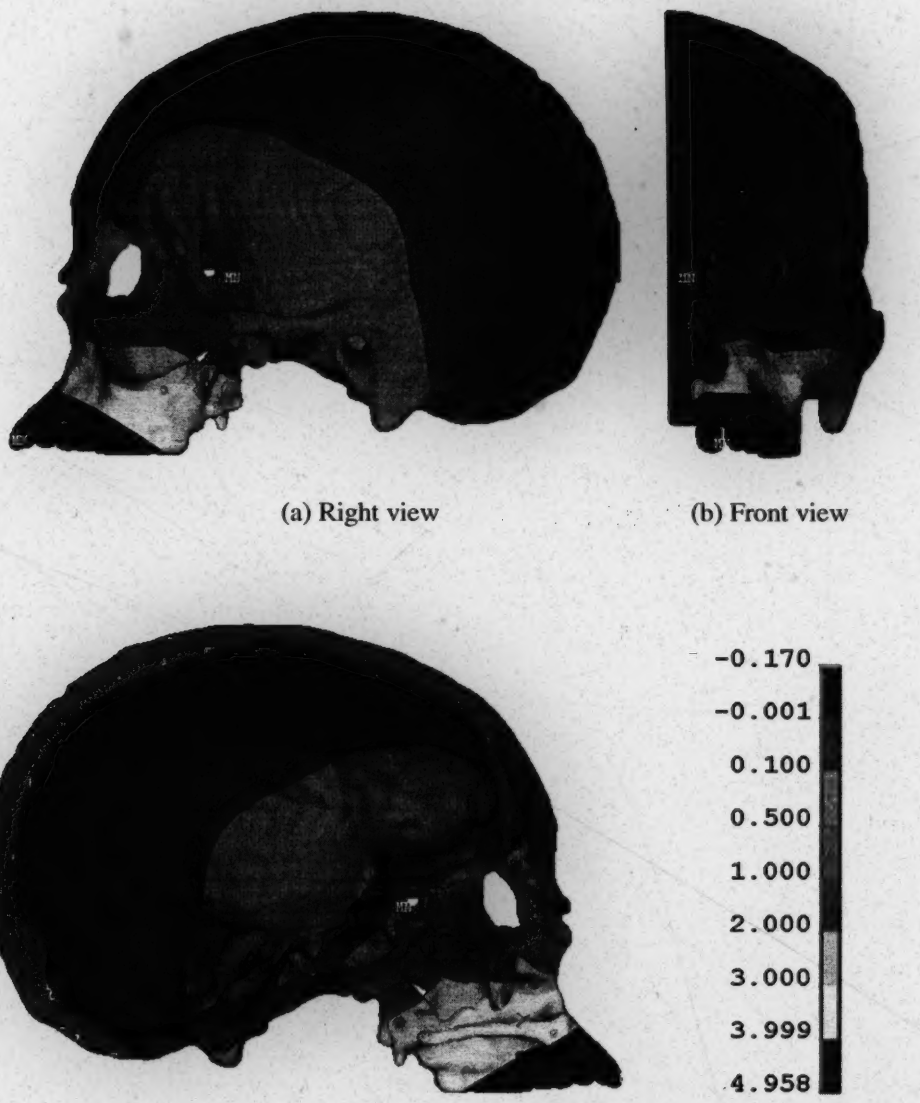

(a) Right view (b) Front view

(c) Left view d) Displacement label (mm)

Figure 5-3: Contour plot of displacement of nodes in transverse direction after 4mm expansion (+ Lateral; - Medial). Deformed skull shown

(a) Right view

(b) Front view

(c) Left view

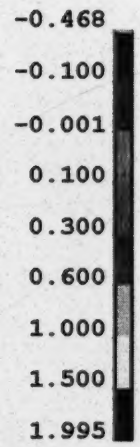

(d) Displacement label (mm)

Figure 5-4: Contour plot of displacement of nodes in vertical direction after 4mm expansion (+ Inferior; - Superior). Deformed skull shown.

(a) Right view (b) Front view

(c) Left view (d) Displacement label (mm)

Figure 5-5: Contour plot of displacement of nodes in sagittal direction after 4mm expansion (+ Posterior; - Anterior). Deformed skull shown.

The resultant displacement contour plot after 4mm expansion is shown in Figure 5-6 and the components in anatomical planes are tabulated in Table 5-1. The maximum displacements, caused mainly by displacements in the transverse direction, were observed at the upper central incisor (5.11 mm) and upper canine (4.82 mm). Teeth displacements and their corresponding root apex were larger than the expansion applied on bone anchor (4mm). Displacements of other superior parts of the maxillary, such as the lateral wall of the inferior nasal cavity and the pterygoid plates were smaller than 4mm. The displacements gradually decreased from inferior-anterior parts to superior-posterior parts of the maxillary structures. In addition to the displacements of the maxillary complex, a large displacement (2.36 mm) was observed in the zygomaticomaxillary region. Displacement results clearly show the expected displacement pattern of maxilla expansion for a solid bone with regions of lower modulus at the sutures, thus bone plates translate as well as rotate.

(a) Right view (b) Front view

(c) Left view (d) Displacement label (mm)

Figure 5-6: Contour plot of resultant displacement of nodes after 4mm expansion

5.3.2 Stress Distribution in Craniofacial and Maxillary Structures

Von Mises stress are the most presented stress in the literature relating results of FE biomechanical studies to state the conditions of bony structures under external forces and displacement load. Additionally, since the isotropic properties were used to define the skull bone properties, it is appropriate in this work to use the effect of the von Mises stress to evaluate the response of bones following maxillary expansions. There are no studies that describe von Mises stresses as clinically relevant. The mathematical definition of von Mises stress is defined with equation 5-1. Similarly, the equivalent strain is used in the study and is defined with equation 5-2.

$$\sigma_e = \frac{1}{2}\left[(\sigma_1 - \sigma_2)^2 + (\sigma_2 - \sigma_3)^2 + (\sigma_3 - \sigma_1)^2\right]^{\frac{1}{2}} \qquad (5\text{-}1)$$

$$\varepsilon_e = \frac{1}{2}\left[(\varepsilon_1 - \varepsilon_2)^2 + (\varepsilon_2 - \varepsilon_3)^2 + (\varepsilon_3 - \varepsilon_1)^2\right]^{\frac{1}{2}} \qquad (5\text{-}2)$$

In Table 5-1 and Figure 5-7, small von Mises stresses were observed in the inferior and anterior regions of maxillary. Elevated stresses occur sporadically throughout the skull, maxilla and at the bone anchor. Maximum stresses are experienced below the zygomatic bone. Large stresses were located in the nasal, pterygomaxillary and zygomaticomaxillary regions while the single largest stress was located in nasal suture. It indicated that the stress applied on the bone anchor was transferred to the superior parts of craniofacial structures during ME, which confirms this to be a point of rotation and material deformation required for a permanent expansion process.

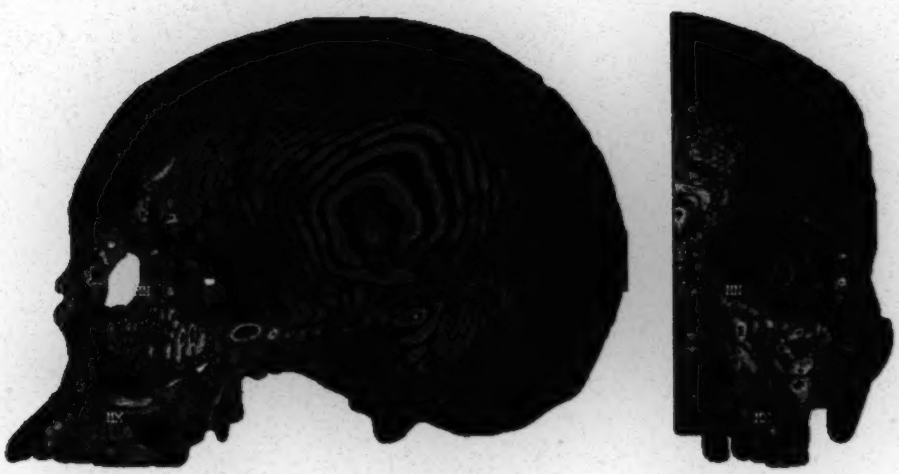

(a) Right view (b) Front view

(c) Left view (d) Stress label (MPa)

Figure 5-7: Contour plot of von Mises stress of nodes

5.3.2 Strain Distribution in Craniofacial and Maxillary Structures

As is the case for von Mises stresses, von Mises strains have no known clinical relevance but are of interest to compare with experiment. Again, the equivalent strain definition is provided with equation 5-2. Largest strains were located in the lateral wall of the inferior nasal cavity (Figure 5-8). Other large strains were located in the anterior wall of the superior nasal cavity and the pterygomaxillary plate. These large strain regions are a result of large ME bone deformation and support patient pain patterns. A region with large stresses does not necessarily relate to a large strain distribution (and vice versa) since the elastic modulus were assigned based on real bone property distribution of skull.

(a) Right view

(b) Front view

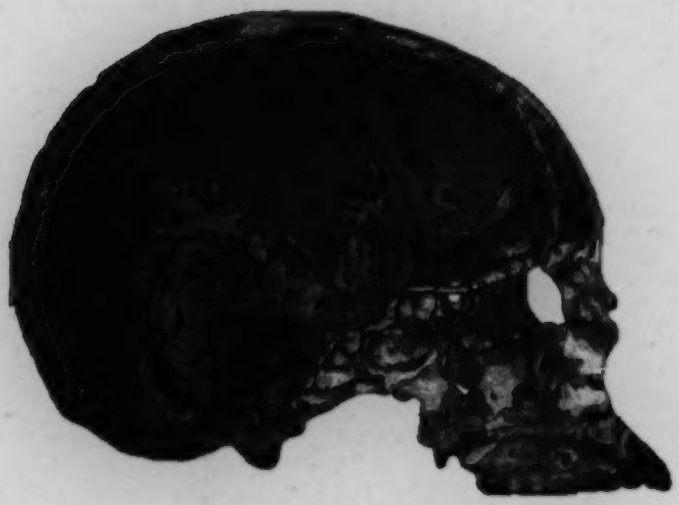

(c) Left view

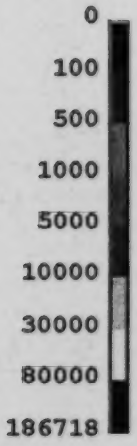

(d) Strain label (με)

Figure 5-8: Contour plot of equivalent strain of nodes

5.4 Discussion

The purpose of the study is to offer clinicians a verified, if not validated, tool for predicting treatment outcome. The first evaluation is to compare predicted and experimental results. Considering the variability and possible sources of error, both experimental and numerical predictions, which were presented earlier, are in agreement with trends seen in experimental work collected in Chapter 4.

Experimental results presented concur with clinically reported craniofacial pain position results during ME, thus showing a link between fresh skull experiments and *in-vivo* situations. Furthermore, predicted trends are in agreement with experimental results in terms of strains. Referring to results presented in Table 4-1 and Table 5-1, appreciable agreement is found. For the sake of the following comparison, it is assumed that experimental results represent principal strains. It is recognized that this is an approximation, but should be well within the error levels associated with the experimental procedure. Predicted and experimental von Mises strain results for the nasomaxillary, zygomaticomaxillary and pterygomaxillary sutures are 11105με and 6825με, 1709με and 1589με, and 8248με and 6523με, respectively. This is equal to 26.4%, 7.5% and 62.7% error, for each suture respectively. The difference can be explained by the sources of error discussed earlier. Trends are in agreement with the predicted results. To further show this agreement, it can be seen that strain data obtained from the experiment and the model has very similar pattern (Figure 5-9), where strain induced in nasomaxillary and pterygomaxillary sutures are much larger

than that induced in zygomaticomaxillary suture. The only difference between experimental and predicted results is that the strain along the pterygomaxillary suture path is larger than that along the nasomaxillary suture path whereas the strain perpendicular to the suture path has a reverse pattern, the latter of which concurs with the model.

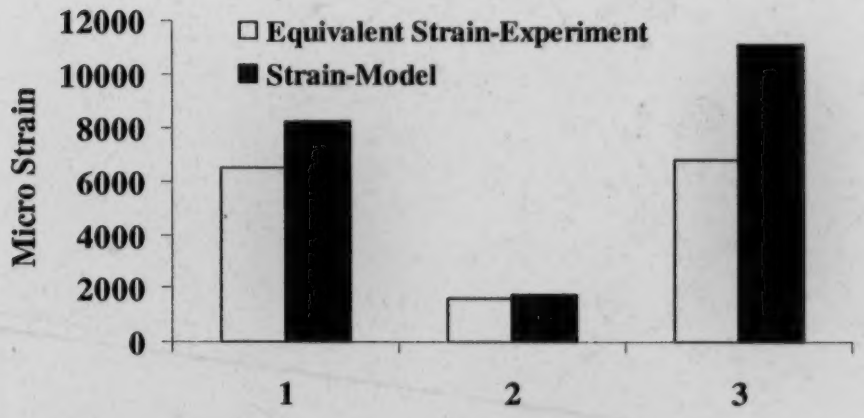

Figure 5-9: Comparison of strain in three craniofacial sutures between experiment and model. Pterygo: Pterygomaxillary suture; Zygo: Zygomaticomaxillary suture; Naso: Nasomaxillary suture

A greater level of difference was expected since the material properties assumed and imaging limitations induce inherent errors and dry skull imaging-based HU are not expected to concur with wet bone HU. Rho's equations (Rho and Hobatho, 1995) have large standard deviations and are also propagated here. Clinically the expansion process is applied at a rate of ¼ mm every 2 days. A total of 4mm transverse expansion is applied on each bone anchor (total of 8 mm expansion) during treatment.

It was therefore expected that a comparison between instantaneous loading results to those incrementally expanded would also lead to variations. Although not yet conclusive, comparing known craniofacial pain locations during ME treatment, experimental strain trends and predicted strains and displacements, it is sensible to assume that the model reasonably predicts ME treatment and current proof-of-concept model provides preliminary data that is at least comparable in accuracy as models developed in other studies.

The reliability and accuracy of the displacement, stress and strain distribution obtained in this work was further evaluated by comparing with results obtained from Jafari et al (2003), where a rapid maxillary expansion of 10mm (5mm per side) was analyzed by using a FE skull model with a single material property for both cancellous and cortical bone. From Table 5-2, stresses in seven craniofacial sutures were compared. The stress obtained from two studies indicated a similar stress distribution pattern and similar stress values. It is to be noted that the results originally reported by Jafari were excessively high because of conversion errors and have been changed in Table 5-2. This had been noticed since the originally reported stresses were significantly higher than the strength of bone which has been reported in the range 100 MPa (Parr et al, 1997). The current model provides more realistic results

Table 5-2: Comparison of stress results with those of Jafari et al

Regions of **Error! Reference source not found.**	Jafari et al (MPa)		Von Mises Stress (MPa)		Resultant Error (%)	
	Max	Mean	Max	Mean	Max	Mean
15. Nasomaxillary suture	25.6	19.5	30.31	22.37	15.5	12.8
16. Nasal suture	55.4	19.2	48.50	31.99	14.2	40.0
17. Frontomaxillary suture	9.4	8.7	6.22	3.16	51.1	175.3
18. Nasofrontal suture	32.7	15.8	49.35	14.37	33.7	10.0
20. Zygomaticomaxillary buttress	9.0	5.7	2.81	2.35	220.3	142.6
23. Zygomaticofrontal	33.0	14.4	30.57	10.42	7.9	38.2
24. Zygomaticotemporal suture	9.3	5.2	7.39	5.05	25.8	3.0
Average error					52.7	60.3

The von Mises stresses contour plot presented in Figure 5-7 indicates that the BA anchorage position is visibly an elevated stress region. This is typical for the loading point and an area of significant elastic property changes.

Seen in Figure 5-8, the largest strains were located in the lateral wall of the inferior nasal cavity. Another large strain was located in the anterior wall of the superior nasal cavity (Nasal regions) and the pterygomaxillary plate. Since large strain represents large deformation, these regions with large strain have large deformation of bones due to the BA-ME and support patient pain patterns.

The strain distribution had a similar pattern as that of stress, which did not necessarily had to be the case because of elastic property heterogeneity. However, a region with big stress does not necessarily result to a big strain distribution (vice versa) since the elastic modulus was assigned based on real bone property distribution of skull. This is

an advantage - that will be further discussed in Chapter 6 - of the current work compared to previous studies.

There are typically two approaches to examine the convergence of FE analysis. One way performs FE analysis with smaller elements and another one performs FE analysis with same size but higher order element (more nodes) (Zienkiewicz et al, 2000). The performance of the convergence examination needs stronger computer capability than was available and more computing time. Because of the limitation of the available computers, it is not practical to perform this kind of investigation. Since the current FE model consists of much smaller sized elements than previous studies (Tanne et al, 1989, 1991; Iseri et al, 1998; Provatidis et al, 2003a,b; Johnson et al, 2005), it is believed that the current model should present better convergence results. In addition, earlier models were not accurate geometrical representation.

5.5 Conclusions

The proposed FE model developed was shown to be an effective tool to predict the outcome of maxillary expansion using bone anchors as force abutment. The model includes 297,800 nodes and 877,400 hexahedra and tetrahedral elements, which leads to a very accurate geometry. The model used Cone Beam Computerized Tomography (CBCT) images to develop accurate bone geometry and assign materials properties through the use of ScanIP/ScanFE (Simpleware, UK). Using individual voxels to build a skull FE model leads to the automatic assignment of elastic properties based

on the HU of individual pixels. Predictions were compared with the literature and experimental work. Some model limitations were identified but can be minimized using effective strategies. In the next chapter, the effect of using a different amount of elastic properties on FE model will be studied.

CHAPTER 6 EVALUATION OF THE EFFECT OF ELASTIC PROPERTIES ON THE PROPOSED MODEL

6.1 Introduction

As detailed in Chapter 3, the elastic properties (EP) of the developed FE model for ME-BA treatment are defined by converting Cone Beam Computed Tomography (CBCT) obtained voxel Hounsfield Unit (HU) values using previously defined empirical equations (Lagravère et al, 2005; Rho and Hobatho, 1995), 156 EPs were originally defined and assigned to the FE model and the Bone Anchor Osseintegrated Interface (BAOI) EP was defined as an average of the heterogeneous elastic moduli of surrounding bone. The error from the resolution of HU distribution of CBCT image data and the experimental equations are the leading source of elastic property definition error. It was introduced in Chapter 2 that the definition and assignment of EPs was critical for the accuracy of FE analysis for bony structures. The objective of this study is to evaluate the influence of the number of EPs assigned to the model on the displacement, stress and strain predictions at twenty five anatomical landmarks and stress predictions at the BAOI of the proposed skull model. Five FE models, two using 2 EP - defined from literature and from calculations based on the exact HU distribution of CBCT image data, respectively -, as well as 20, 39 and 78 EPs divided between cancellous and cortical bones, will be used to perform FE analysis of maxillary expansion. Results will be compared to those detailed in Chapter 5 for the control FE model (156 EP). Furthermore, the effect of BAOI EP on local stresses will be evaluated using a ± 50% EP sensitivity schemes.

6.2 Materials and Methods

6.2.1 Elastic Property Assignment

EPs were assigned to FE model elements based on CBCT image individual voxel Hounsfield Units (HU) values using the relationship between HU and apparent density for NewTom Volume Scanner (NEwTom 3G, Aperio, Italy) (Lagravère et al, 2005) and Rho's (Rho and Hobatho, 1995) empirical relationships for cancellous and cortical bone.

The detailed process for developing a three dimensional finite element model of a skull was presented in Chapter 3. Since the CBCT scanner provides high resolution imaging data and small element size (1.06mm×1.06mm×1mm) were used, the FE model developed possesses accurate geometrical features. This allows greater latitude in assigning bone EP distribution for specific subject than those developed in previous studies. Six EP assignment schemes, presented in Table 6-1, one control and five for comparison were used to define material properties of the FE model based on the HU distribution of CBCT image data. Presented in the table are the number of cancellous EP, cortical EP, HU difference between each level of EP and density difference between each level of EP.

Table 6-1: Summary of six material assignment schemes. [1]The elastic properties for cancellous and cortical bones were defined from literature. [2]The elastic properties for cancellous and cortical bones were defined with average elastic modulus of corresponding elements of the developed subject-specific FE model

EP Assignment scheme	Number of Elastic Properties		HU range	Density range (kg/m^3)
	Cancellous	Cortical		
156 (control)	125	31	8	16
78	63	15	16	32
39	32	7	32	64
20	16	4	64	128
2 (Literature) [1]	1 (7.9GPa)	1 (13.7GPa)	240	480
2 (Subject-specific) [2]	1 (1.8GPa)	1 (15.4GPa)	240	480

6.2.2 Bone Anchor Osseointegration Interface

As detailed earlier, a 3mm diameter titanium cylindrical bone anchor was modeled to be included in the FE skull model, as shown in Figure 3-6. Titanium was used since it has been shown to be successfully implanted (Hansson et al, 1983); properties of which are in Table 3-1. The bone anchor osseointegration interface was defined as perfectly bonded along the 4mm length and tip of the BA. BA features such as threading were neglected in the model as it was assumed that they were an integral part of the BAOI thickness.

In the first part of the study, measuring the effect of the number of assigned bone EPs, the EP of BAOI was assigned a uniform value equal to the average of elastic modulus of anchor-surrounding-bones; however, in clinical conditions the denser bone material is most likely distributed on the surface of the palatal bones, this could lead to a different stress distribution in the BAOI compared with that from the FE model

applied (Fang et al, 2005).

In the second part of this study, the effect of the BAOI EP was verified in the control FE model (156 EP) using a ±50% sensitivity scheme from the original 2.4 GPa elastic modulus value. BOAI elastic modulus was either set as 1.2 GPa, 2.4 GPa or 3.6 GPa with a major Poisson's ratio of 0.3.

6.2.3 Osseointegration Boundary and Constraint Conditions

To simulate a clinical maxillary expansion treatment with a bone anchored appliance, a 4mm unilateral transverse displacement was applied to the bone anchor neck. A zero transverse displacement is defined on the model plane of symmetry. A free constraint was applied on the regions of maxillary suture. To eliminate rigid body motion, zero displacement constraint is defined at the peripheral region of the foramen magnum and posterior region of the symmetry plane.

6.3 Results

6.3.1 Model Sensitivity to Number of Assigned EPs

To determine the influence of EPs, von Mises stress, equivalent strain and resultant displacement values at 25 anatomical landmarks on the craniofacial structures were obtained by performing the expansion simulation with the developed 6 FE models and presented in Table 6-1, Table 6-2 and Table 6-3 respectively.

Table 6-2: Maximum von Mises stress distributed in craniofacial and maxillary structures obtained with 6 material assignment schemes

Region	156 EP	78 EP		39 EP		20 EP		2 EP (Subject-specific)		2 EP (Literature)	
	MPa	MPa	%	MPa	%	MPa	%	MPa	%	MPa	%
1	0.00	0.00	0.0	0.00	0.0	0.00	0.0	0.00	0.0	0.00	0.0
2	0.02	0.02	0.0	0.03	50.0	0.03	50.0	0.03	50.0	0.22	1000.0
3	0.29	0.29	0.0	0.37	27.6	0.50	72.4	0.47	62.1	1.88	548.3
4	0.94	0.93	1.1	1.09	16.0	1.42	51.1	2.88	206.4	22.11	2252.1
5	0.06	0.06	0.0	0.08	33.3	0.09	50.0	0.04	33.3	0.37	516.7
6	0.39	0.39	0.0	0.48	23.1	0.59	51.3	0.74	89.7	3.83	882.1
7	4.09	4.11	0.5	5.07	24.0	6.22	52.1	4.60	12.5	27.88	581.7
8	3.31	3.33	0.6	3.50	5.7	3.84	16.0	5.10	54.1	39.27	1086.4
9	0.71	0.72	1.4	0.96	35.2	1.16	63.4	1.36	91.5	4.60	547.9
10	6.59	6.59	0.0	9.58	45.4	14.77	124.1	37.88	474.8	170.73	2490.7
11	1.43	1.43	0.0	1.41	1.4	1.35	5.6	4.32	202.1	16.64	1063.6
12	1.79	1.77	1.1	1.83	2.2	2.22	24.0	3.72	107.8	13.72	666.5
13	34.90	32.22	7.7	28.41	18.6	30.25	13.3	40.49	16.0	159.62	357.4
14	16.96	16.98	0.1	19.58	15.4	22.17	30.7	20.50	20.9	85.93	406.7
15	30.31	30.71	1.3	35.06	15.7	42.71	40.9	28.89	4.7	118.45	290.8
16	48.50	48.32	0.4	56.28	16.0	63.63	31.2	47.69	1.7	191.44	294.7
17	6.22	6.26	0.6	9.27	49.0	17.34	178.8	24.41	292.4	98.24	1479.4
18	49.35	49.89	1.1	57.95	17.4	66.39	34.5	53.05	7.5	207.03	319.5
19	2.53	2.53	0.0	3.06	20.9	3.73	47.4	4.23	67.2	8.11	220.6
20	2.81	2.75	2.1	3.32	18.1	5.35	90.4	4.83	71.9	19.45	592.2
21	16.36	16.33	0.2	15.74	3.8	14.77	9.7	13.62	16.7	56.59	245.9
22	10.63	10.56	0.7	10.08	5.2	9.71	8.7	21.47	102.0	84.46	694.5
23	30.57	30.63	0.2	39.47	29.1	51.00	66.8	33.38	9.2	123.48	303.9
24	7.39	7.40	0.1	9.66	30.7	12.90	74.6	21.05	184.8	85.42	1055.9
25	1.87	1.87	0.0	2.79	49.2	4.15	121.9	9.18	390.9	35.84	1816.6

In Table 6-2, the difference between 156 and 78 EP is nearly null, with the exception of 7.7% difference at landmark 13. Clearly other schemes present large differences.

Table 6-3: Equivalent strain distribution in craniofacial and maxillary structures obtained with 6 material assignment schemes

Region	156 Mat	78 Mat		39 Mat		20 Mat		2 Mat (Subject-specific)		2 Mat (Literature)	
	με	με	%	με	%	με	%	με	%	με	%
1	0	0	0.0	0	0.0	0	0.0	0	0.0	0	0.0
2	3	3	0.0	3	0.0	4	33.3	9.0	200.0	23	666.7
3	69	69	0.0	87	26.1	114	65.2	276.0	300.0	246	256.5
4	217	218	0.5	248	14.3	319	47.0	1607.0	640.6	2809	1194.5
5	14	14	0.0	18	28.6	23	64.3	21.0	50.0	46	228.6
6	134	135	0.7	163	21.6	196	46.3	287.0	114.2	458	241.8
7	917	920	0.3	1139	24.2	1394	52.0	2581.0	181.5	3537	285.7
8	1110	1119	0.8	1169	5.3	1251	12.7	2869.0	158.5	4991	349.6
9	1733	1703	1.7	1797	3.7	1645	5.1	763.0	56.0	582	66.4
10	10604	11022	3.9	16685	57.3	21300	100.9	21169.0	99.6	21734	105.0
11	321	324	0.9	356	10.9	515	60.4	2410.0	650.8	2121	560.7
12	482	487	1.0	465	3.5	515	6.8	2086.0	332.8	1750	263.1
13	50171	49295	1.7	48484	3.4	515	99.0	22541.0	55.1	20240	59.7
14	3717	3718	0.0	4242	14.1	4751	27.8	11420.0	207.2	10903	193.3
15	11105	11062	0.4	13018	17.2	15075	35.7	16239.0	46.2	15216	37.0
16	15006	15101	0.6	18000	20.0	20404	36.0	26645.0	77.6	24388	62.5
17	2134	2139	0.2	2837	32.9	4243	98.8	13622.0	538.3	12485	485.1
18	21720	21025	3.2	31366	44.4	43543	100.5	29722.0	36.8	26447	21.8
19	294	294	0.0	363	23.5	449	52.7	1206.0	310.2	917	211.9
20	1709	1710	0.1	1457	14.7	2093	22.5	2685.0	57.1	2462	44.1
21	8248	8198	0.6	7622	7.6	6765	18.0	7595.0	7.9	7193	12.8
22	8648	8067	6.7	9879	14.2	10910	26.2	11941.0	38.1	10704	23.8
23	3091	3092	0.0	3888	25.8	5116	65.5	14827	379.7	13293	8819
24	2456	2473	0.7	3496	42.3	6175	151.4	11730.0	377.6	10845	341.6
25	456	451	1.1	671	47.1	989	116.9	2817.0	517.8	4476	881.6

In Table 6-3, the difference between 156 and 78 EP is minimal, with a 3.9% difference at landmark 10 being the only exception. Clearly other schemes present much larger differences.

Table 6-4: Resultant displacement distribution in craniofacial and maxillary structures obtained with 6 material assignment schemes

Region	156 Mat	78 Mat		39 Mat		20 Mat		2 Mat (Subject-specific)		2 Mat (Literature)	
	mm	mm	%	mm	%	mm	%	mm	%	mm	%
1	5.11	5.11	0.0	5.24	2.5	5.41	5.9	5.89	15.3	5.95	16.4
2	4.82	4.82	0.0	4.92	2.1	5.04	4.6	5.39	11.8	5.42	12.4
3	4.67	4.67	0.0	4.75	1.7	4.84	3.6	5.08	8.8	5.08	8.8
4	4.34	4.34	0.0	4.37	0.7	4.40	1.4	4.39	1.2	4.29	1.2
5	4.64	4.64	0.0	4.70	1.3	4.78	3.0	5.04	8.6	5.02	8.2
6	4.37	4.37	0.0	4.40	0.7	4.45	1.8	4.63	5.9	4.57	4.6
7	4.21	4.21	0.0	4.22	0.2	4.24	0.7	4.33	2.9	4.24	0.7
8	4.13	4.13	0.0	4.14	0.2	4.14	0.2	4.12	0.2	4.00	3.1
9	4.23	4.23	0.0	4.24	0.2	4.25	0.5	4.32	2.1	4.23	0.0
10	3.87	3.87	0.0	3.84	0.8	3.81	1.6	3.72	3.9	3.57	7.8
11	4.09	4.09	0.0	4.08	0.2	4.07	0.5	4.05	1.0	3.95	3.4
12	3.77	3.77	0.0	3.73	1.1	3.67	2.7	3.38	10.3	3.25	13.8
13	3.49	3.49	0.0	3.42	2.0	3.36	3.7	3.29	5.7	3.13	10.3
14	1.37	1.37	0.0	1.58	15.3	1.77	29.2	2.21	61.3	2.11	54.0
15	1.08	1.08	0.0	1.10	1.9	1.07	0.9	0.86	20.4	0.84	22.2
16	1.31	1.31	0.0	1.37	4.6	1.37	4.6	1.09	16.8	1.05	19.8
17	0.82	0.82	0.0	0.81	1.2	0.76	7.3	0.57	30.5	0.57	30.5
18	1.10	1.10	0.0	1.15	4.5	1.14	3.6	0.9	18.2	0.87	20.9
19	0.11	0.11	0.0	0.11	0.0	0.09	18.2	0.02	81.8	0.02	81.8
20	2.36	2.36	0.0	2.63	11.4	2.84	20.3	3.1	31.4	2.97	25.8
21	3.55	3.55	0.0	3.47	2.3	3.36	5.4	2.9	18.3	2.70	23.9
22	0.24	0.24	0.0	0.23	4.2	0.20	16.7	0.12	50.0	0.11	54.2
23	0.61	0.61	0.0	0.66	8.2	0.68	11.5	0.74	21.3	0.70	14.8
24	1.30	1.30	0.0	1.47	13.1	1.65	26.9	2.05	57.7	1.99	53.1
25	0.27	0.27	0.0	0.25	7.4	0.21	22.2	0.09	66.7	0.08	70.4

In Table 6-4 no difference is found between 156 and 78 EP, even the 39 EP scheme only presents a maximum difference of 15.3%, between 1.37 mm and 1.58 mm, for landmark 14; a clinically irrelevant level of difference. Lower number EP schemes show larger percentage difference, however few could be deemed clinically relevant.

The average percentage difference and standard deviation for resultant displacement, von Mises stress and strain at the 25 anatomical landmarks between the control and other five simulations following the expansion simulation are presented in Table 6-5. The difference between using 78 elastic properties and the control (156 elastic

properties) is on average less than or equal to 1.0% ± 1.5 %. The results were specifically 0.0 ± 0.1 % for displacement, 0.8 ± 1.6 % for von Mises stress and 1.0% ± 1.5 % for strain, which shows convergence of the results.

The average percentage differences increased as the number of EP used decrease. When using 39 EP, the displacement percentage difference tripled compared to 78EP. At 20 EP, the displacement difference remains below 8%, but jumps nearly three-fold 22.5% ± 22.7% when using 2 EP.

Table 6-5: Average percentage difference (± standard deviation) between using 2, 20, 39 and 78 versus 156 material properties for displacement, von Mises stresses and strains at 25 bony landmark positions detailed in Figure 5-2

	Number of Elastic Properties				
	78	39	20	2 (Subject-specific)	2 (Literature)
Resultant Displacement	0.0% ± 0.1%	3.5%±4.3%	7.9%±8.9%	22.1%±23.3%	22.5%±22.7%
Von Mises Stress	0.8% ± 1.6%	22.1%±15.3%	52.4%±42.0%	102.8%±125.3%	788.6%±634.9%
Von Mises Strain	1.0% ± 1.5%	20.1%±15.5%	53.8%±39.0%	217.3%±202.2%	276.9%±293.4%

In terms of strain for the 2 EP schemes, there is a jump of 276.9% (literature) and 217.3% (subject-specific) difference with the control, as well as 788.6% (literature) and 102.8% (subject-specific) in terms of stress with nearly equivalent standard deviations. It was found that elastic properties have less of an effect on the resultant displacement distribution, while stress and strain distributions are very sensitive to material property assignment. It is clear that the use of two elastic properties, one for

cancellous bone and one for cortical bone is undesirable, and the use of more than 78 elastic properties is more reliable for the FE analysis of BA-ME treatments

The percentage average difference and standard deviation of von Mises stresses at the BAOI after the expansion treatment is presented in Table 6-6. It can be seen that as the number of elastic properties decreases the percentage difference with the control increases significantly. Again, using 78 EP presents little average difference with the control, while 2 EP presents nearly 400% (Literature) and 100% (Subject-specific) of difference with an equally high standard deviation.

Table 6-6: Average percentage difference of von Mises stress distributed in BAOI between control and four trial models.

	Number of Elastic Properties				
	78	39	20	2 (Subject-Specific)	2 (Literature)
Average percentage difference ± standard deviation	0.24% ± 0.04%	13.4% ± 6.6%	30.7% ± 20.5%	100.8% ± 110.2%	390.5% ± 382.0%

The stress distribution was evaluated along eight BA longitudinal lines, as shown in Figure 6-1a. It can be observed from Figure 6-1b that the anchorage point exhibits in general terms the largest von Mises stresses in the model, as does the cut out section shown in Figure 6-1c.

Figure 6-2a,b show the significant difference between 2 EP and other models for BA longitudinal lines 2 and 8, selected because they are representative of the other longitudinal line results. Figure 6-2a shows the convergence between the stress from models with 78 and 156 EPs, while the use of 2 EP presents erroneous and reverse trends. Figure 6-2b shows again the significant difference between 2 EP and other trials and the control model. Results along the other lines appear in Appendix 1. Clearly, the use of two elastic properties, one for cancellous bone and one for cortical bone is an undesirable approach for large and complex models such as is presented here. Depending on the intended use of the FE model, a larger or smaller number of elastic properties should be employed.

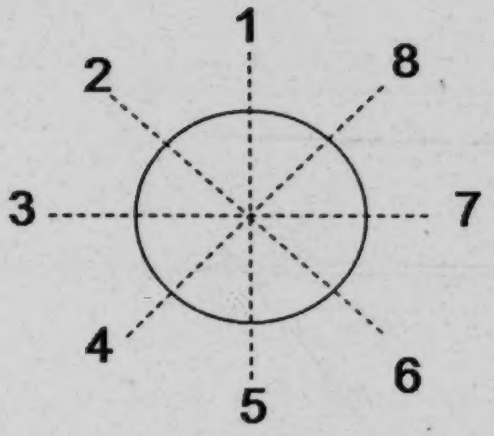

a. Bone anchor evaluation lines

b. Front view FE model

c. Cut out section B with stress scale

Figure 6-1: (a) Bone anchor cross section and evaluation lines; (b) front view of FE model; (c) cut view B of (b) showing the stress at the implant

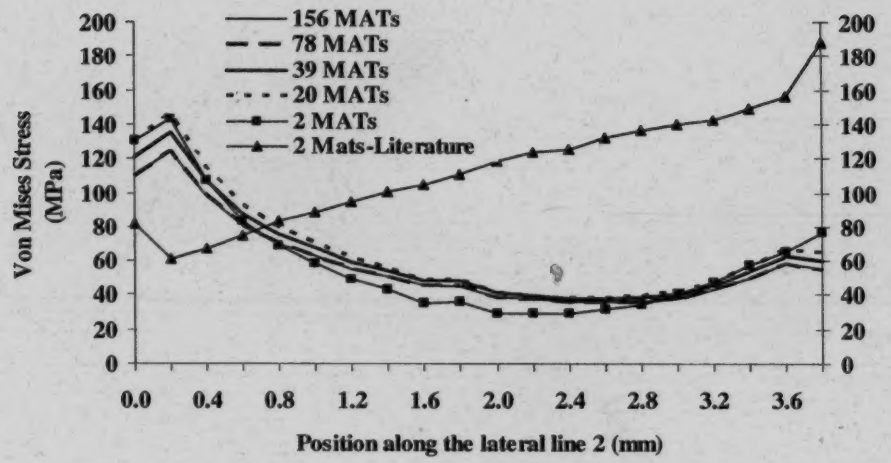

(a)

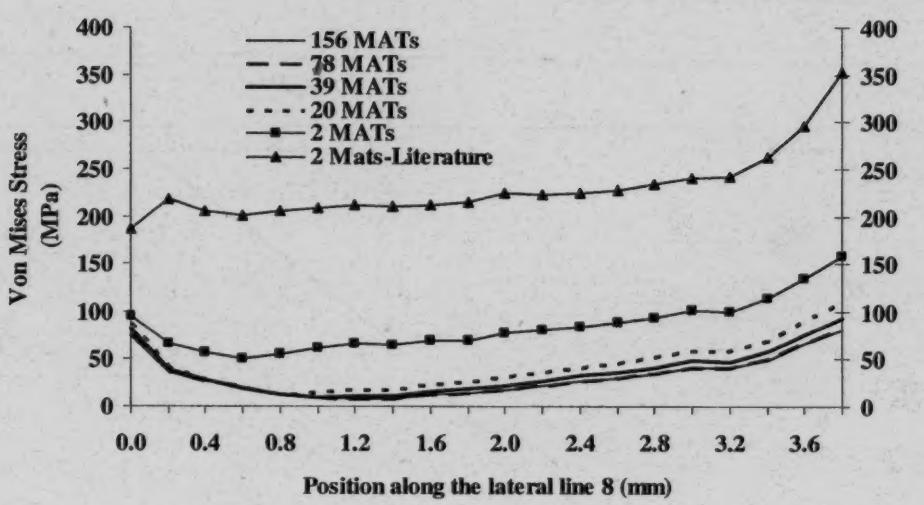

(b)

Figure 6-2: Comparison of von Mises stress distribution along (a) line 2 and (b) line 8

6.3.2 BAOI Von Mises Stresses Sensitivity to EP

Typical results of the sensitivity of the BAOI von Mises stresses to a ± 50% variation in BAOI elastic modulus are presented in Figure 6-3a,b for BA longitudinal lines 2 and 8, respectively; again these were selected because results were representative of the range of results obtained along all eight BA longitudinal lines, the complete results are presented in Appendix 2. Average percentage differences between von Mises stresses in the BAOI for the control 2.4 GPa were 18.8% and 12.3% for 1.2 GPa and 3.6 GPa, respectively. As expected, greater elastic modulus resulted in greater stresses. However, the von Mises stress error is less than the difference in EP with the control, which indicates that BAOI EP selection may not be as critical if proper estimation and assumptions are made. This is also confirmed by another study that has shown that the osseointegration interface surrounded with cortical bone has larger induced stresses than those surrounded by cancellous bone (Koca et al, 2005). Shown in Figure 6-3, the discrepancy between stress levels is larger at the BAOI neck and tip.

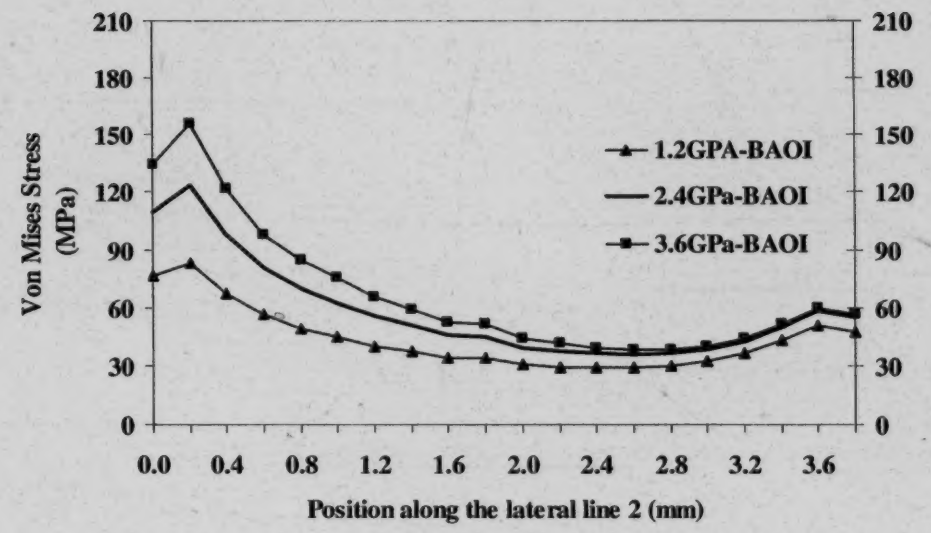

(a)

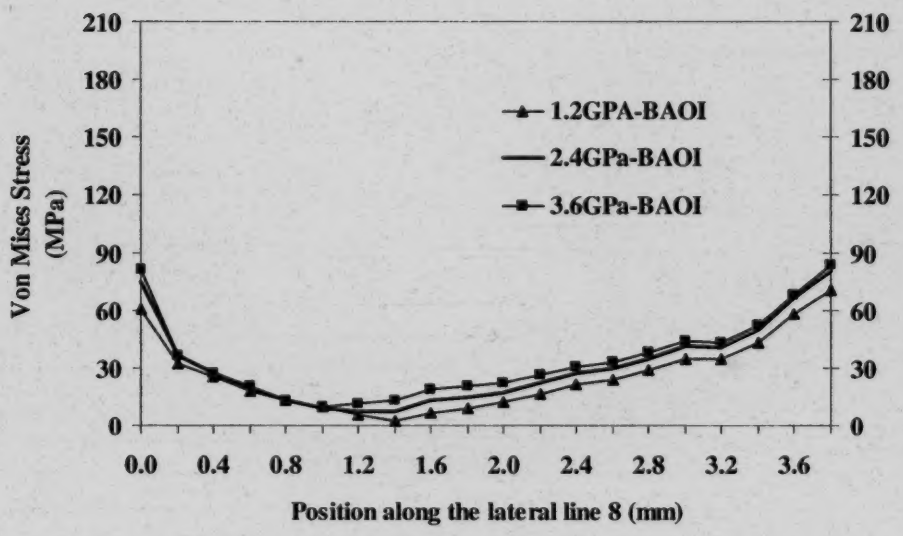

(b)

Figure 6-3: Von Mises stress distribution in (a) line 2 and (b) line 8 with a ± 50% variation of BAOI elastic modulus.

6.4 Discussion

The number of elastic properties required to properly define a model largely depends on the intended use and the research question. Since elastic properties were defined by converting HU value of CT image data with experimental equations, the accuracy of FE analyses was mostly dependent on the resolution of HU distribution of CBCT image data and the experimental equations which were used to define the relationship between HU and bone density and EP. The largest source of error were due to the relationships found in the literature (Lagravère et al, 2005; Rho and Hobatho, 1995) since, as expected, low correlation between density and EP were observed. The regression coefficients for Rho's relationships between density and elastic modulus were $R^2 = 0.95$ for distal femur and $R^2 = 0.54$ for mandible cortical bone specimens, which were used in this study for cancellous and cortical bone, respectively.

Results presented for 25 anatomical landmarks in this orthodontic representative treatment study show that when using more than 2 EP, von Mises stresses and strains results are within 54% and the displacement results are within 8% of the control model. In addition, these models have similar trends to the control model in terms of BAOI von Mises stress distribution along eight BA longitudinal lines. Again, the 2 EP scheme showed much higher stresses than the other schemes.

The importance of material heterogeneity can be seen between the two graphs of Figure 6-4, which shows the von Mises stresses and strains for each of the twenty five landmarks.

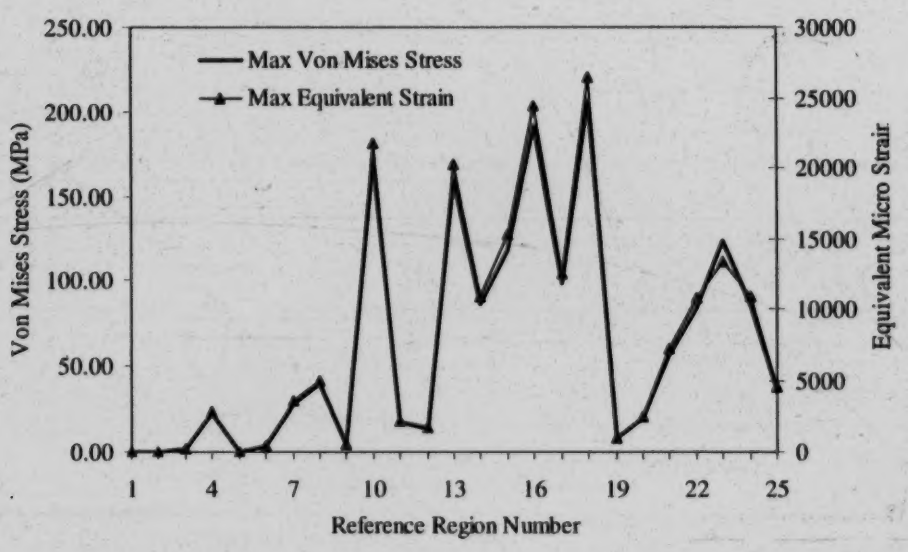

(a)

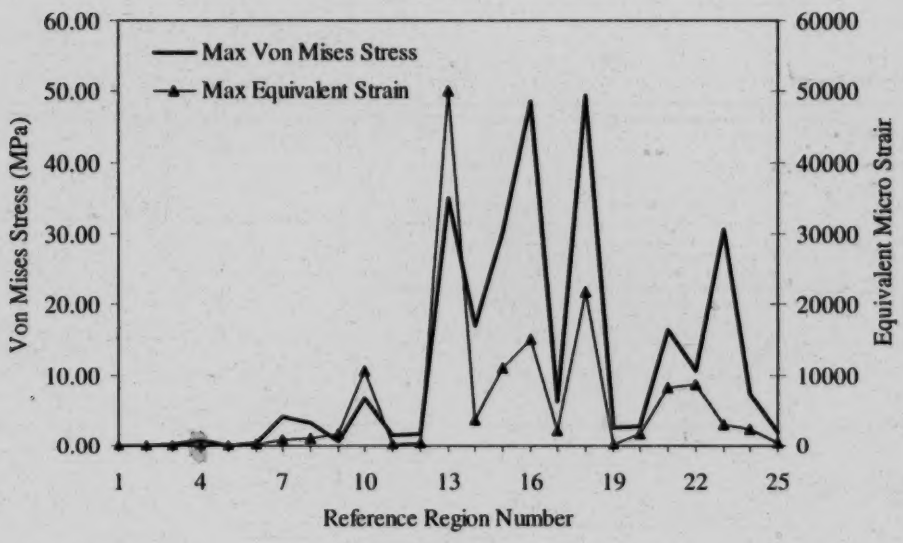

(b)

Figure 6-4: Von Mises stress and strain at 25 reference position for (a) 2 EP and (b) 156 EP.

Using 2 EP (Figure 6-4a) shows that the strain is always proportional to the stress; this indicates that the bone elastic modulus is constant over the surface of the skull, which does not realistically occur. Conversely, Figure 6-4b shows discrepancies between the stress and strain curve shape, a more plausible occurrence resulting from EP heterogeneity.

The purpose of the developed FE model is to offer clinicians a tool for predicting treatment outcome. The absence of experimental data to validate the FE model is problematic. To further verify the reliability of the results, the models were used to predict the force that would have been required to perform transverse maxillary expansion with using all five EP assignment schemes. A transverse horizontal force was assumed to be applied on the center of the BA neck. The forces calculated to obtain 4 mm unilateral transverse expansion were 285N, 285.4N, 412.8N, 603.7N and 1390N for 156, 78, 39, 20 and 2 (subject-specific) assigned EP, respectively. From maxillary expansion clinical literature, the reported cumulative force to obtain 8 mm total (4mm unilateral) expansion during a rapid maxillary expansion (RME) treatment was reported as approximately 100N (Ficarelli, 1978; Bell, 1982). Considering that RME is performed over the course of days, it can be said that the predicted forces from a single event 4mm unilateral expansion using 78 and 156 EP, 285N and 285.4N, are in good agreement with clinical situations considering the difference between the model and wet bone. The difference can be explained by difference in treatment time and the viscoelastic nature of bone.

From these results an argument can be made that, until better definition of the EP of soft tissue, be it craniofacial or other, models cannot be highly accurate and thus a low number of EP can be used without major detriment. It can also be argued that minimizing model-based uncertainty, by increasing the number of EP, considering the heterogeneity and anisotropy of the material and precisely representing the geometry can bring current models to the threshold of applicability and that studies which will better define specific bone EP will soon be available. Although the current 156 or 78 EP models do not address all of these concerns, it was shown that predictions converged and appeared more representative with clinically observed results. Conversely, it can be argued that depending on the requirements such as stress and strain evaluation, an argument can be made that 30% difference (20 EP case) is an acceptable difference to minimize model complexity since EPs obtained from the literature present such large levels of errors.

6.5 Conclusion

It was shown in this chapter that EP play a large role in the accuracy of a model but accurate experimental EP data is not yet available. This gives most predictions a high level of inherent error.

ME treatment is largely dependent on the force being applied to the craniofacial structure. The magnitude of effective force being applied to the bone anchors is largely dependent on the bone anchor inclination angle with respect to the wall of the palatine process. The effect of bone anchor inclination angle is studied in the next chapter.

CHAPTER 7 EVALUATION OF BONE ANCHOR IMPLANTATION INCLINATION ANGLE AND POSITION IN THE PALATE

7.1 Introduction

For maxillary expansion treatments using bone anchor, rigid endosseous bone anchors are ideal orthodontic anchorage conditions since they provide stable abutment for expansion load (Roberts et al, 1984, 1989; Gray et al, 1983). Following expansion force application to the BA, large stresses are induced in the Bone Anchor Osseointegrated Interface (BAOI). Loss of stable abutment can occur due to a failure of osseointegrated bone anchors, which mainly results from a large stress exceeding interface strength (Hoshaw et al, 1994; Duyck et al, 2001).

Previous studies have reported that the selection of the appropriate BA anchorage position and its inclination alignment is vital for the reduction of failure of oseointegrated BA. Based on literature and clinical experience, the BA anchorage positions should be chosen with high level of bone quality and quantity, with enough space between teeth to place bone anchor. During most clinical situations, an appropriate BA anchorage position ranges from 6 to 10mm from the mid-palatal suture and between the second premolar and first molar. The bone anchor long axis should be perpendicular to the surface of palatal bones. At that inclination condition,

the effective contact area between BA and surrounding bones as well as contact area between cap and surface of palatal bones is maximized and is optimal to reduce the stress concentration in BAOI.

However, clinically, a perfectly perpendicular alignment of the bone anchor long axis to surface of palatal bones is nearly unfeasible. In addition, for some subjects with existing space condition limitations between teeth, placing BA at an angle is necessary to prevent contact between BA and teeth roots. The objectives of this study were to investigate the influence of anchorage inclination angle (AIA) on von Mises stress distributed in bone-anchor osseointegration interface, verify the conceived notion that BA positioned perpendicular to the bone is optimal and assess the general effect of AIA on overall maxillary expansion treatment.

7.2 Materials and Methods

The 3D FE model presented is used to model an osseointegrated bone anchor at 6 different anchoring inclination angles (AIA). The CBCT data acquisition, segmenting and bony structure generation process was detailed in Chapter 3. The BA was modeled as a 3mm diameter cylinder with a 4mm BAOI effective length for every test case. The BA elastic modulus and major Poisson ratio of implant were defined as those of titanium (Table 3-1). BAs were placed in the palatal bone between 2nd premolar and 1st permanent molar teeth, where support bone is typically strong and plentiful (Bernhart et al, 2000). As shown in Figure 7-1a,b, using this configuration,

long axis of BAs would be optimally set perpendicular to palatal shelf of the maxillary bone to avoid teeth roots, roughly along the transverse (T) axis and inclined along the implant axis in the coronal view (Figure 7-1b).

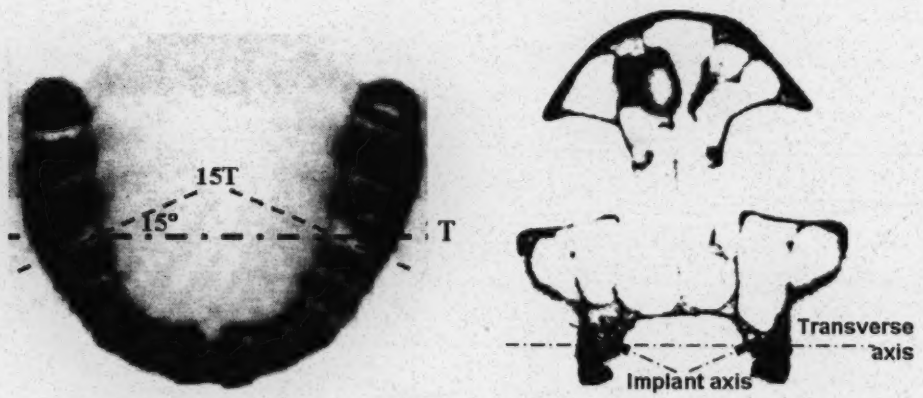

Figure 7-1: Schematic of implant anchorage position and inclination direction; a) BA long axis projection along transverse axis (T) and along a 15° offset from the transverse axis in the transverse plane (15T); b) implant anchorage position in skull in coronal view

BAOI was defined as perfectly bonded along the 4mm length and tip of the bone anchor. Solid tetrahedral elements were selected for bone anchor and BAOI. Functional osseointegrated BAs demonstrate interfacial bone density similar to that of the bone in which the bone anchor was placed (Albrektsson et al, 2001). An average of the heterogeneous elastic modulus of surrounding elements was used to define BAOI property. BA features such as threads were not included in the model. Such features are not deemed critical to larger models although it is recognized that they will cause stress concentration factors. It was assumed that threading was an integral

portion of the BAOI thickness and contributed to the validity of the perfect bonding assumption. The elastic modulus and Poisson's ratio used for the bone anchor are given in Table 3-1.

A total of six BA inclinations were considered. These were selected based on typical permissible bone anchor offset due to available maneuverability between teeth. Sectioned views of the skull and BA are presented in Figure 7-2 for clarification. The first three AIA conditions were modeled with bone anchor long axis located along a transverse axis positioned perpendicular to the surface of palatal bone (0-T), +10° (U10-T) or -10° (D10-T) in the vertical plane, respectively. The other three AIA conditions were modeled with bone anchor long axis located at a 15° offset in the vertical plane with bone anchor long axis perpendicular to surface of palatal bone (0-15T), +10° (U10-15T) or -10° (D10-15T) respectively.

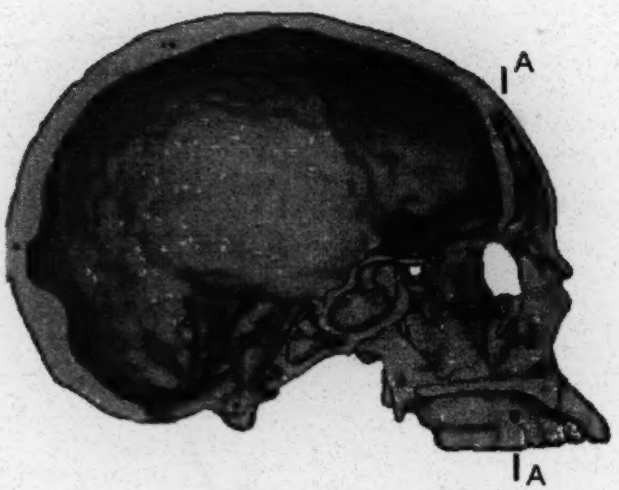

(a) Left view showing cut line AA

(b)

(b) Cross section view A-A for 3 anchoring inclination angles in the vertical plane

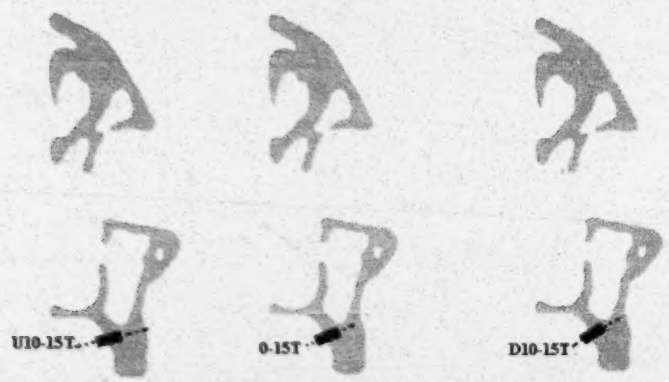

(c) Cross section view A-A for 6 anchoring inclination angles in the 15° offset vertical plane

Figure 7-2: FE skull model with 6 AIA conditions

As in previous chapters, to simulate a clinical 8mm total transverse expansion situation, a 4mm unilateral transverse displacement was applied to the bone anchor neck. A zero transverse displacement is defined on the model plane of symmetry. Since for adult patients, an osteotomy of maxillary suture surgery was carried out before expansion (Harzer et al, 2004), a free constraint was applied on the regions of maxillary suture. To eliminate rigid body motion, zero displacement constraint is defined at the peripheral region of the foramen magnum and posterior region of the symmetry plane.

7.3 Results

The study objectives were two-fold; namely, evaluate the effect of various anchorage inclination angles on BAOI stress and on anatomical landmark displacement expected from transverse expansion.

7.3.1 BAOI FE Predicted Stress Results

It is recognized that the lack of information on precise BAOI properties, and other EP issues raised in Chapter 6 are limitations of the model; however this holds true for all existing models since BAOI properties have yet to be accurately experimentally measured and will be patient and bone anchor material specific.

Expansion loads are transferred from the BA to the bone through the BAOI along all surfaces. Von Mises stresses at BAOI were analyzed along 8 lines (Figure 6-1a)

positioned every 45 along the longitudinal length of the BA for six AIA. The average and maximum stresses found at each inclination are presented in Figure 7-3 and Figure 7-4. No singular pattern emerges from the data of as to a common line on which the maximum stress occurs for any of the six AIA; what is apparent is that higher maximum and average stresses occur at a 15° offset from the transverse axis. However, from observation of the results, no statistically significant difference can be found between the results.

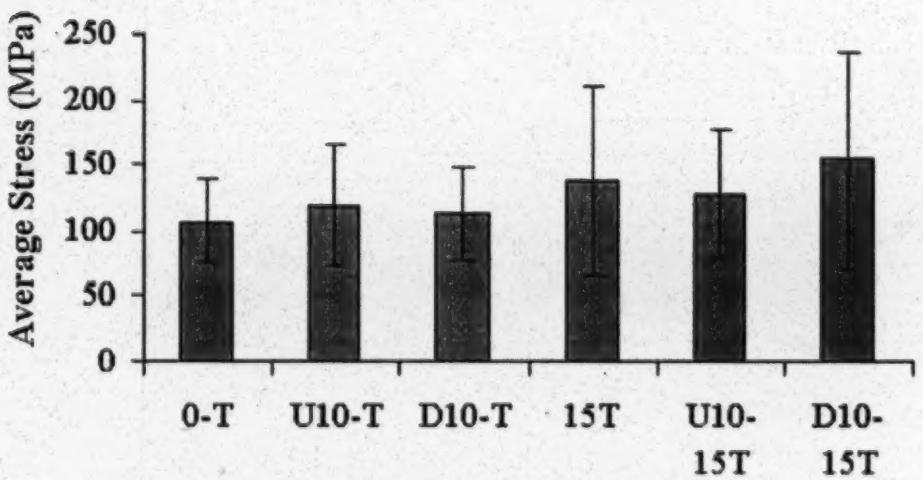

Figure 7-3: Average stress and standard deviations on BA

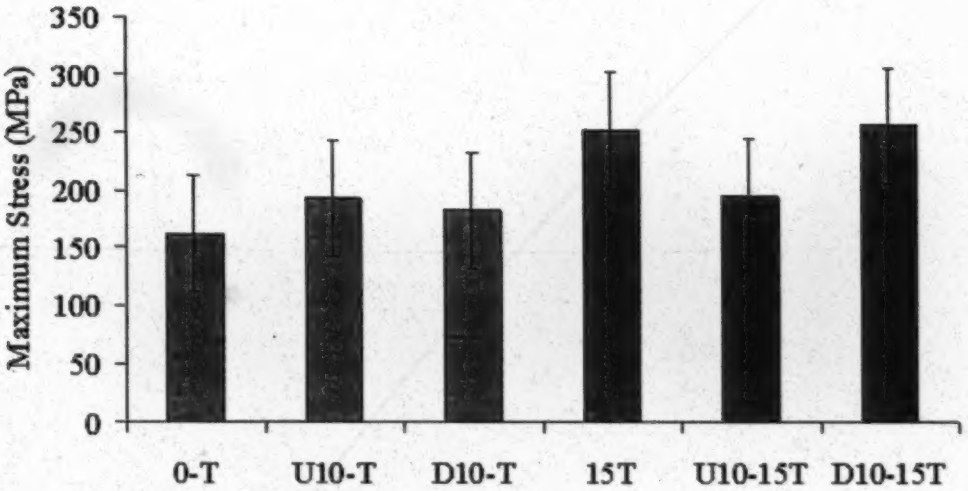

Figure 7-4: Average maximum stress

In Figure 7-5 are presented the results for two BAOI longitudinal lines (5 and 8) which represent the range of results (full results in Appendix 3). The majority of the maximum stresses occurred at the neck of the BA at the inner wall of the maxilla - where BA protrudes from the bone. Most of the stress distributions along the eight BAOI longitudinal lines of analysis showed peaks at both extremities with a gradual decrease inwards from the edges. This is expected since stress concentrations are cause by changes in material properties or abrupt dimensional variations as well as by off-axis loading causing force-couples and localized compressive stresses. At these positions micro cracks could develop and lead to a BAOI failure from an excessive load. High stresses were also present at the distal end surface (inside the bone) of the BA where the transverse compressive load is transmitted from the BA to the bone.

The largest stress (255MPa) was measured at line 5 for the case D10-15T. Also noticeable was the occurrence of the maximum stress at 0.2mm from the neck (0.0mm-position) for some loading patterns (0-T, U10-T, U10-15T Figure 7-5a). AIA had little to no effect on the stress past 0.8mm. Stresses were nearly constant. The lowest maximum stresses were found at line 8 (Figure 7-5b). AIA slightly affected the position of the minima of the curves presented for line 8; however, overall, stresses were very similar in range and average.

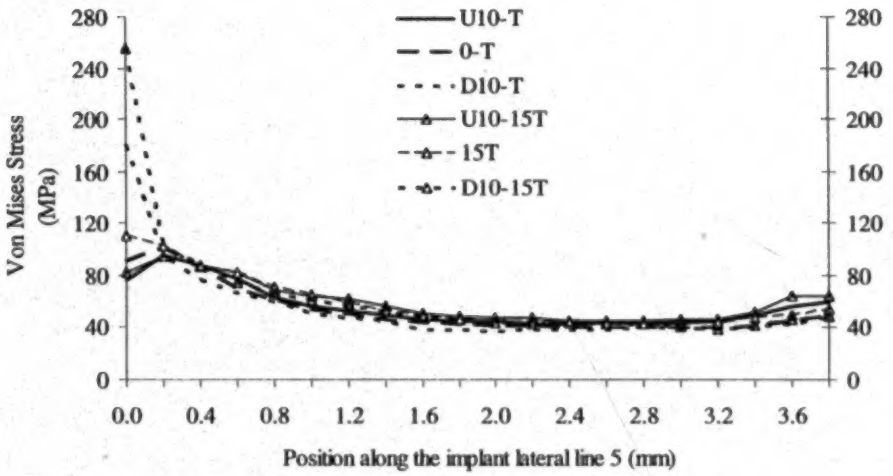

(a)

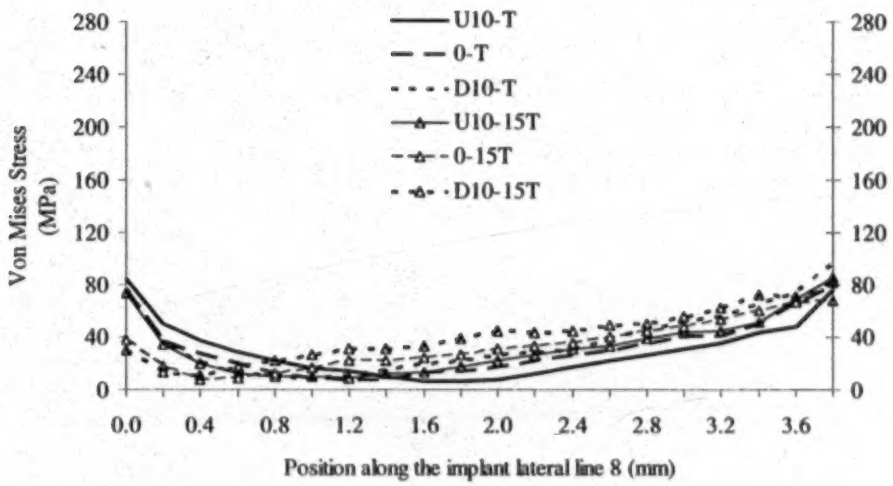

(b)

Figure 7-5: Stress distribution in BAOI from model with 6 implantation inclination angles found along (a) line 5 and (b) line 8.

7.3.2 Predicted Expansion Treatment Results

In Table 7-1 and Table 7-2 are presented the results of total displacement and von Mises stresses, respectively, for twenty five (25) anatomical landmarks shown in Figure 5-2. For this comparison, AIA 0-T was selected as control since it is generally agreed to be the target clinical AIA. There were very little difference of displacement; the average resultant difference between 0-T results and other AIA were equal or less than 0.25%. A maximum difference of 1.37% with an original displacement of 5.11 mm for region 7 was found for the D10-15T AIA. Average resultant differences in Von Mises stresses differences between control and five AIA were all less than 2%; however, differences of up to 9.6% were found at region 4, the upper first molar (0.94 MPa versus 0.85 MPa).

Table 7-1: Displacement distribution under 6 implantation inclination angles. Comparison is done with 0-T, clinically accepted AIA.

	0-T	U10-T		D10-T		U10-15T		0-15T		D10-15T	
Regions	mm	mm	%	mm	%	mm	%	mm	%	mm	%
1	5.11	5.09	0.39	5.16	0.98	5.11	0.00	5.14	0.59	5.18	1.37
2	4.82	4.81	0.21	4.85	0.62	4.82	0.00	4.84	0.41	4.87	1.04
3	4.67	4.65	0.43	4.69	0.43	4.66	0.21	4.67	0.00	4.7	0.64
4	4.34	4.34	0.00	4.35	0.23	4.33	0.23	4.33	0.23	4.34	0.00
5	4.64	4.62	0.43	4.67	0.65	4.63	0.22	4.65	0.22	4.68	0.86
6	4.37	4.35	0.46	4.39	0.46	4.36	0.23	4.38	0.23	4.4	0.69
7	4.21	4.2	0.24	4.22	0.24	4.2	0.24	4.21	0.00	4.23	0.48
8	4.13	4.13	0.00	4.14	0.24	4.12	0.24	4.12	0.24	4.13	0.00
9	4.23	4.22	0.24	4.25	0.47	4.23	0.00	4.24	0.24	4.26	0.71
10	3.87	3.86	0.26	3.87	0.00	3.86	0.26	3.86	0.26	3.86	0.26
11	4.09	4.08	0.24	4.1	0.24	4.08	0.24	4.09	0.00	4.1	0.24
12	3.77	3.77	0.00	3.76	0.27	3.75	0.53	3.75	0.53	3.75	0.53
13	3.49	3.48	0.29	3.49	0.00	3.48	0.29	3.49	0.00	3.5	0.29
14	1.37	1.37	0.00	1.37	0.00	1.36	0.73	1.37	0.00	1.36	0.73
15	1.08	1.08	0.00	1.07	0.93	1.07	0.93	1.07	0.93	1.07	0.93
16	1.31	1.31	0.00	1.31	0.00	1.31	0.00	1.31	0.00	1.31	0.00
17	0.82	0.82	0.00	0.82	0.00	0.81	1.22	0.81	1.22	0.81	1.22
18	1.1	1.1	0.00	1.1	0.00	1.1	0.00	1.1	0.00	1.1	0.00
19	0.11	0.11	0.00	0.11	0.00	0.11	0.00	0.11	0.00	0.11	0.00
20	2.36	2.36	0.00	2.35	0.42	2.35	0.42	2.35	0.42	2.34	0.85
21	3.55	3.56	0.28	3.54	0.28	3.53	0.56	3.52	0.85	3.51	1.13
22	0.24	0.24	0.00	0.24	0.00	0.24	0.00	0.24	0.00	0.24	0.00
23	0.61	0.61	0.00	0.61	0.00	0.61	0.00	0.61	0.00	0.61	0.00
24	1.3	1.3	0.00	1.3	0.00	1.3	0.00	1.3	0.00	1.3	0.00
25	0.27	0.27	0.00	0.27	0.00	0.27	0.00	0.27	0.00	0.27	0.00

Table 7-2: Stress (MPa) distribution through the skull under 6 implantation inclination angles. Comparison is done with 0-T, clinically accepted AIA.

Regions	0-T	U10-T		D10-T		U10-15T		0-15T		D10-15T	
	MPa	MPa	%	MPa	%	MPa	%	MPa	%	MPa	%
1	0.00	0.00	0.0	0.00	0.0	0.00	0.0	0.00	0.0	0.00	0.0
2	0.02	0.02	0.0	0.02	0.0	0.02	0.0	0.02	0.0	0.02	0.0
3	0.29	0.3	3.4	0.28	3.4	0.3	3.4	0.29	0.0	0.28	3.4
4	0.94	0.96	2.1	0.9	4.3	0.89	5.3	0.88	6.4	0.85	9.6
5	0.06	0.06	0.0	0.06	0.0	0.06	0.0	0.06	0.0	0.06	0.0
6	0.39	0.4	2.6	0.38	2.6	0.4	2.6	0.4	2.6	0.39	0.0
7	4.09	4.1	0.2	4.05	1.0	4.19	2.4	4.17	2.0	4.13	1.0
8	3.31	3.41	3.0	3.16	4.5	3.34	0.9	3.26	1.5	3.12	5.7
9	0.71	0.71	0.0	0.69	2.8	0.71	0.0	0.71	0.0	0.7	1.4
10	6.59	6.59	0.0	6.59	0.0	6.48	1.7	6.47	1.8	6.48	1.7
11	1.43	1.41	1.4	1.45	1.4	1.39	2.8	1.42	0.7	1.42	0.7
12	1.79	1.79	0.0	1.77	1.1	1.73	3.4	1.73	3.4	1.71	4.5
13	34.90	34.78	0.3	35.03	0.4	34.86	0.1	34.99	0.3	35.12	0.6
14	16.96	16.96	0.0	16.92	0.2	16.9	0.4	16.9	0.4	16.86	0.6
15	30.31	30.29	0.1	30.28	0.1	30.22	0.3	30.24	0.2	30.22	0.3
16	48.50	48.47	0.1	48.45	0.1	48.34	0.3	48.36	0.3	48.33	0.4
17	6.22	6.21	0.2	6.23	0.2	6.2	0.3	6.21	0.2	6.22	0.0
18	49.35	49.31	0.1	49.3	0.1	49.19	0.3	49.22	0.3	49.18	0.3
19	2.53	2.53	0.0	2.53	0.0	2.52	0.4	2.52	0.4	2.52	0.4
20	2.81	2.82	0.4	2.76	1.8	2.78	1.1	2.76	1.8	2.72	3.2
21	16.36	16.54	1.1	15.86	3.1	16.11	1.5	15.9	2.8	15.44	5.6
22	10.63	10.62	0.1	10.63	0.0	10.6	0.3	10.61	0.2	10.61	0.2
23	30.57	30.56	0.0	30.52	0.2	30.46	0.4	30.47	0.3	30.43	0.5
24	7.39	7.36	0.4	7.45	0.8	7.39	0.0	7.42	0.4	7.48	1.2
25	1.87	1.86	0.5	1.89	1.1	1.88	0.5	1.89	1.1	1.91	2.1

7.4 Discussion

The model applies a clinically representative unilateral displacement of 4mm to the BA. Assuming the expansion appliance to be rigid, expansion displacement is more representative than applying an expansion force to BA.

Results show that anchorage inclination angle does have an affect on the stress level at the bone anchor osseointegration interface. This is not unexpected since a 4mm unilateral expansion is applied at BA; this study shows that at different AIA, BAOI failure is possible since stress levels are sufficiently high. BAOI strength is typically associated with compressive stresses (Watanabe et al, 2003). It has been previously reported (Brochers et al, 1983) that upper limit for bone remodeling was 24.5 MPa in compression. Buser et al (1999) found, depending on surface morphology, that implant removal torque ranged 0.13 to 1.56 Nm, which represents failure shear stresses of 24.5 to 294.3 MPa for a 3mm diameter BA using typical torque/shear stress equations. These results accentuate the importance of proper alignment of BA. Von Mises stress levels seen in Figure 7-3 and Figure 7-4 are caused by a combination of compressive and shear stresses. However, the stress levels presented can be slightly misleading since ME is a progressive process. Expansion is performed up to a rate of 0.25 to 0.5mm every day permitting bone to remodel and alleviate internal and residual stresses which this model cannot yet do. It can be shown that if 0.5mm of unilateral expansion was applied, the stresses would be an eighth of the stresses from 4mm of unilateral expansion because of the linear elastic material assumptions.

Referring to Figure 7-3 and Figure 7-4 this would indicate that most stresses would be below 24.5MPa; only lines 3 and 7 at AIA 15T and lines 5 and 6 at AIA D10-15T could possibly fail under these conditions, assuming the stresses are entirely compressive, which is improbable. In addition, it is unlikely that stresses at the BA neck would necessarily lead to BAOI failure since over the length of the interface stresses are within acceptable range.

7.5 Conclusion

It is apparent that AIA offset with the transverse axis in the transverse plane should be avoided as BAOI stresses were greater. Most misalignment will lead to couples being applied to BAOI, an undesirable effect since it causes a decrease in ME effective expansion loads. When the clinical situation has two axes of misalignment such as in the three 15T cases, greater expansion loads will be needed to obtain similar maxillary expansion, this could lead to BAOI failure. Results also show that AIA has very little effect on the efficacy of the treatment as compared to previous results found in the literature (Jafari et al, 2003).

This work leads to a better understanding of influence of AIA conditions on the stress induced during maxillary expansion treatments using bone anchor abutments. Placing bone anchors in perpendicular to the wall of the maxillary bone is optimal to reduce the quantity of stress in BAOI. If an offset is necessary to prevent bone anchor teeth root contact, upward rotation is recommended as an alternative since the BAOI

stresses are lower. The optimal AIA conditions could lead to a decrease in anchorage failure rates due to interface failure. Finally, AIA has little effect on the efficacy of the treatment; displacement of bony structures was largely unaffected.

CHAPTER 8 SUMMARY, CONCLUSIONS AND FUTURE WORK

8.1 Summary

The present work focused on developing a preliminary subject-specific 3D FE skull model and used the model to predict the displacement, stress and strain distribution in craniofacial as well as stress distribution in BAOI following a bone anchor assisted maxillary expansion. The model was verified through the literature and experimental work. FE model was used to determine the influence of elastic properties and to evaluate the influence of anchorage inclination angles on stress distribution in BAOI.

8.1.1 Development of a 3D FE Model of Skull with Bone Anchors

The FE model developed in this work is an accurate representation of the geometric features and heterogeneous bone properties of the scanned skull. A CBCT scan was used to obtain the original image data of a skull. The ScanIP&FE^{TM} imaging processing program was utilized to establish a 3D FE model by automatically segmenting bone tissues from every 2D image slices and generating the elements. The bone elastic properties were defined by converting the HU value of individual pixels with experimental equations and assigned to corresponding individual element as well. The bone anchor was modeled simulating a perfect osseointegration condition. Besides the above advanced merits, other advantages of the developed FE model

include small element size which leads to a better convergence of FE analysis, as well as the smooth surfaces consisting of tetrahedral elements.

8.1.2 Finite Element Analysis of Maxillary Expansion Treatments

The biomechanical response including the craniofacial deformation, stress and strain distribution was simulated and analyzed. The craniofacial deformations matched well with experimental results and predicted results found in the literature. The strain and stress distributions were clearly indicative of assessed patient treatment pain responses. Due to the heterogeneous bone properties of the model, the stress induced in craniofacial bones have the same trends as results found in previous studies.

8.1.3 Effect of Elastic Properties

The objective of this secondary study was to evaluate the influence of using different Elastic Properties on the displacement, stress and strain predictions at twenty five anatomical landmarks and on stress predictions at the Bone Anchor Osseintegrated Interface (BAOI). It was hypothesized that the number of elastic properties would have an effect on predicted maxillary expansion treatment anatomical landmark displacement, von Mises stresses and strains. Five different FE models were built with 78, 39, 20 and 2 (literature and subject-specific defined respectively) elastic properties assigned based on the Hounsfield unit value distribution obtained from CBCT image data. By comparing the FE analysis from these models with the control (156 EPs), it was found that elastic property assignment present an insignificant effect

on the resultant displacement distribution, while stress and strain distributions are sensitive to it. The FE models assigned with heterogeneous elastic properties, specifically with 156 and 78 elastic properties, were more reliable for the FE analysis of BA-ME treatments

8.1.4 Effect of Anchorage Inclination Angles of Bone Anchors

The approach used in the 1st study was used to investigate the influence of anchorage inclination angle on the stresses distributed in the bone-anchor osseointegration interface, and on overall maxillary expansion. For this study it was hypothesized that the optimal anchorage inclination condition would be perfect perpendicular alignment with the bone surface. Six anchorage inclination angles were modeled and evaluated. It was found that placing bone anchors perpendicular to the wall of the maxillary bone is optimal to reduce the quantity of stress in BAOI. If an offset is necessary to prevent bone anchor teeth root contact, upward rotation is recommended as an alternative. Little difference was observed in the maxillary expansion treatment displacement and stress levels in craniofacial structures due to inclination angle variations for small expansion increments (0.5mm). This confirms the clinical 0.5mm per two days incremental expansion process; greater increments could lead to BAOI failure.

8.2 Conclusion

The three dimensional FE model developed to simulate maxillary expansion using bone anchors was shown to provide an excellent representation of the maxillary expansion process. It exhibits the trends for strains measured during experiments on fresh skulls and stress-induced pain observed in patients. The use of 156 material properties provides more plausible results than earlier models. The principle objective of this work was to develop an initial FE skull model that will eventually be used to predict patient specific treatment outcomes. The model does have some limitations. In its current state it could not be used by clinicians to predict treatment for the following reasons:

- The work required to define the model from a CBCT scan is too complex. However, this proof-of-concept model has demonstrated that once the FE model production process is fully automated, the work will have clinical relevance.
- The model cannot be relevant until craniofacial bone elastic properties are accurately determined experimentally accounting for the large variations.
- The model must account for bone orthotropic behaviour.

This work lead to a better understanding of influence of AIA conditions on the stress induced during transverse expansion. Transverse maxillary expansion was selected as a representative orthodontic treatment; however, the model and its results can be extrapolated to other similar treatments using bone anchor abutments.

8.3 Future Work

The role of elastic properties has been partially shown in this work. However because of the absence of literature in craniofacial elastic properties, future effort is required to build an acceptable database of elastic properties. As other relevant studies stated, most bone tissues have anisotropicéorthotropic behaviour, this should be considered in future work. This will also require future imaging processing programs, such as Simpleware™, to provide techniques to accurately define bone anisotropic properties. Furthermore, since live bone is adaptive, future work will also be required to focus on analyzing the effect of the viscoelastic properties of bones as well as modeling time dependent effects during slow maxillary expansion process. ME-BA treatments are mostly used with young patients. Since the tissue morphology and properties of craniofacial sutures are very different from surrounding connective bones, it is necessary to evaluate the effect of treatments on the craniofacial sutures including their deformation and stress distributions, therefore a future model is required to represents the tissue morphology and properties of craniofacial sutures to reach this end. Once a skull model includes the above considerations, *in vivo* orthodontic treatment studies should be performed to validate the patient-specificity of the FE model. Finally, the elastic properties of BAOI and the failures of BA osseointegration conditions are also required further studies.

REFERENCES

Albrektsson, T., Johansson, C., 2001. Osteoinduction, osteoconduction and osseointegration. European Spine Journal, 10, Suppl 2: S96-101.

Athanasiou, A.E., 1995. Orthodontic cephalometry. Mosby-Wolfe, Baltimore.

Au, A.G., Huang, X.H., Carey, J., Lambert, R.G., Amirfazli, A., 2006. Towards a patient specific finite element model for knee bones, Canadian Society for Mechanical Engineering, accepted. Kananaskis, AB, CA, May 21-23, 2006.

Barker, D.S., Netherway, D.J., Krishnan, J., Hearn, T.C., 2005. Validation of a finite element model of the human metacarpal. Medical Engineering & Physics, 27(2):103-113.

Bell, R.A., 1982. A review of maxillary expansion in relation to rate of expansion and patient's age. American Journal of Orthodontics, 81(2), 32-37.

Bernhart T, Freudenthaler J, Dortbudak O, Bantleon HP, Watzek G., 2001. Short epithetic implants for orthodontic anchorage in the paramedian region of the palate. A clinical study. Clinical Oral Implants Research, 12(6):624-631

Bernhart, T., Vollgruber, A., Gahleitner, A., Dortbudak, O., Haas, R., 2000. Alternative to the median region of the palate for placement of an orthodontic implant. Clinical Oral Implants Research, 11(9): 595-601.

Branemark PI, Aspegren K, Breine U, 1964. Microcirculatory studies in man by high resolution vital microscopy. Angiology, 15:329-332

Branemark PI, Adell R, Breine U, Hansson BO, Lindstrom J, Ohlsson A, 1969. Intra-osseous anchorage of dental prostheses. I. Experimental studies. Scandinavian Journal of Plastic & Reconstructive Surgery, 3(2):81-100

Branemark PI, Breine U, Hallen O, Hanson B, Lindstrom J, 1970. Repair of defects in mandible. Scandinavian Journal of Plastic & Reconstructive Surgery, 4(2):100-108

Branemark PI, Lindstrom J, Hallen O, Breine U, Jeppson PH, Ohman A, 1975. Reconstruction of the defective mandible. Scandinavian Journal of Plastic & Reconstructive Surgery, 9(2):116-128

Branemark PI, Hansson BO, Adell R, Breine U, Lindstrom J, Hallen O, 1977. Osseointegrated implants in the treatment of the edentulous jaw. Experience from a 10-year period. Scandinavian Journal of Plastic & Reconstructive Surgery, Supplement, 16:1-132

Breine U, Branemark PI, 1980. Reconstruction of alveolar jaw bone. An experimental and clinical study of immediate and preformed autologous bone grafts in combination with osseointegrated implants. Scandinavian Journal of Plastic & Reconstructive Surgery, 14(1):23-48.

Brochers, L. and Reichant, P., 1983. Three-dimensional stress distribution around a dental implant at different stages of interface development. Journal of Dental Research 62(2):155–9

Brosh, T., Vardimon, A.D., Ergatudes, C., Spiegler, A., Lieberman, M., 1998. Rapid palatal expansion. Part 3: Strains developed during active and retention phases. American Journal of Orthodontics and Dentofacial Orthopedics, 114(2):123-133

Buser, D., Nydegger, T., Oxland, T., Cochran, D.L., Schenk, R.K., Hirt, H.P., Snetivy, D., and Nolte, L.P., 1999. Interface shear strength of titanium implants with a sandblasted and acid-etched surface: a biomechanical study in the maxilla of miniature pigs. Journal of Biomedical Materials Research, 45(2):75-83.

Cattaneo, P.M., Dalstra, M., Frich, L.H., 2001. A three-dimensional finite element model from computed tomography data: a semi-automated method. Proceedings of the Institution of Mechanical Engineers, Part H, Journal of Engineering in Medicine, 215(2): 203-213

Chang, Wei-Chun; Linden, M.J.; Robbins, S.; Mayott, C.; Engler, P., 1993. Computer aided stress analysis of the femur with prosthetic hip stem utilizing computed tomography. Proceedings of the Northeast Conference, IEEE 19th Annual Northeasrt Bioengineering Conference, 60-61

Chen X. and Chen H., 1998. The influence of alveaolar structures on the torsional strain field in a gorilla corporeal cross-section. Journal of Human Evolution, 35(6): 611-633.

Coleman, J.C., Roberts, M.D, 2000. Solid model creation from CT image data, Technical report TU-Bone-2000-03, Bone Tissue Mechanics Lab, Department of Biomedical Engineering, Tulane University

Coleman, J.C., Hart, RT., Owan, I, Tankano, Y, Burr, DB, 2002. Characterization of dynamic three-dimensional strain fields in the canine radius. Journal of Biomechanics 35(12): 1677-1683.

Currey JD, 1988. The effect of porosity and mineral content on the Young's modulus of elasticity of compact bone. Journal of Biomechanics 21(2):131-9

Danforth RA, Dus I, Mah J, 2003. 3-D volume imaging for dentistry: a new dimension. Journal of the California Dental Association, 31(12):817-823.

Duyck, J., Renold, H.J., Van Oosterwyck, H., Naert, I., Vander Sloten, J., Ellingsen, J.E., 2001. The influence of static and dynamic loading on the marginal bone behaviour around implants: an animal experimental study. Clinical Oral Implant Research, 12(3):207-218

Erverdi, N., Okar, I., Kucukkeles, N., Arbak, S., 1994. A comparison of two different rapid palatal expansion techniques from the point of root resorption. American Journal of Orthodontics and Dentofacial Orthopedics, 106(1), 47-51.

Fang Y., Lagravère M.O., Carey J., Major P.W., Amirfazli, A., Evaluation of materials properties effect on finite element maxillary expansion model. Journal of Biomechanics Submitted 2006

Fang, Y., Lagravère, M.O., Carey, J., Major, P.W., Toogood R., 2005. A new method for developing accurate three dimensional finite element model of skull based on CT imaging data: Application to maxillary expansion treatment, Society of Craniofacial Genetics, 28th Annual Meeting and Scientific Symposium, Salt Lake City, Utah.

Ficarelli, J.P., 1978. A brief review of maxillary expansion. Journal of Pedodontics, 3(1): 29-35.

Finnigan, P., Hathaway, A., Lorensen, W., 1990. Merging CAT and FEM, Mechanical Engineering, 112(7): 32-38.

Gray, J.B., Steen, M.E., King, G.J., Clark, A.E., 1983. Studies on the efficacy of implants as orthodontic anchorage. American Journal of Orthodontics, 83(4): 311-317.

Gupta, S., van der Helm, F.C.T., Sterk, J.C., van Keulen, F., Kaptein, B.L., 2004. Development and experimental validation of a three-dimensional finite element model of the human scapula. Proc. Institution of Mechanical Engineers, Part H: Journal of Engineering in Medicine, 218(2):127-142.

Hansson HA, Albrektsson T, Branemark PI, 1983. Structural aspects of the interface between tissue and titanium implants. Journal of Prosthetic Dentistry, 50(1):108-113.

Harzer, W., Schneider, M., Gedrange, T., 2004. Rapid maxillary expansion with palatal anchorage of the hyrax expansion screw—Pilot study with case presentation. Journal of Orofacial Orthopedics, 65(5), 419-24.

Hekimoglu, C., Anil, N., Cehreli, M.C., 2004. Analysis of strain around endosseous

dental implants opposing natural teeth or implants. The Journal of Prosthetic Dentistry 92(5):441-6

Holberg, C., 2005. Effects of rapid maxillary expansion on the cranial base-an FEM analysis. Journal of Orofacial Orthopedics, 66(1): 54-66.

Hoshaw, S.J., Brunski, J.B., Cochran, G.V.B., 1994. Mechanical loading of Branemark implants affects interfacial bone modeling and remodeling. International Journal of Oral Maxillofacial Implants, 9:345-360

Iseri, H., Tekkaya, A.E., Oztan, O., Bilgic, S., 1998. Biomechanical effects of rapid maxillary expansion on the craniofacial skeleton, studied by the finite element method. European Journal of Orthodontics, 20(4): 347-356.

Jaecques, S.V.N, Muraru, L., Lierde, C.Van, De Smet, E., Van Oosterywck, H, M. Wevers, I., 2004. In vivo micro-CT-based FE models of guinea pigs with titanium implants: an SLT-based approach. International Congress Series, 1268:579-583

Jafari, A., Shetty, K.S., Kumar, M., 2003. Study of stress distribution and displacement of various craniofacial structures following application of transverse orthopedic forces--a three-dimensional FEM study. Angle Orthodontics, 73(1):12-20.

Johnson, E.A.C., Young, P.G., 2005. On the use of a patient-specific rapid prototyped model to simulate the response of the human head to impact and comparison with analytical and finite element models from serial MR images. Journal of Biomechanics, 38(1):39-45.

Koca OL., Eskitascioglu G., Usumez A., 2005. Three-dimensional finite-element analysis of functional stresses in different bone locations produced by implants placed in the maxillary posterior region of the sinus floor. Evaluation Studies. Journal of Prosthetic Dentistry, 93(1):38-44

Lagravère, M.O., Fang, Y., Carey, J., Major, P.W., 2005. Density conversion factor determined from cone-beam computer tomographer NewTom 9000. (in print) Dentomaxillofacial Radiology.

Lavernia, C. J.; Cook, S. D.; Weinstein, A. M.; Klawitter, J. J.,1981. Analysis of stresses in a dental implant system. Journal of Biomechanics, v 14, n 8, 555-560

Lim, D., Seliktar R., Sun, W., Holman, J., Nunes, L., 2002. Finite element (FE) modeling of the shoulder complex: A pilot study using the realistic Mechanical Parameters, Loading and Boundary Conditions. 4th Meeting of the International Shoulder Group, Cleveland, OH, June 17-18.

Major, P.W., Johnson, D.E., Hesse, K.L., Glover, K.E., 1994. Landmark identification error in posterior anterior cephalometrics. Angle Orthodontics, 64(6): 447-454.

Major, P.W., Maxillary expansion with an implant bone borne appliance, and in vitro skull pilot study, HREB file number B-240704, approved July 2005

McNamara, James A., 2000. Maxillary transverse defiency, American Journal of Orthodontics and Dentofacial orthopedics. 117(5): 567-570

Mehta B. V., Rajani S., Sinha G, 1997. Comparison of image processing techniques (magnetic resonance imaging, computed tomography scan and ultrasound) for 3D modeling and analysis of the human bones. Journal of Digital Imaging, 10(3), sup 1:203-206

Movassaghi K, Altobelli DE, Zhou H, 1995. Frontonasal suture expansion in the rabbit using titanium screws. Journal of Oral & Maxillofacial Surgery, 53(9):1033-42

Norton MR, Gamble C, 2001. Bone classification: an objective scale of bone density using the computerized tomography scan. Clin Oral Implants Res 12:79-84.

Nuno, N.; Amab Nuno, N.; Amabili, M., 2002. Modelling debonded stem-cement interface for hip implants: Effect of residual stresses. Clinical Biomechanics, v17, n1, 41-48

Parr, J.A., Garetto, L.P., Wohlford, M.E., Arbuckle, G.R., Roberts, W.E., 1997. Sutural expansion using rigidly integrated endosseous implants: an experimental study in rabbits. Angle Orthodontics, 67(4):283-290.

Peterson, J., and Dechow, P.C., 2003. Material properties of the human cranial vault and zygoma. Anatomical Record, Part A: Discoveries in Molecular, Cellular, & Evolutionary Biology, 274(1):785-97.

Provatidis, C., Georgiopoulos, B., Kotinas, A., McDonald, J.P., 2003a. Simplified finite element model for the simulation of relaxation during rapid maxillary expansion. Integrated systems in dental healthcare, European Symposium, May, 29-31.

Provatidis, C., Georgiopoulos, B., Kotinas, A., McDonald, J.P., 2003b. In-vitro validation of a FEM model for craniofacial effects during rapid maxillary expansion. Proceedings of the IASTED International Conference on Biomechanics, 68-73.

Pugh, J. W.; Rose, R. M.; Radin, E. L., 1973. Structural model for the mechanical behavior of trabecular bone. Journal of Biomechanics, v 6, n 6, Nov 657-670

Reddi AH, Wientroub S, Muthukumaran N., 1987. Biologic principles of bone induction. Orthopedic Clinics of North America, 18(2):207-12,.

Rho, J.Y., Hobatho, M.C., 1995. Relations of mechanical properties to density and CT numbers in human bone, Medical Engineering and Physics, 17(5):347-355.

Rice JC, Cowin SC, Bowman JA,1988. On the dependence of the elasticity and strength of cancellous bone on apparent density. Journal of Biomechanics, 21(2):1231-6

Roberts, W.E., Smith, R.K., Zilberman, Y., Mozsary, P.G., Smith, R.S., 1984. Osseous adaptation to continuous loading of rigid endosseous implants. American Journal of Orthodontics, 86(2): 95-111.

Roberts, W.E., Helm, F.R., Marshall, K.J., Gongloff, R.K., 1989. Rigid endosseous implants for orthodontic and orthopedic anchorage. Angle Orthodontics, 59(4): 247-256.

Schaffler MB. Burr DB, 1988. Stiffness of compact bone: effects of porosity and density. Journal of Biomechanics, 21(1):13-6.

Schiel HJ, Klein J, Widmer B, 1996. Das enossale implantat als kieferorthopadisches verankerungselement. Zeitschrift fur Zahnarztliche Implantologie, 12:183-188

Shapiro, P.A., Kokich, V.G., 1989. Uses of implants in orthodontics. Dental Clinics of North America, 32(2):539-550.

Smalley, W.M., Shapiro, P.A., Hohl, T.H., Kokich, V.G., Branemark, P.I., 1988. Osseointegrated titanium implants for maxillofacial protraction in monkeys. American Journal of Orthodontics and Dentofacial Orthopedics, 94(4):285-295.

Snyder SM., Schneider E., 1991. Estimation of mechanical properties of cortical bone by computed tomography. Journal of Orthopaedic Research, 9(3):422-431

Strait, D.S., Wang,Q., Dechow, P.C., 2005. Modeling elastic properties in finite element analysis: How much precision is needed to produce an accurate model? Anatomical Record, Part A, Discoveries in Molecular, Cellular, & Evolutionary Biology, 283(2):275-87.

Tanne, K., Hiraga, J., Kakiuchi, K., Yamagata, Y., Sakuda, M., 1989. Biomechanical effect of anteriorly directed extraoral forces on the craniofacial complex: a study using the finite element method. American Journal of Orthodontics and Dentofacial Orthopedics, 95(3): 200-2007.

Tanne, K., 1991. Biomechanical responses of craniofacial and alveolar bones to mechanical forces in orthodontics. Interfaces in medicine and mechanics, 2:299-308.

Thomason, J.J., Grovum L.E., Deswysen, A.G., Bignell, W.W., 2001. In vivo surface strain and stereology of the frontal and maxillary bones of sheep: Implications for the structural design of the mammalian skull. Anatomical record, 264(4):325-338

Ulrich, D., Rietbergen, B., Laib, A., Ruegsegger, P., 1998. Mechanical analysis of bone and its microarchitecture based on in vivo voxel images. Technology and Health Care, 6(5-6):421-427

Watanabe, F., Hata, Y., Komatsu, S., 2003. Finite element analysis of the influence of implant inclination, loading position, and load direction on stress distribution. Odontology, 91(1):31-36

Weber, I., Yong, P.G., 2004. Automating the generation of 3D finite element models based on medical imaging data: application to head impact, Simpleware Ltd.

Yacoub N., Mao, J.J., 1999. Transmission of bone strain in the craniofacial bones of edentulous human skulls upon dental implant loading. Annual Meeting of the International Association for Dental Research, Vancouver, Canada

Zienkiewicz, O.C., Taylor, R.L., 2000. The finite element method. 5th edition, Volume 1: The Basis, Oxford, Boston, Butterworth-Heinemann.

APPENDIX 1

Effect of number of EP on Von Mises stress along BA longitudinal lines

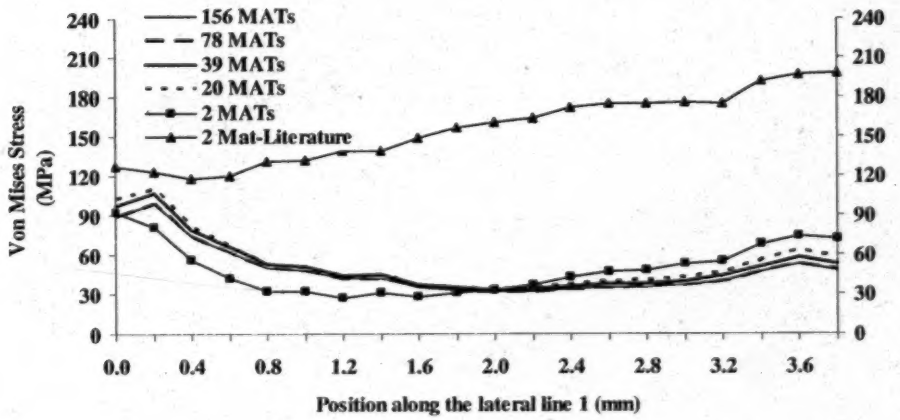

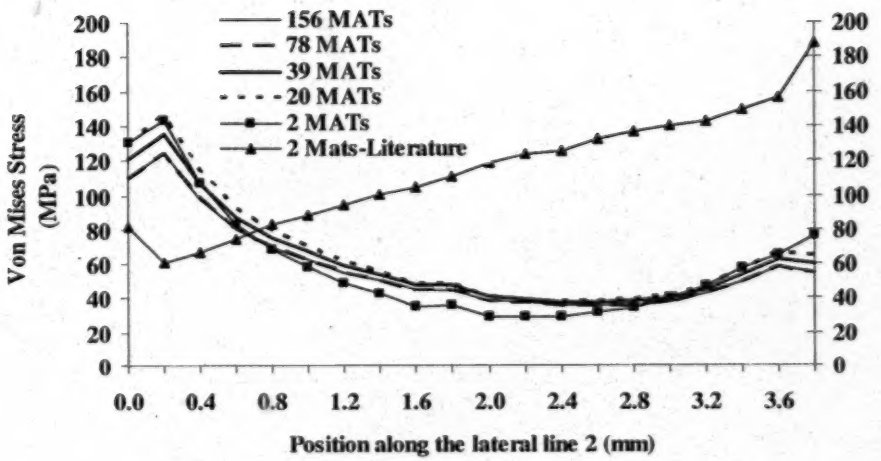

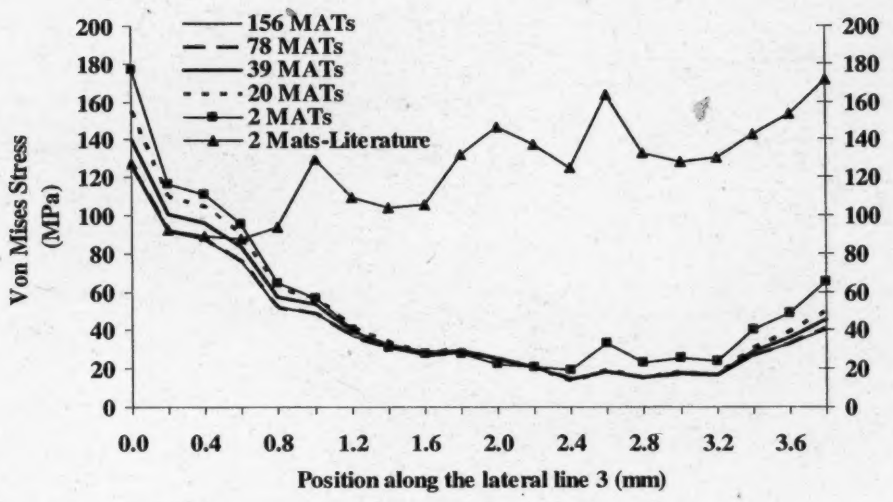
156 MATs
78 MATs
39 MATs
20 MATs
2 MATs
2 Mats-Literature
Von Mises Stress (MPa)
Position along the lateral line 3 (mm)

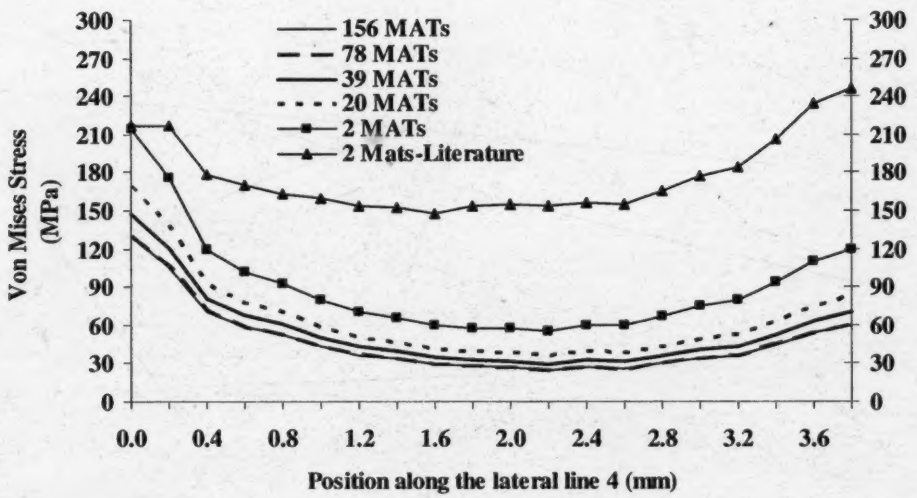
156 MATs
78 MATs
39 MATs
20 MATs
2 MATs
2 Mats-Literature
Von Mises Stress (MPa)
Position along the lateral line 4 (mm)

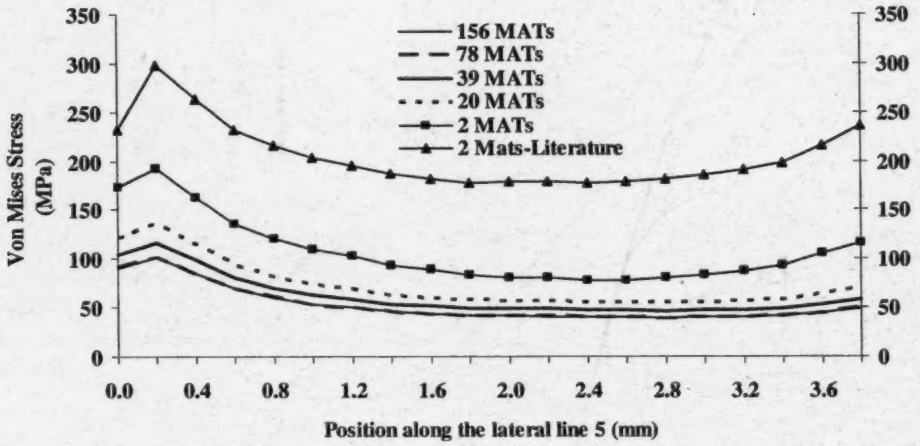
156 MATs
78 MATs
39 MATs
20 MATs
2 MATs
2 Mats-Literature
Von Mises Stress (MPa)
Position along the lateral line 5 (mm)
0
50
100
150
200
250
300
350
0.0
0.4
0.8
1.2
1.6
2.0
2.4
2.8
3.2
3.6

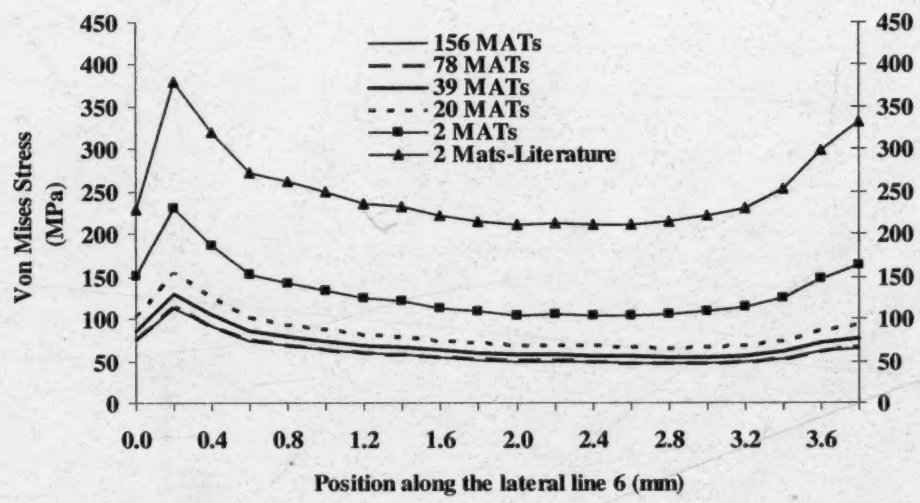
156 MATs
78 MATs
39 MATs
20 MATs
2 MATs
2 Mats-Literature
Von Mises Stress (MPa)
Position along the lateral line 6 (mm)
0
50
100
150
200
250
300
350
400
450
0.0
0.4
0.8
1.2
1.6
2.0
2.4
2.8
3.2
3.6

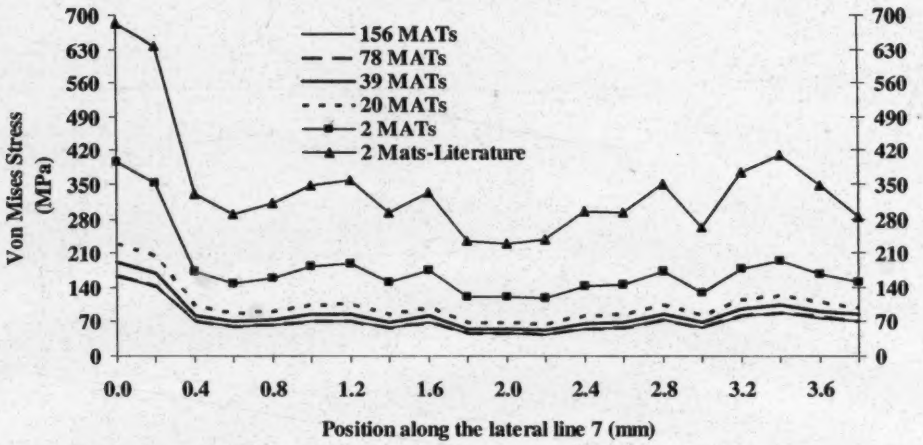
156 MATs
78 MATs
39 MATs
20 MATs
2 MATs
2 Mats-Literature
Von Mises Stress (MPa)
700
630
560
490
420
350
280
210
140
70
0
0.0
0.4
0.8
1.2
1.6
2.0
2.4
2.8
3.2
3.6
Position along the lateral line 7 (mm)

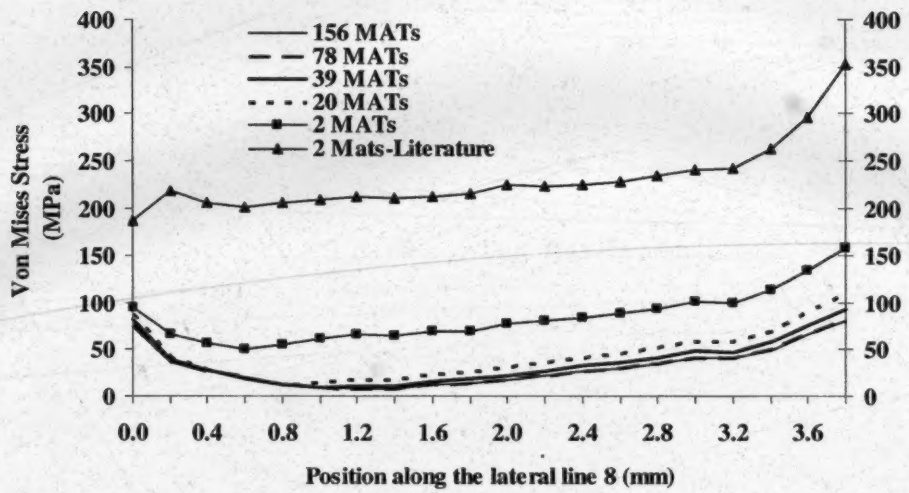
156 MATs
78 MATs
39 MATs
20 MATs
2 MATs
2 Mats-Literature
Von Mises Stress (MPa)
400
350
300
250
200
150
100
50
0
0.0
0.4
0.8
1.2
1.6
2.0
2.4
2.8
3.2
3.6
Position along the lateral line 8 (mm)

APPENDIX 2

Sensitivity of Von Mises stress along BA longitudinal lines to BAOI EP

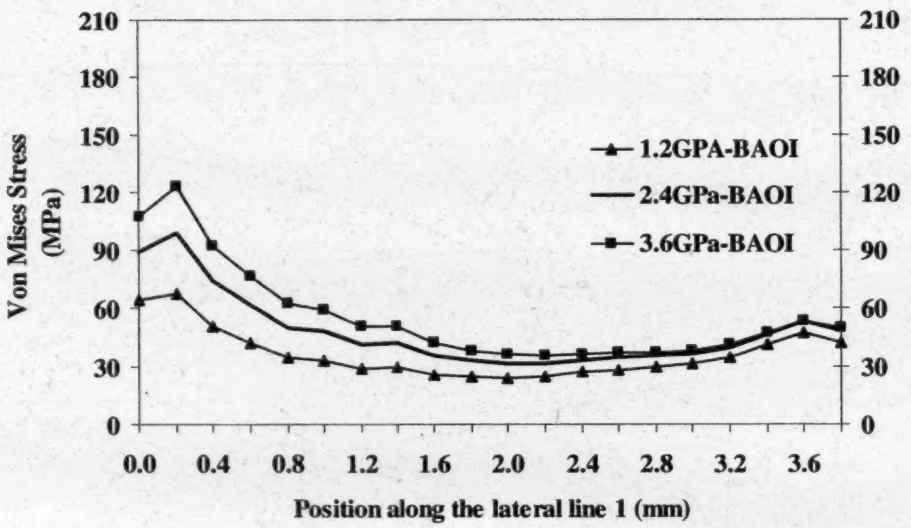

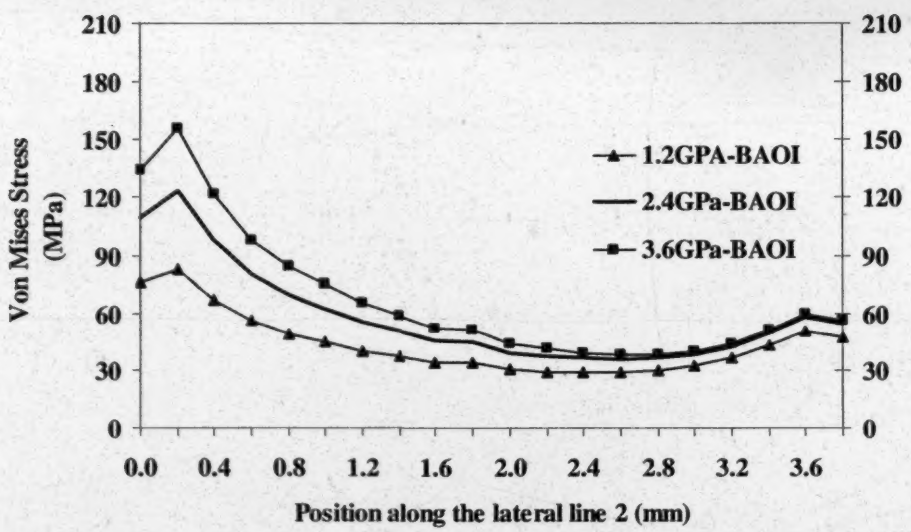

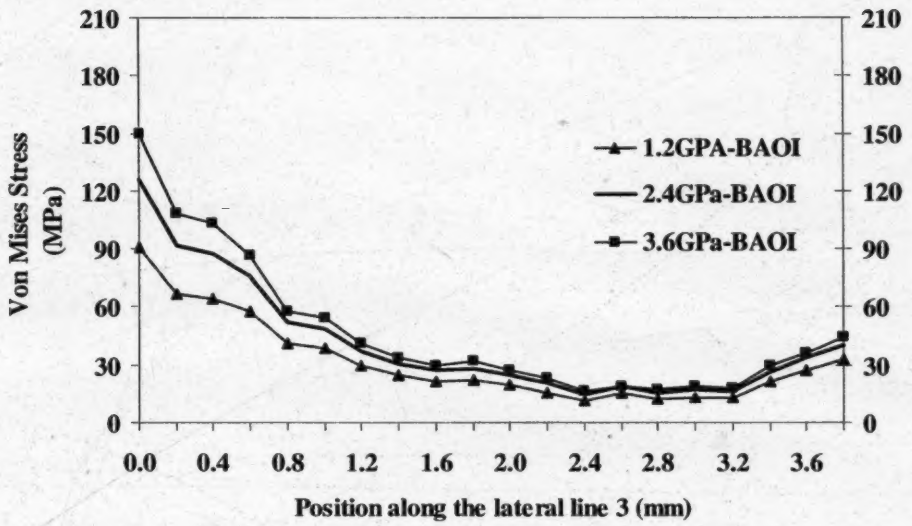
Von Mises Stress (MPa)
210
180
150
120
90
60
30
0
0.0
0.4
0.8
1.2
1.6
2.0
2.4
2.8
3.2
3.6
1.2GPA-BAOI
2.4GPa-BAOI
3.6GPa-BAOI
Position along the lateral line 3 (mm)

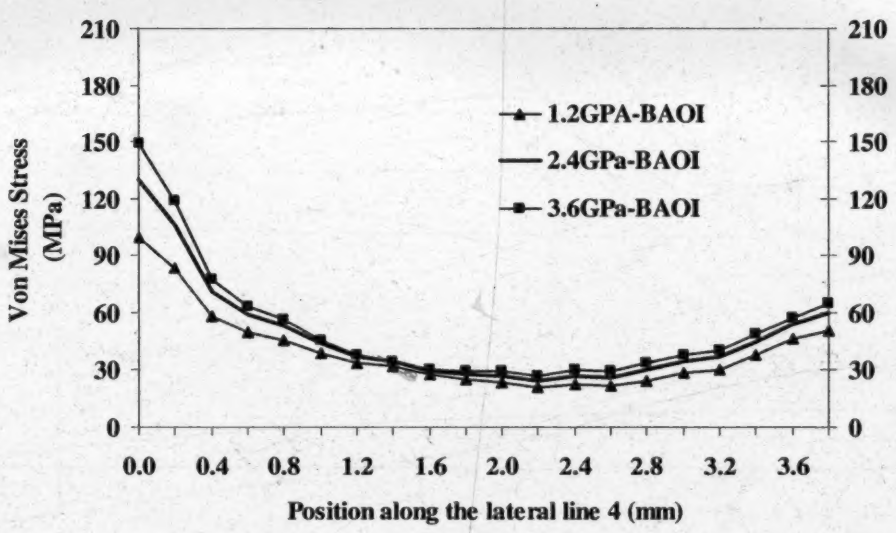
Von Mises Stress (MPa)
210
180
150
120
90
60
30
0
0.0
0.4
0.8
1.2
1.6
2.0
2.4
2.8
3.2
3.6
1.2GPA-BAOI
2.4GPa-BAOI
3.6GPa-BAOI
Position along the lateral line 4 (mm)

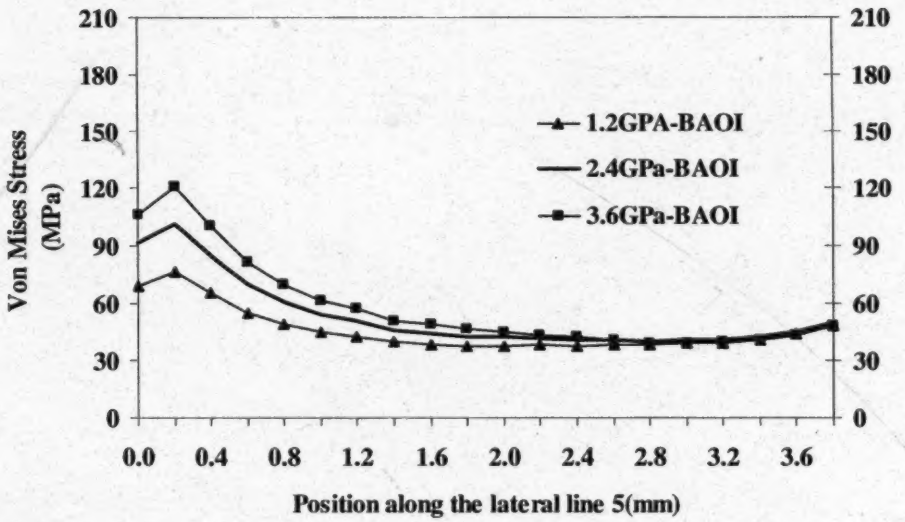
Von Mises Stress (MPa)
210
180
150
120
90
60
30
0
1.2GPA-BAOI
2.4GPa-BAOI
3.6GPa-BAOI
0.0
0.4
0.8
1.2
1.6
2.0
2.4
2.8
3.2
3.6
Position along the lateral line 5(mm)

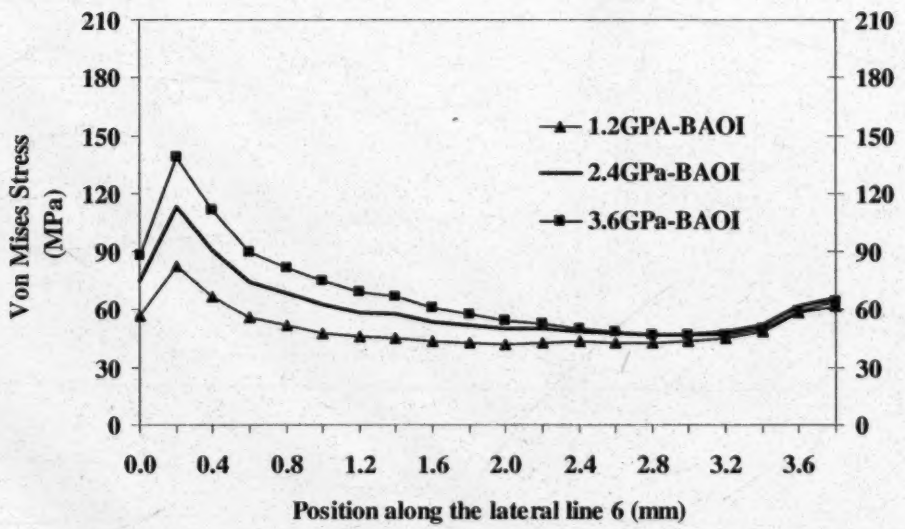
Von Mises Stress (MPa)
210
180
150
120
90
60
30
0
1.2GPA-BAOI
2.4GPa-BAOI
3.6GPa-BAOI
0.0
0.4
0.8
1.2
1.6
2.0
2.4
2.8
3.2
3.6
Position along the lateral line 6 (mm)

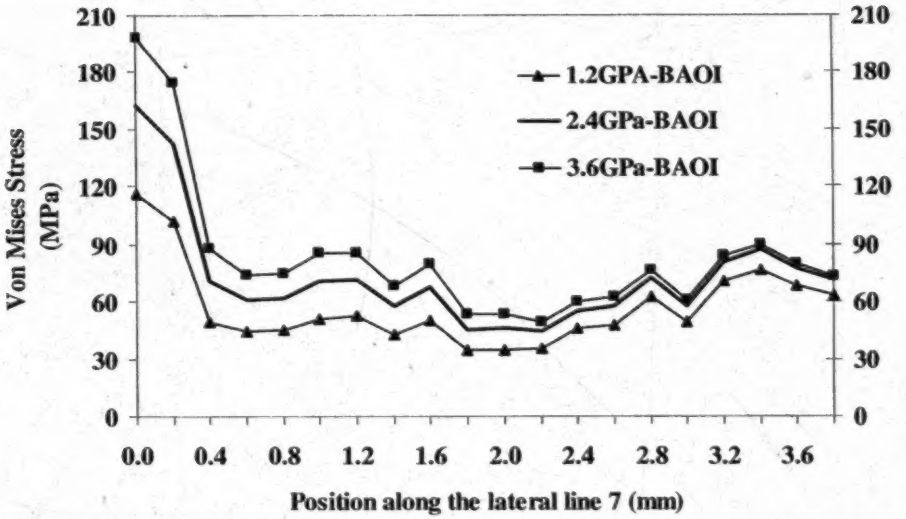
Von Mises Stress (MPa)
1.2GPA-BAOI
2.4GPa-BAOI
3.6GPa-BAOI
Position along the lateral line 7 (mm)

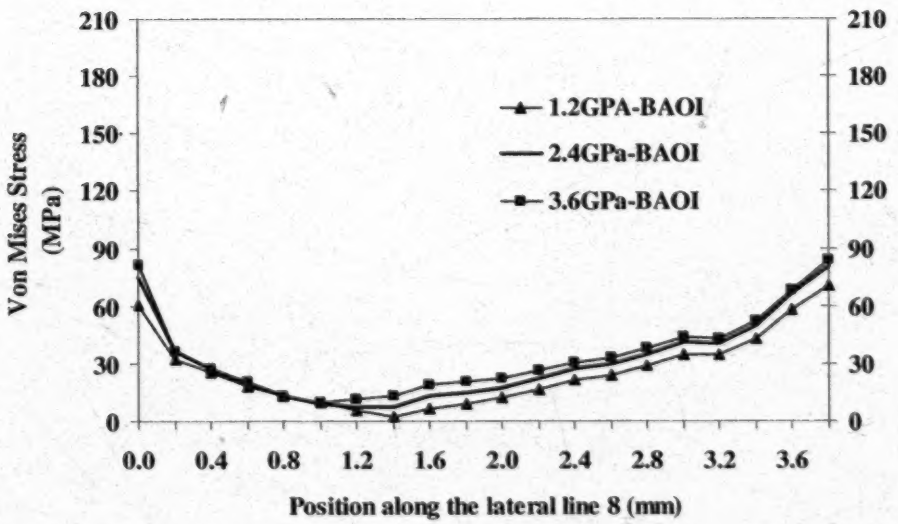
Von Mises Stress (MPa)
1.2GPA-BAOI
2.4GPa-BAOI
3.6GPa-BAOI
Position along the lateral line 8 (mm)

APPENDIX 3

Effect of AIA on Von Mises stress along BA longitudinal lines

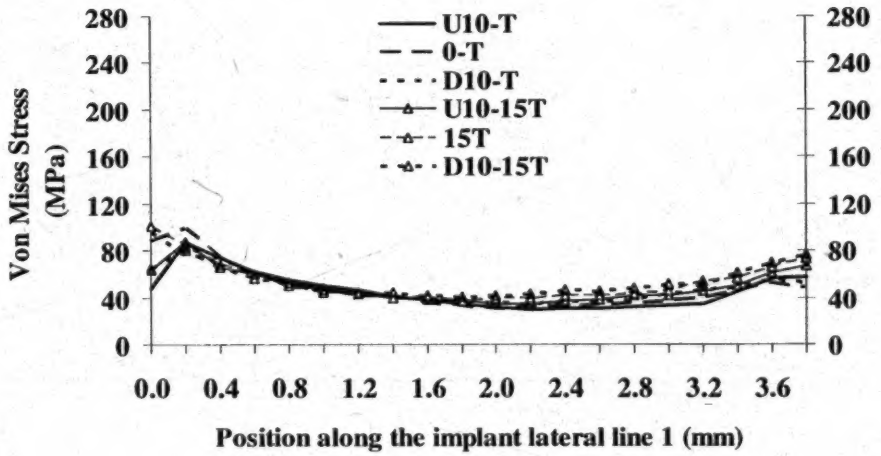

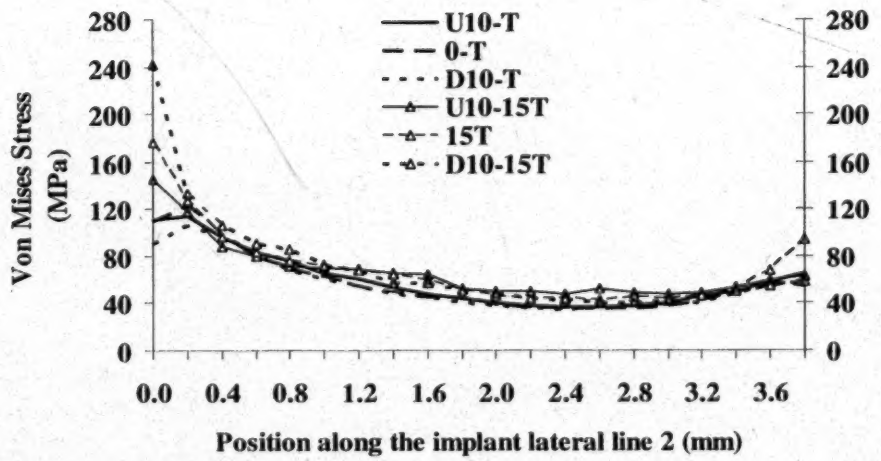

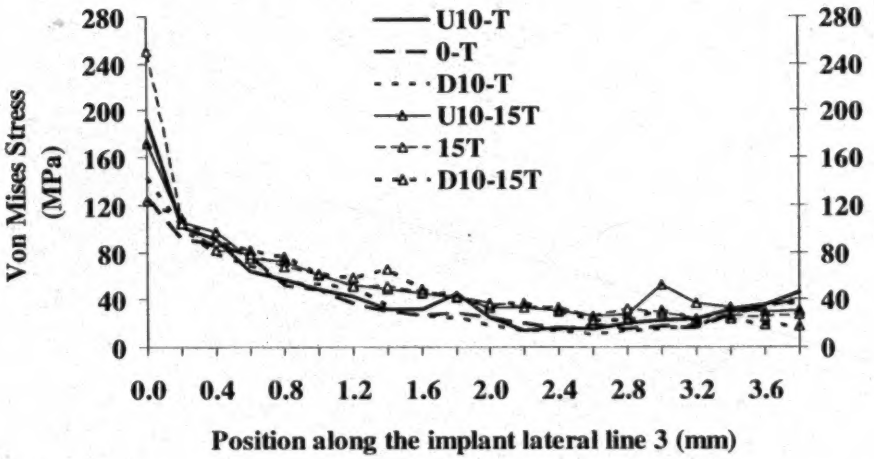
U10-T
0-T
D10-T
U10-15T
15T
D10-15T
Von Mises Stress (MPa)
280
240
200
160
120
80
40
0
0.0
0.4
0.8
1.2
1.6
2.0
2.4
2.8
3.2
3.6
Position along the implant lateral line 3 (mm)

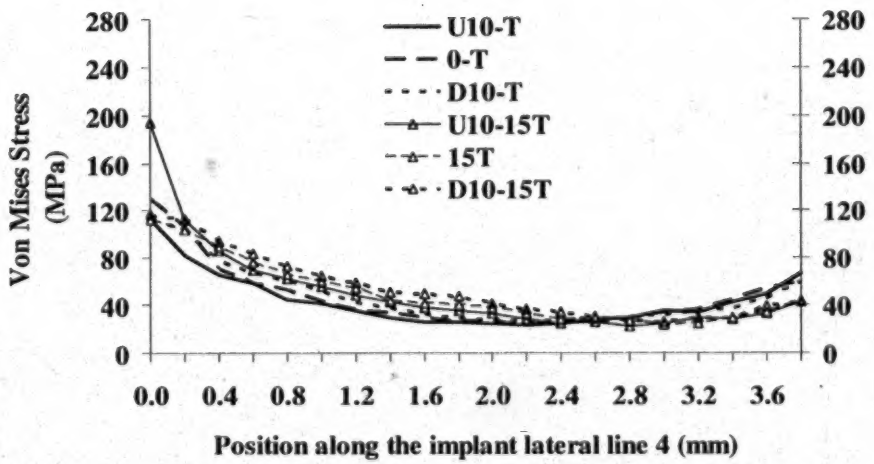
U10-T
0-T
D10-T
U10-15T
15T
D10-15T
Von Mises Stress (MPa)
280
240
200
160
120
80
40
0
0.0
0.4
0.8
1.2
1.6
2.0
2.4
2.8
3.2
3.6
Position along the implant lateral line 4 (mm)

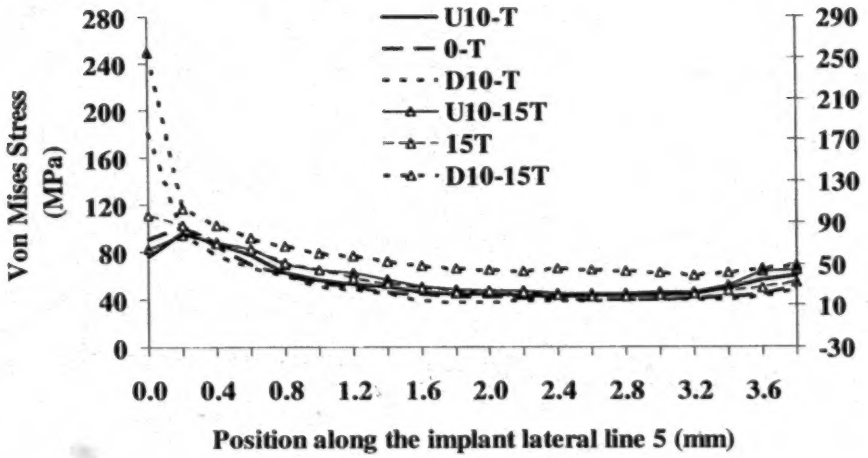
U10-T
0-T
D10-T
U10-15T
15T
D10-15T
Von Mises Stress (MPa)
280
240
200
160
120
80
40
0
290
250
210
170
130
90
50
10
-30
0.0
0.4
0.8
1.2
1.6
2.0
2.4
2.8
3.2
3.6
Position along the implant lateral line 5 (mm)

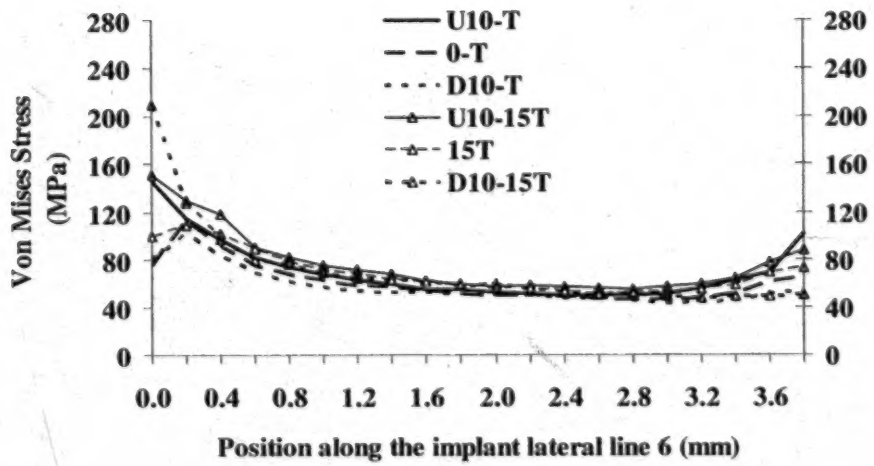
U10-T
0-T
D10-T
U10-15T
15T
D10-15T
Von Mises Stress (MPa)
280
240
200
160
120
80
40
0
0.0
0.4
0.8
1.2
1.6
2.0
2.4
2.8
3.2
3.6
Position along the implant lateral line 6 (mm)

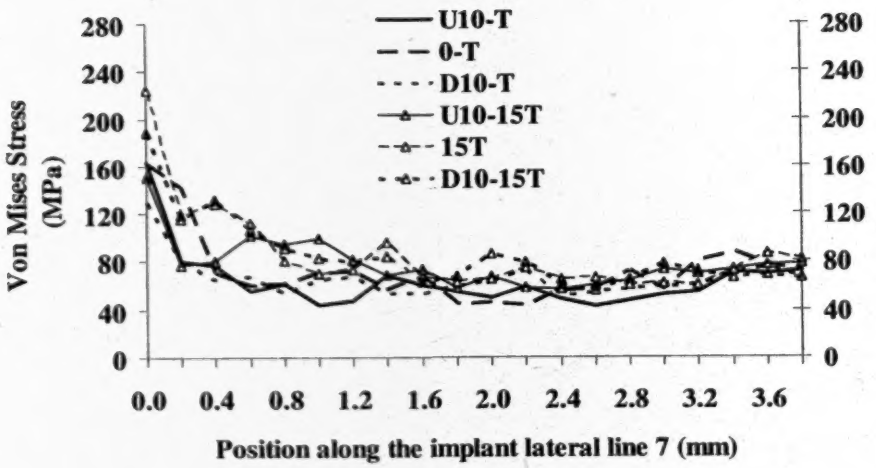
U10-T
0-T
D10-T
U10-15T
15T
D10-15T
Von Mises Stress (MPa)
280
240
200
160
120
80
40
0
0.0
0.4
0.8
1.2
1.6
2.0
2.4
2.8
3.2
3.6
Position along the implant lateral line 7 (mm)

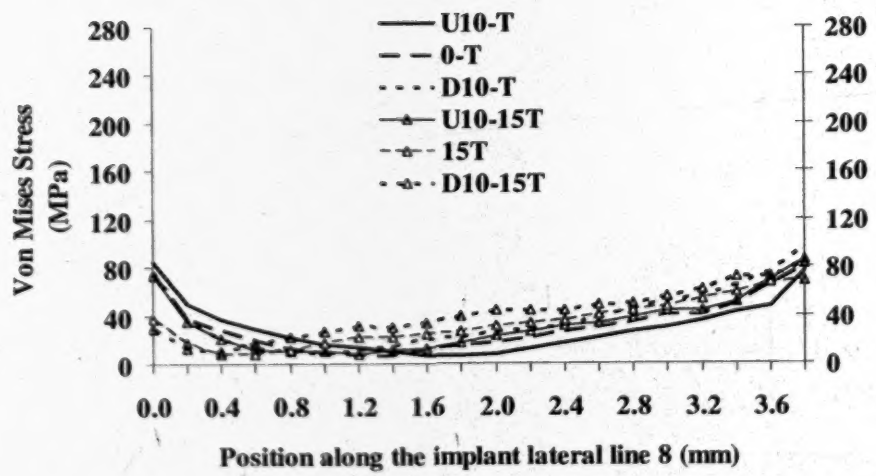
U10-T
0-T
D10-T
U10-15T
15T
D10-15T
Von Mises Stress (MPa)
280
240
200
160
120
80
40
0
0.0
0.4
0.8
1.2
1.6
2.0
2.4
2.8
3.2
3.6
Position along the implant lateral line 8 (mm)